NATIONAL ASSOCIATION OF SURVEYING AND GEOINFORMATICS LECTURERS (NASGL)

BOOK OF PROCEEDINGS

FOR THE

4TH ANNUAL GENERAL MEETING & CONFERENCE (ABUJA 2023)

EDITORS:

- Dr. T.T. Youngu
- Dr. N. Zitta

THEME:

Geospatial Solutions for Good Governance; Issues and Prospects

VENUE:

National Space Research and Development Agency (NASRDA), Obasanjo Space Centre, Airport Road, Abuja, Nigeria

Date: 31st July - 3rd August, 2023

BOOK OF PROCEEDINGS

VOLUME 2 **2023** **ISBN: 978- 978 – 55067 – 3 – 0**

Editors

Dr. T. T. Youngu Ahmadu Bello University, Zaria, Kaduna State – Nigeria (Chief Editor)

Dr. N. Zitta Federal University of Technology, Minna, Niger State – Nigeria

Published by the:

National Association of Surveying and Geoinformatics Lecturers (NASGL), A sub-group of Nigerian Institution of Surveyors.

C/O 30 S.O Williams Crescent, Off Anthony Enahoro Street, Off Okonjo Iweala Way, Utako Berger, P.M.B 763, Garki, Abuja.

Preface

The proceeding is a compendium of presentations at the 4th National Association of Surveying and Geoinformatics Lecturers (NASGL) AGM/Conference Abuja 2023 from July 31st to August 3rd 2023.

The conference provides forum for researchers and professionals in the geospatial industry and allied professions to address fundamental problems and challenges of National Development - *Geospatial Solutions for Good Governance: Issues and Prospects*. The conference is a platform where recognized best practices, theories and concepts are shared and discussed amongst academics, practitioners and researchers. The scope and papers are quite broad but have been organised around the sub-themes listed below:

- Spatially-enabled Election Management
- Geospatial Information for Ensuring Government Accountability
- Geospatial Information to Enhance Disaster and Emergency Management
- Geospatial Information in Ensuring Census Data Accuracy
- Emerging Geospatial Data Acquisition Techniques that Support Good Governance
- Geospatial Sciences for Effective Public Infrastructure Projects
- Geospatial Sciences for Effective Delivery of Public and Social Services

All the papers were subjected to peer-reviews by a team of assessors from amongst our seasoned academics before they were subjected to this electronic publishing. We hope you have a pleasurable and rewarding reading on topical issues in the geospatial environment and academia in the Book of Proceedings**.**

LOC Chairman

National Association of Surveying and Geoinformatics Lecturers (NASGL) 4th AGM/Conference Abuja 2023

September 2023

Copyright Statements

Scientific/Review Committee

We wish to express our deepest and sincere gratitude to the following people who provided comprehensive scientific reviews and made commendable suggestions towards improving the abstracts and full papers submitted to NASGL AGM/Conference Abuja 2023.

Dr. T. T. Youngu	Department of Geomatics, Ahmadu Bello University, Zaria (Chaiman)
Dr. N. Zitta	Department of Surveying and Geoinformatics, Federal University of Technology, Minna
Dr. L. Hart	Department of Surveying and Geomatics, Rivers State University, Port-Harcourt
Dr. E. G. Ayodele	Department of Surveying and Geoinformatics, University of Lagos, Akoka

Local Organising Committee

Dr. J. D. Dodo	Chairman
Dr. L. Hart	Secretary
Dr. T. T. Youngu	Head, Technical/Review Subcommittee
Surv. A. Bala	Head, Publicity Subcommittee
Surv. H. A. Samaila-Ija	Member
Dr. N. Zitta	Member
Dr. E. G. Ayodele	Member
Surv. Y. Umar	Member
Surv. N. Lawal	Member
Dr. (Mrs.) N. Johnson	Member
Surv. Y. Yinang	Member
Surv. D. U. Agada	Member
Surv. (Mrs.) F. Adamu	Member
Surv. G. C. Mohammed	Member
Surv. I. Musa	Member

National Association of Surveying and Geoinformatics Lecturers

(NASGL) Executive

Surv. Dr. Y. D. Opaluwa	NASGL Chairman
Surv. Dr. K. O. Odedare	NASGL Vice -Chairman
Dr. L. Hart	NASGL Secretary General
Surv. (Mrs.) K. Z. Atta	NASGL Assistant Secretary General
Surv. (Mrs). V. N. Asogwa	NASGL Treasurer
Surv. Dr. E. G. Ayodele	NASGL Financial Secretary
Surv. S. O. Olaosegba	NASGL Publicity Secretary
Surv. Dr. O. G. Ajayi	NASGL Internal Auditor
Prof. L. M. Ojigi	NASGL Ex-Officio
Surv. (Mrs.) O. O. Opatoyinbo	NASGL Ex-Officio
Surv. H. A. Samaila-Ija	North Central Zonal Coordinator
Surv. A. A. Fusami	North-East Zonal Coordinator
Surv. Chief Maleeks Ya'u	North-West Zonal Coordinator
Dr. (Mrs.) C. N. Baywood	South-East Zonal Coordinator
Surv. (Mrs.) A. S. Dienye	South-South Zonal Coordinator
Surv. Dr. S. O. Ogunlade	South-West Zonal Coordinator

Table of Contents

Cover Page 0

Title Page i

Preface ii

Copyright Statement iii

Scientific / Review Committee iv

Local Organising Committee v

NASGL National Executive vi

Table of Contents vii

SUB THEME 01: Spatially-enabled Election Management

Computer-based Solution for Geospatial Data Visualization and Analysis of Nigeria 2023 Presidential Election Results

Ibrahim, M., Umar, Y. & Adeyemi, W. 2

Fair Election: A Review of Geospatial Techniques and Forensic GIS in Monitoring Election Process in Nigeria

Morgan, V. U., Francisca, O. O., Johnson, N. G. & Godwin, S. **27**

SUB THEME 02: Geospatial Information for Ensuring Government Accountability

Integration of Geospatial Techniques and Artificial Intelligence in Mapping Multidimensional Poverty in Africa. A Review

Nzelibe, I. U. 34

SUB THEME 03: Geospatial Information to Ensure Disaster and Emergency Management

SUB THEME 04: Geospatial Information in Ensuring Census Data Accuracy

SUB THEME 05: Emerging Geospatial Data Acquisition Techniques that Support Good Governance

Evaluation of Spectral Distance for Effective Feature Mapping in a Multiclass Problem

Zitta, N., Adeniyi, G. & Fimba, E. D. 60

SUB THEME 06: Geospatial Sciences for Effective Public Infrastructure Projects

The Comparative Temporal Variation Evaluation of Kainji and Shiroro Hydropower Plant Reservoirs Storage Water Level in Niger State, Nigeria

Akinwale, A. S. & Musa, A. A. 71

Geospatial Mapping for Effective Public Infrastructure: A Scenario of Bus Stops in Akure South, Ondo State, Nigeria

Tata, H. & Olaoye 88

SUB THEME 07: Geospatial Sciences for Effective Delivery of Public and Social Services

Geospatial Land Use Mapping in Crop Farming Purview

Ogunlade, S. O. 101

Spatial Pattern Analysis of COVID-19 in Nigeria

Akpee, D., Eludoyin, O. S. & Ogoro, M. 109

SUB THEME 01

Spatially-enabled Election Management

COMPUTER-BASED SOLUTION FOR GEOSPATIAL DATA VISUALIZATION AND ANALYSIS OF NIGERIA 2023 PRESIDENTIAL ELECTION RESULTS

Musa Ibrahim.[1]*, Yusuf Umar.[1], Waheed Adeyemi.[1]

[1] Department of Surveying and Geoinformatics, Federal Polytechnic Nasarawa,

Nasarawa state Nigeria.

*Corresponding author: ibrahimmusa283@yahoo.com

Phone: +2348067763648

Abstract

Geospatial data visualization is a powerful tool that helps better understand complex spatially related data by presenting it in a visual graphics format. Geospatial data visualization and analysis is often used in the dissemination of election results to both the general public and decision makers. There are several computer-based tools for visualizing and analyzing geospatial data ranging from no-code tools like PowerBI and Tableau to online visualization platforms like DataWrapper and Google Charts, and specific libraries in popular programming languages, such as Python, JavaScript and R. This paper uses 'Geopandas', a python-based library to visualize and analyze dataset on Nigeria 2023 presidential election published by the Independent National Electoral Commission (INEC). This research intends to provide a flexible solution for visually communication of election results. Tabular dataset on 2023 presidential election were obtained from INEC in PDF formats while geospatial map of Nigeria for the three levels of polling units (State, LGA and Ward) where sourced from the 'Geo-referenced Infrastructure and Demographic Data for Development' (GRID3) in GeoJSON format. These datasets where integrated into python scripting environment for pre-processing (data cleaning) and Geopandas with its associated libraries were used for the processing. The geospatial visualization types created in this paper include choropleth maps, symbol maps, locator maps, bar charts, election donuts, hexagon bin plots, kernel density estimate (KDE) plots and scatter plots. The geospatial visualization and analysis technique employed in this paper can be used to develop and deploy an election management dashboard that can be managed on the web, mobile and desktop platforms. This paper is recommended to be a vital tool that will demonstrate transparency and good governance for both the general public and decision makers to quickly visualize and analyze the outcome of an election pictorially and also create academic gap for further researcher on same or related research to employ other tools rather than python-based library to visualize and analyze data set.

Keywords: Geospatial Visualization, Python, Geopandas, Election Results, Election Map

1.0 INTRODUCTION

Python is an open-source programming language developed with the community-based model [8]. Python is integrated into Geographical Information System software such as QGIS and ArcGIS mainly used for automating the geo-processes [1]. Python has reach ecosystem of

geospatial data visualization and analysis libraries that includes matplotlib, seaborn, pandas, geopandas, plotly, bokeh, geoplotlib, folium, ggplot, and pygal [7]. This paper focuses on using 'geopandas' and its complementary libraries. Pandas provides data structures and data analysis tools whereas GeoPandas extends the data types used by pandas to allow spatial operations on geometric types [1]. It is also common to see geopandas used together with matplotlib and folium libraries for geospatial visualization and analysis. Geopandas is a python library that makes working with geospatial data in python easier. It combines the powerful features of the popular Pandas library to use DataFrames and of Shapely library to work with geometrical data, providing geospatial operations with the familiar syntax of Pandas while extending its functionality to work with geometries to create beautiful maps. The geometric operations are performed by Shapely library and it further depends on Fiona library for geospatial file access and Matplotlib library for plotting.

Geospatial data visualization is a powerful tool that helps better understand complex spatially related data by presenting it in a visual graphics format. Python has rich set of geo-visualization libraries and tools thanks to its versatility and ease of use. Python greatly enhance the ability to derive insights and communicate findings in election data to others. With the help of pictorial representations, such as charts, graphs, maps, and dashboards, analysts can better understand the underlying data and spot potential anomalies or outliers [6].

Eighteen political parties featured candidates for the 2023 presidential elections, however only four of them got significant number of votes across the states. Hence this paper only focuses on the four frontrunners: Bola Tinubu of the ruling All Progressives Congress (APC), Atiku Abubakar of the leading opposition People's Democratic Party, Peter Obi of the Labour Party, and Rabiu Kwankwaso of the New Nigeria People's Party (NNPP).

1.1 Scope and Limitations

In this paper, we have seen that Geopandas is a versatile and powerful geospatial library for Python, but like any software tool, it has the following limitations: -

i. Simplistic Cartographic Options: Geopandas provides a basic level of cartographic capabilities for visualizing geospatial data, but these options are not as advanced or customizable as what you might find in dedicated cartography software or more specialized GIS tools. If you need more advanced and customized cartographic features, you might need to integrate it with other libraries like Matplotlib. It supports creating choropleth maps, where areas are shaded based on a variable's value. However, you might find limited control over color gradients, classification methods, and legend styling compared to dedicated cartography tools. Labeling features on a map, especially when dealing with crowded areas, can be challenging in Geopandas. You might need to resort to using additional libraries or manual adjustments to achieve desired labeling effects.

ii. Performance with Large Datasets: Geopandas might encounter performance issues when dealing with very large datasets. Operations involving extensive data can lead to slower processing times and increased memory usage.

iii. Limited 3D and Time Support: Geopandas primarily focuses on 2D geospatial data. While it does have some support for working with 3D and time-related data, it's not as comprehensive as its 2D capabilities.

iv. Limited Geometric Operations: Geopandas doesn't offer the full range of geometric operations that dedicated GIS software might provide. Complex geospatial analyses might require additional libraries or tools.

v. Spatial Indexing: Geopandas uses a spatial indexing mechanism to speed up spatial queries. However, the spatial indexing might not be as optimized as what you'd find in specialized GIS software.

vi. Dependency Complexity: Geopandas relies on several other libraries, including Fiona and Shapely, which can sometimes result in version compatibility issues or complex dependency chains.

vii. Limited Data Editing Capabilities: While Geopandas can read and write various geospatial data formats, its data editing capabilities are more limited compared to dedicated GIS software.

viii. Lack of Advanced GIS Functionality: Geopandas is focused on providing a simplified interface for geospatial data manipulation and analysis. It might lack some of the more advanced features and tools found in full-fledged GIS software.

ix. Less User-Friendly for graphical user interface (GUI) Tasks: Geopandas is primarily used in scripting environments, which might make it less user-friendly for tasks that require a GUI.

In summary, while Geopandas is fantastic for its data manipulation and analysis capabilities, creating highly customized and sophisticated cartographic outputs might require supplementing it with other tools or libraries that provide more advanced cartographic features.

2.0 STUDY AREA

Nigeria has a total area of 923,770km square [10]. with maximum North-South and East-West extent of about 1,050km and 1,150km respectively. Nigeria lies in the tropical zone of West Africa between latitudes 4°N and 14°N of the equator and between longitudes 2°E and 14°E, of the Greenwich Meridian (Figure 1). The country is bordered in the West by Benin, in the Northwest and in the North by Niger, in the Northeast by Chad and in the East by Cameroon, while the Atlantic Ocean forms the Southern limits of Nigerian territory.

Nigeria has a democratic constitution with a federal system modelled on the United State of America [4]. The executive is headed by the president, the legislature is formed by the

National Assembly of Senate and House of Representatives, and the judiciary is headed by a supreme court.

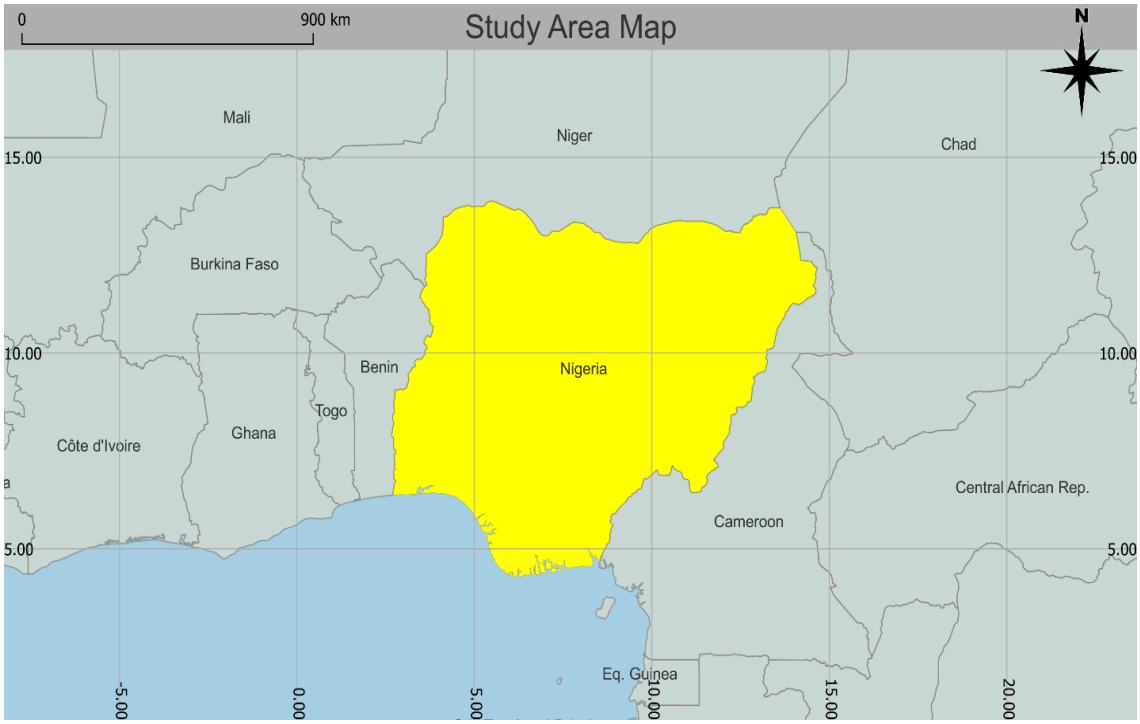

Figure 1: The Study Area. Map of Nigeria showing its place in Africa

Nigeria is a Federation consisting of 774 Local Governments, 36 States and a Federal Capital Territory in ascending order of hierarchy and each headed by Chairman, Governors and President-appointed minister respectively. Subject to the provisions of the 1999 Constitution, the executive power of the Federation is vested in the President and the executive rule of law vested in a State under the Constitution shall be so exercised as not to impede or prejudice the exercise of the executive powers of the Federation. The system of local government by democratically elected local government councils headed by the Chairman is under this Constitution guaranteed [12]. There are six geopolitical zones within the Federal Republic of Nigeria (Table 1). These zones are a form of administrative division and were initiated in 1993 by the then head of state and commander-in-chief of the armed forces of the Federal Republic of Nigeria President General Sani Abacha's administration to group the nation's states. The six zones were not wholly divided based on geography; rather, states with comparable ethnic populations and/or shared political histories were grouped together.

Table 1: Geopolitical Zones, their States and Ethnicity (adopted from Olabanjo, 2022)

S/N	Zone	States	Ethnicity
1.	North Central	Benue, Kogi, Kwara, Nasarawa, Niger, and Plateau States, as well as the Federal Capital Territory.	Hausa & Fulani
2.	North East	Adamawa, Bauchi, Borno, Gombe, Taraba, and Yobe States.	
3.	North West	Jigawa, Kaduna, Kano, Katsina, Kebbi, Sokoto, and Zamfara States.	
4.	South East	Abia, Anambra, Ebonyi, Enugu, and Imo States.	

5.	South South	Akwa Ibom, Bayelsa, Cross River, Delta, Edo, and Rivers States.	Igbo and Niger Deltans
6.	South West	Ekiti, Lagos, Ogun, Ondo, Osun, and Oyo States.	Yoruba

3.0 DATA AND METHODOLOGY

This paper seeks to spatially visualize and analyze the result outcome of 2023 Nigeria presidential election for its four prominent contesting candidates and this section describes in detail the approach used in python geopandas and its related libraries to generate high quality print ready geospatial visualization. Figure 2 illustrates the sequence of steps used in this paper.

Generally, we used two kinds of datasets, tabular data sourced from INEC and the vector map data sourced from GRID3. The two were put together to make the geospatial visualizations and analyses as seen in Figure 4, Figure 5, Figure 6, Figure 7, Figure 8 and Figure 9.

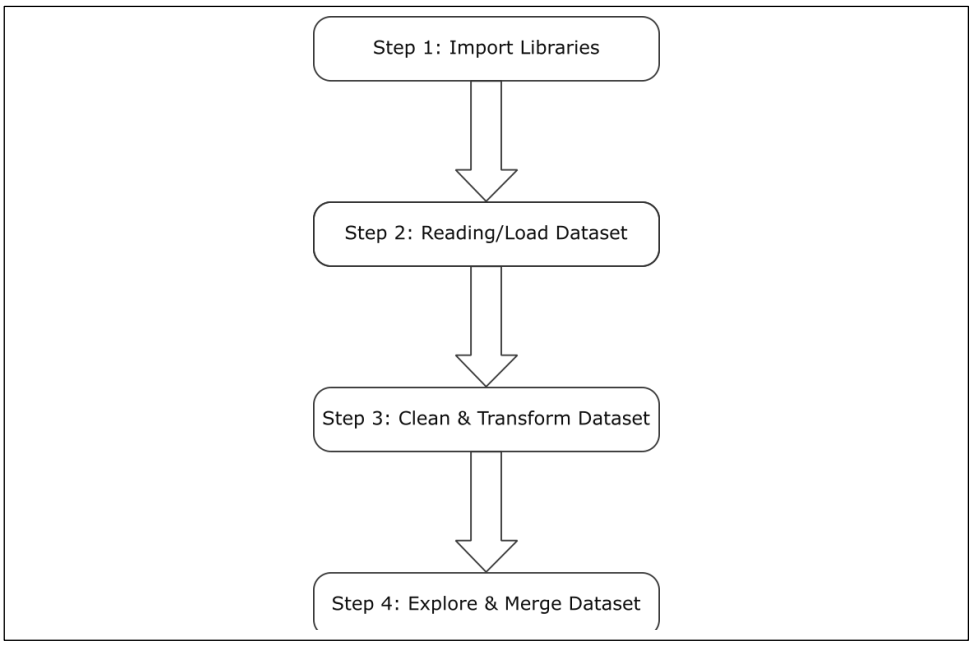

Figure 2: Sequence of steps in geopandas geospatial visualization

3.1 Tabular Election Dataset

INEC provided these datasets in portable document format (PDF) as seen in figure 3, so we used object-character recognition (OCR) technique to extract the tables into comma-delimited variable (CSV) files that can be read by geopandas in python. The resulting table is presented in table 1 below. This tabular dataset when join to the geospatial data is referred to as “metadata”. That is additional information that characterize each individual geospatial feature.

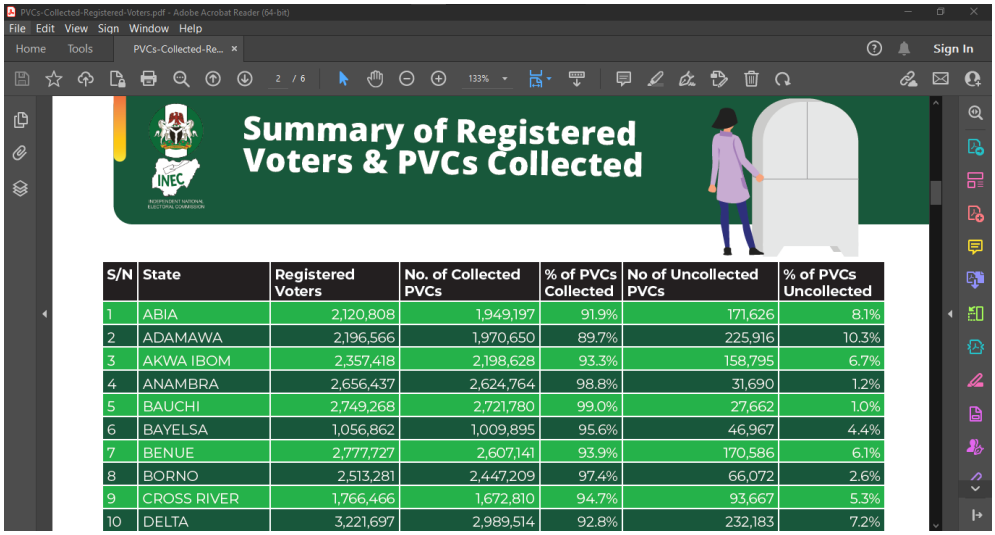

S/N	State	Registered Voters	No. of Collected PVCs	% of PVCs Collected	No of Uncollected PVCs	% of PVCs Uncollected
1	ABIA	2,120,808	1,949,197	91.9%	171,626	8.1%
2	ADAMAWA	2,196,566	1,970,650	89.7%	225,916	10.3%
3	AKWA IBOM	2,357,418	2,198,628	93.3%	158,795	6.7%
4	ANAMBRA	2,656,437	2,624,764	98.8%	31,690	1.2%
5	BAUCHI	2,749,268	2,721,780	99.0%	27,662	1.0%
6	BAYELSA	1,056,862	1,009,895	95.6%	46,967	4.4%
7	BENUE	2,777,727	2,607,141	93.9%	170,586	6.1%
8	BORNO	2,513,281	2,447,209	97.4%	66,072	2.6%
9	CROSS RIVER	1,766,466	1,672,810	94.7%	93,667	5.3%
10	DELTA	3,221,697	2,989,514	92.8%	232,183	7.2%

Figure 3: Summary of Registered Voters & PVCs Collected (Source: INEC Nigeria, 2023).

Table 2: OCR result of "Presidential Election Results by States"

S/N	STATE	APC	PDP	LP	NNPP
1	ABIA	8,914	22,676	327,095	1,239
2	ABUJA	90,902	74,194	281,717	4,517
3	ADAMAWA	182,881	417,611	105,648	8,006
4	AKWA IBOM	160,620	214,012	132,683	7,796
5	ANAMBRA	5,111	9,036	584,621	1,967
6	BAUCHI	316,694	426,607	27,373	72,103
7	BAYELSA	42,572	68,818	49,975	540
8	BENUE	310,468	130,081	308,372	4,740
9	BORNO	252,282	190,921	7,205	4,626
10	CROSS RIVER	130,520	95,425	179,917	1,644
11	DELTA	90,183	161,600	341,866	3,122
12	EBONYI	42,402	13,503	259,738	2,661
13	EDO	144,471	89,585	331,163	2,743
14	EKITI	201,494	89,554	11,397	264
15	ENUGU	4,772	15,749	428,640	1,808
16	GOMBE	146,977	319,123	26,160	10,520
17	IMO	66,406	30,234	360,495	1,552
18	JIGAWA	421,390	386,587	1,889	98,234
19	KADUNA	399,293	554,360	294,494	92969

S/N	STATE	APC	PDP	LP	NNPP
20	KANO	517,341	131,716	28,513	997,279
21	KATSINA	482,283	489,045	6,376	69,386
22	KEBBI	248,088	285,175	10,682	5,038
23	KOGI	240,751	145,104	56,217	4238
24	KWARA	263,572	136,909	31,166	3,142
25	LAGOS	572,606	75,750	582,454	8,442
26	NASARAWA	172,922	147,093	191,361	12,715
27	NIGER	375,183	284,898	80,452	21,836
28	OGUN	341,554	123,831	85.829	2,200
29	ONDO	369,924	115,463	44,405	930
30	OSUN	343,945	354,366	23,283	713
31	OYO	449,884	182,977	99,110	4,095
32	PLATEAU	307,195	243,808	466,272	8,869
33	RIVERS	231,591	88,468	175,071	1,322
34	SOKOTO	285,444	288,679	6,568	1,300
35	TARABA	135,165	189,017	146,315	12,818
36	YOBE	151,459	198,567	2,406	18,270
37	ZAMFARA	298,396	193,978	1,660	4,044

3.2 Geospatial Data Visualization

To create the visualizations in this paper we adopted the steps outlined in Figure 2. We launched the jupyter lab python development environment and imported the required libraries pandas, geopandas and matplotlib in this case. We followed the process in order as outlined below; -

a. Import Libraries

b. Reading/Load Dataset

c. Clean & Transform Dataset

d. Explore & Merge Dataset

e. Plot Map/Chart

3.2.1 Import Libraries: By default, the libraries used in the study are not available in the python environment, so they have to be imported. As a convention, this is usually done from the very top of the script or code file (figure 10).

3.2.2 Reading/Load Dataset: Next we have to load in the datasets. The geospatial file was read in using geopandas *read_file()* function while the tabular CSV dataset was read using pandas *read_csv()* function. This is an important step as it avails us access to the data used for the visualization.

3.2.3 Clean & Transform Dataset: This step and the next can be done interchangeably depending on your workflow. Here we decided to do some cleaning on the dataset to get rid of unwanted noise before merging the geospatial data to the tabular data.

3.2.4 Explore & Merge Dataset: We carried out exploratory data analysis (EDA) and make sure the two datasets were properly combined together. The pandas *merge()* function was used to accomplish the merging.

3.2.5 Plot Map/Chart: Finally, we used several functions from pandas, geopandas and matplotlib to visualize the election result. For choropleth and labeled maps we used geopandas *plot()* function together with matplotlib *subplots()* function, for the interactive locator map, we used geopandas *explore()* function, for the donut chart, we used matplotlib *pie()* function, for the horizontal and stacked bar charts, we used matplotlib *plot()* function, for the scatter plot, we used the matplotlib *scatter()* function, and for the hexagon and kernel density estimate (KDE) charts, we used matplotlib *plot()* function with *kind* argument set as hexbin, kde respectively,

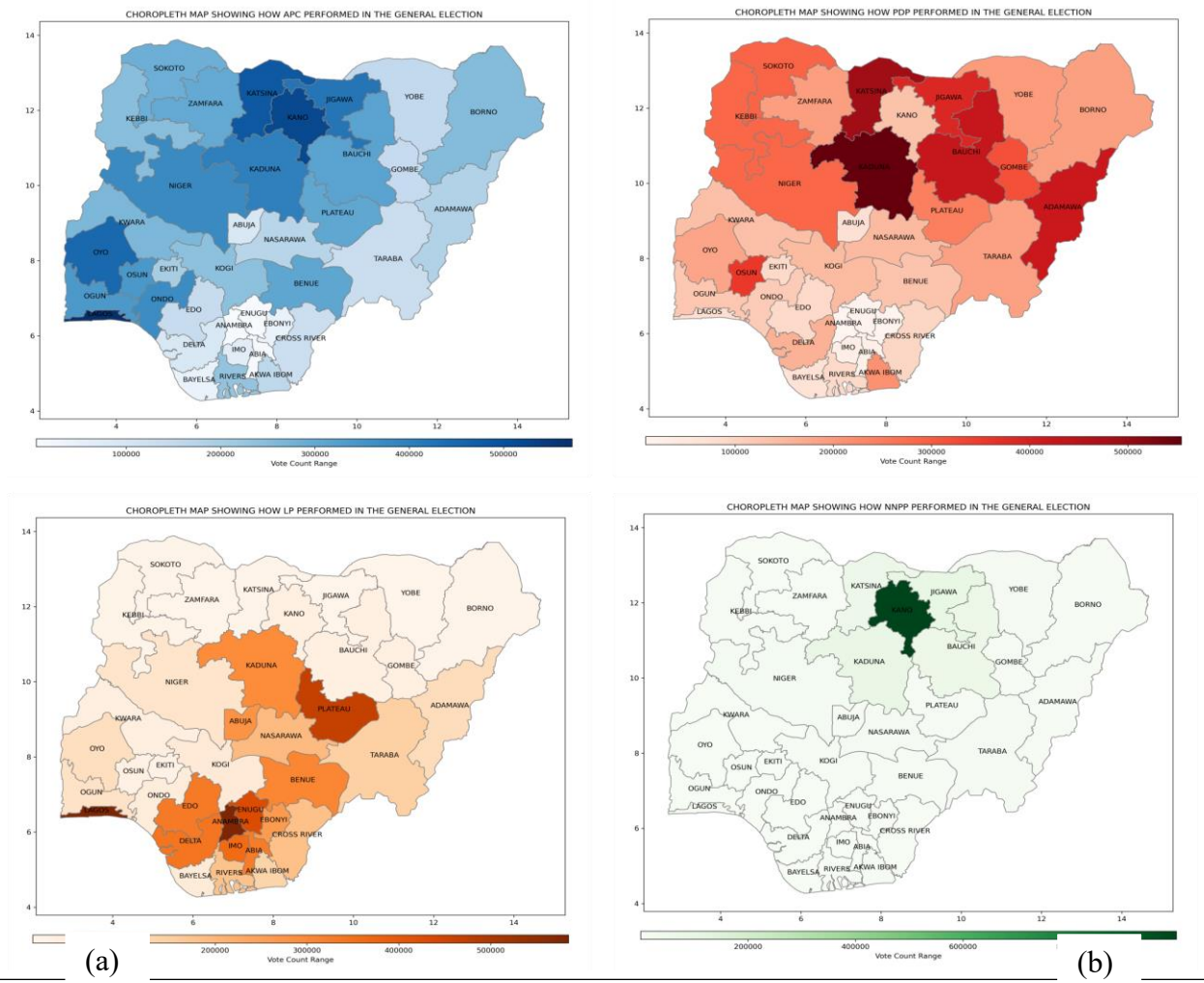

Figure 4 (a): Choropleth map showing how the four major political parties performed in the general election across the country. (b) Choropleth map showing how the four major political parties performed in North Central Geopolitical Zone

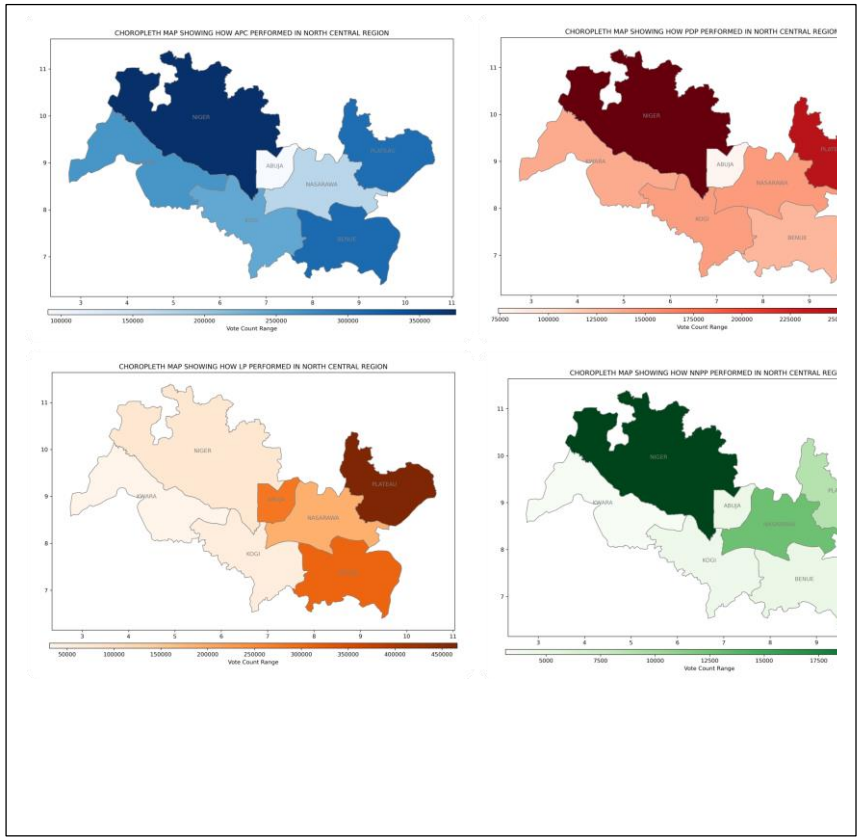
CHOROPLETH MAP SHOWING HOW APC PERFORMED IN NORTH CENTRAL REGION
CHOROPLETH MAP SHOWING HOW PDP PERFORMED IN NORTH CENTRAL REGION
CHOROPLETH MAP SHOWING HOW LP PERFORMED IN NORTH CENTRAL REGION
CHOROPLETH MAP SHOWING HOW NNPP PERFORMED IN NORTH CENTRAL REGION
Vote Count Range

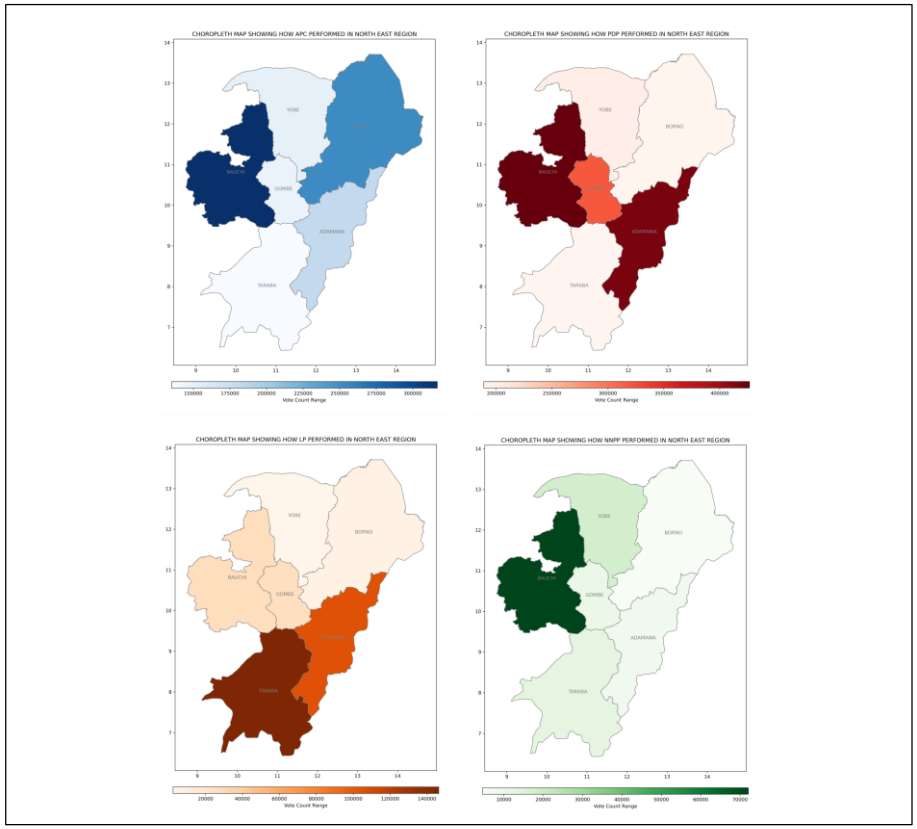
CHOROPLETH MAP SHOWING HOW APC PERFORMED IN NORTH EAST REGION
CHOROPLETH MAP SHOWING HOW PDP PERFORMED IN NORTH EAST REGION
CHOROPLETH MAP SHOWING HOW LP PERFORMED IN NORTH EAST REGION
CHOROPLETH MAP SHOWING HOW NNPP PERFORMED IN NORTH EAST REGION
Vote Count Range

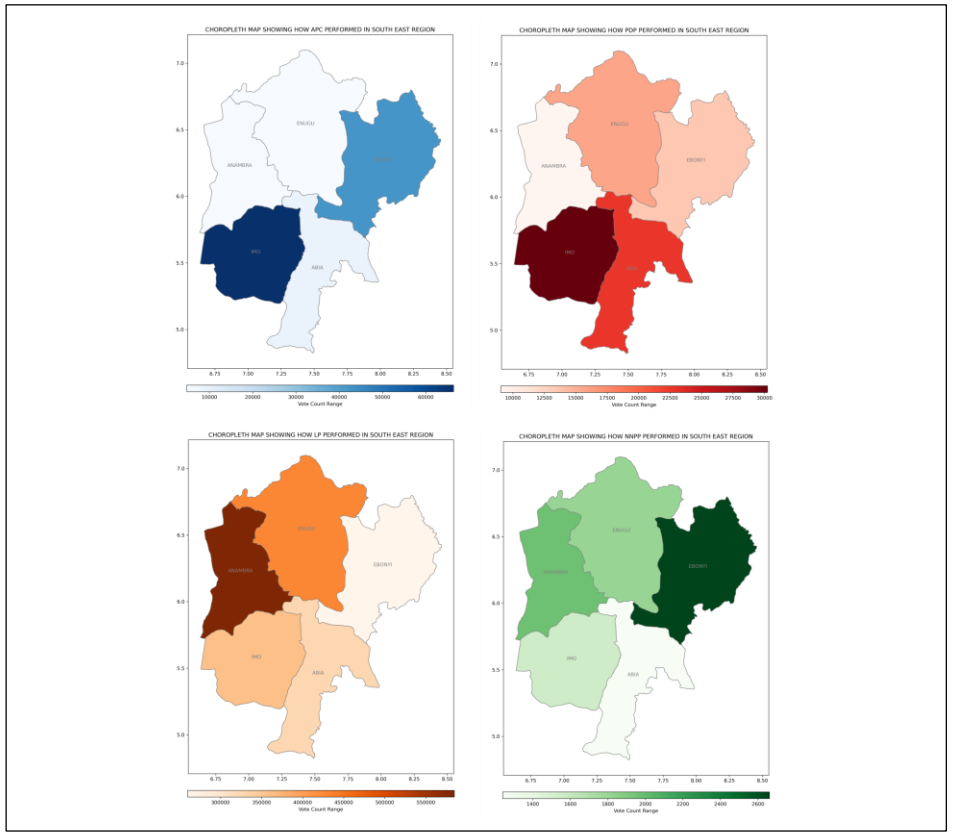
CHOROPLETH MAP SHOWING HOW APC PERFORMED IN SOUTH EAST REGION
CHOROPLETH MAP SHOWING HOW PDP PERFORMED IN SOUTH EAST REGION
CHOROPLETH MAP SHOWING HOW LP PERFORMED IN SOUTH EAST REGION
CHOROPLETH MAP SHOWING HOW NNPP PERFORMED IN SOUTH EAST REGION
ENUGU
ANAMBRA
EBONYI
IMO
ABIA
Vote Count Range

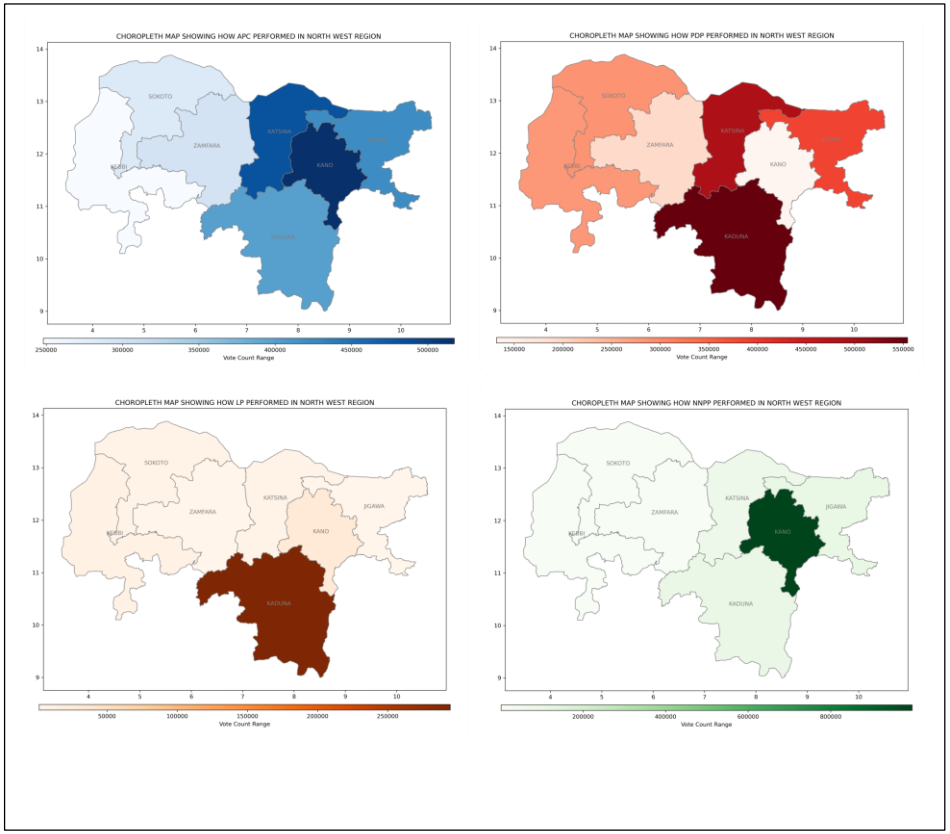
CHOROPLETH MAP SHOWING HOW APC PERFORMED IN NORTH WEST REGION
CHOROPLETH MAP SHOWING HOW PDP PERFORMED IN NORTH WEST REGION
CHOROPLETH MAP SHOWING HOW LP PERFORMED IN NORTH WEST REGION
CHOROPLETH MAP SHOWING HOW NNPP PERFORMED IN NORTH WEST REGION
SOKOTO
ZAMFARA
KATSINA
JIGAWA
KEBBI
KANO
KADUNA
Vote Count Range

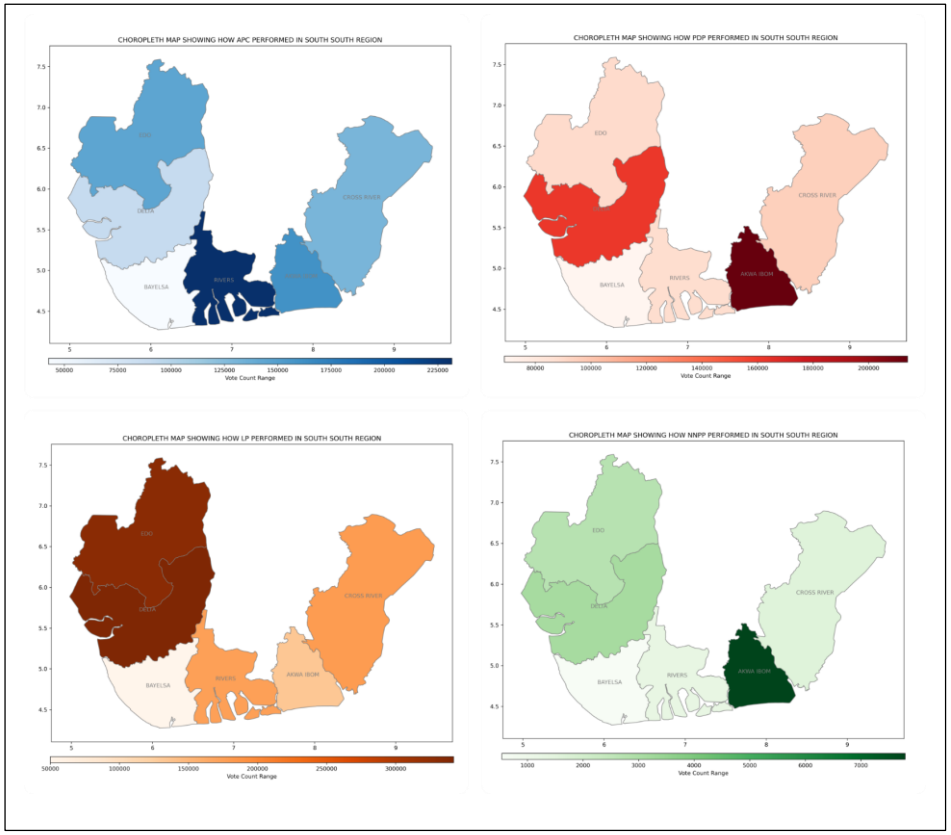
CHOROPLETH MAP SHOWING HOW APC PERFORMED IN SOUTH SOUTH REGION
CHOROPLETH MAP SHOWING HOW PDP PERFORMED IN SOUTH SOUTH REGION
CHOROPLETH MAP SHOWING HOW LP PERFORMED IN SOUTH SOUTH REGION
CHOROPLETH MAP SHOWING HOW NNPP PERFORMED IN SOUTH SOUTH REGION
Vote Count Range

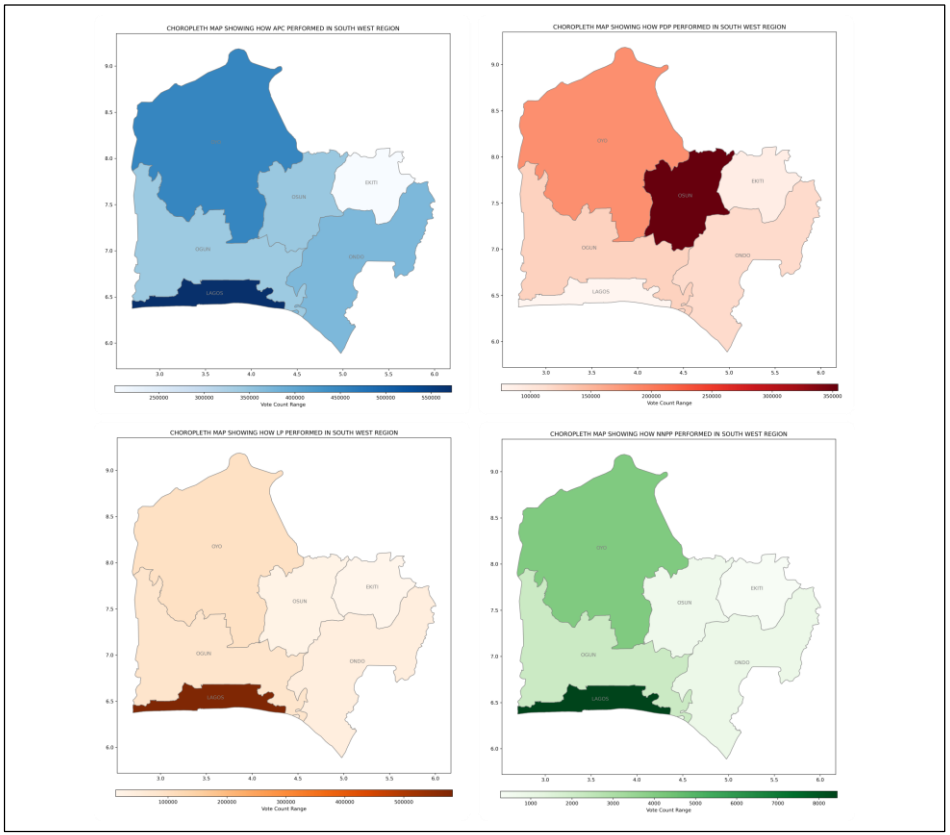
CHOROPLETH MAP SHOWING HOW APC PERFORMED IN SOUTH WEST REGION
CHOROPLETH MAP SHOWING HOW PDP PERFORMED IN SOUTH WEST REGION
CHOROPLETH MAP SHOWING HOW LP PERFORMED IN SOUTH WEST REGION
CHOROPLETH MAP SHOWING HOW NNPP PERFORMED IN SOUTH WEST REGION
Vote Count Range

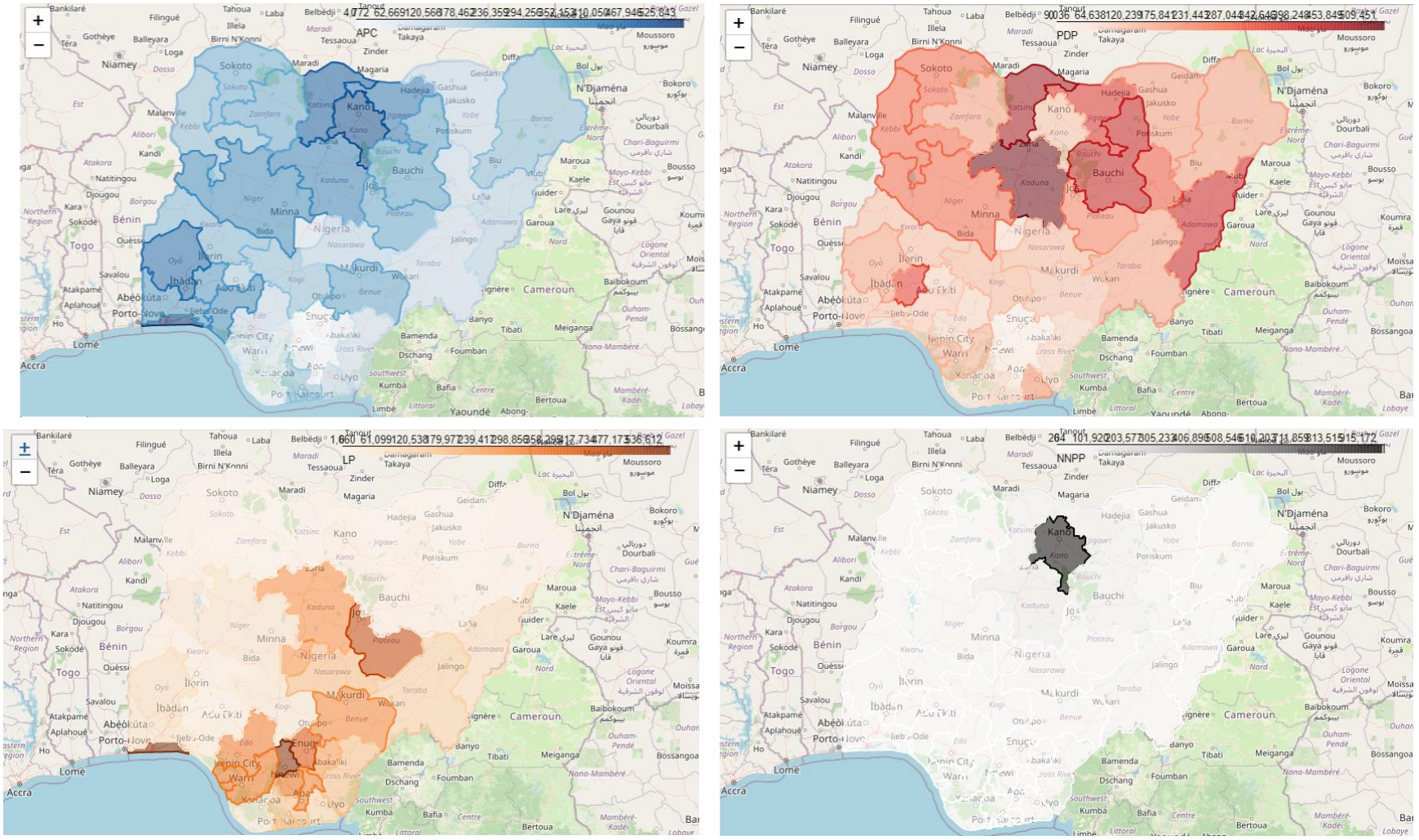

Figure 5: Locator map showing how the parties performed in the election.

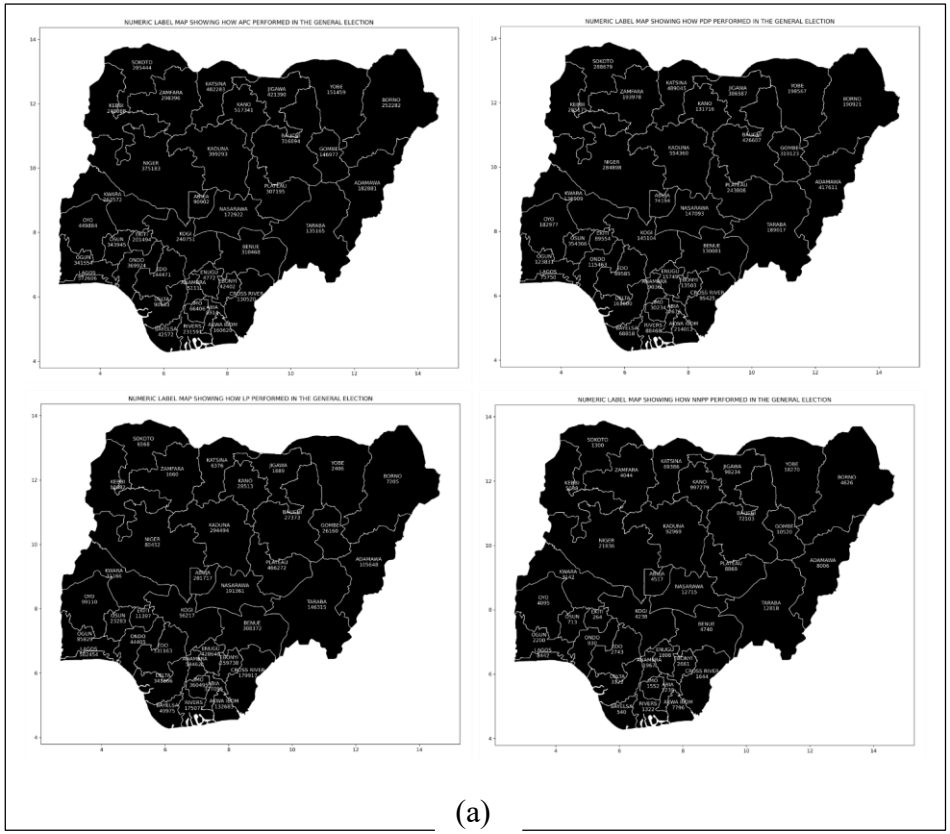

(a)

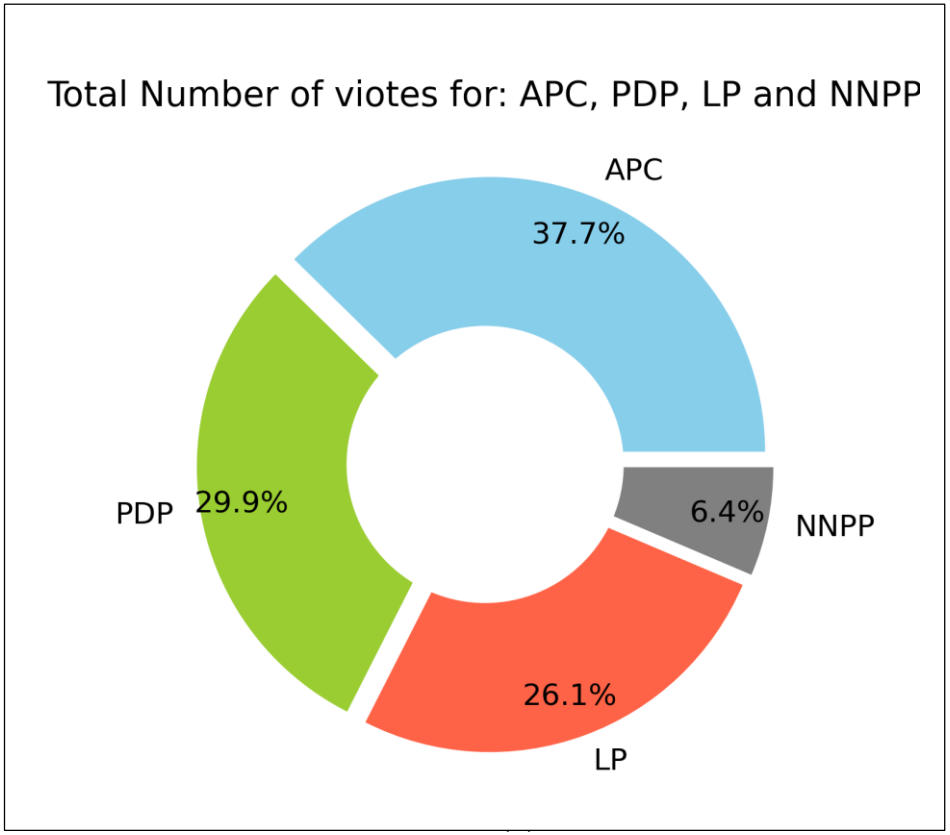

Figure 6: (a) Numeric labeled map showing how the four major political parties performed in the general election. (b) Donut chart showing total number of votes for each party.

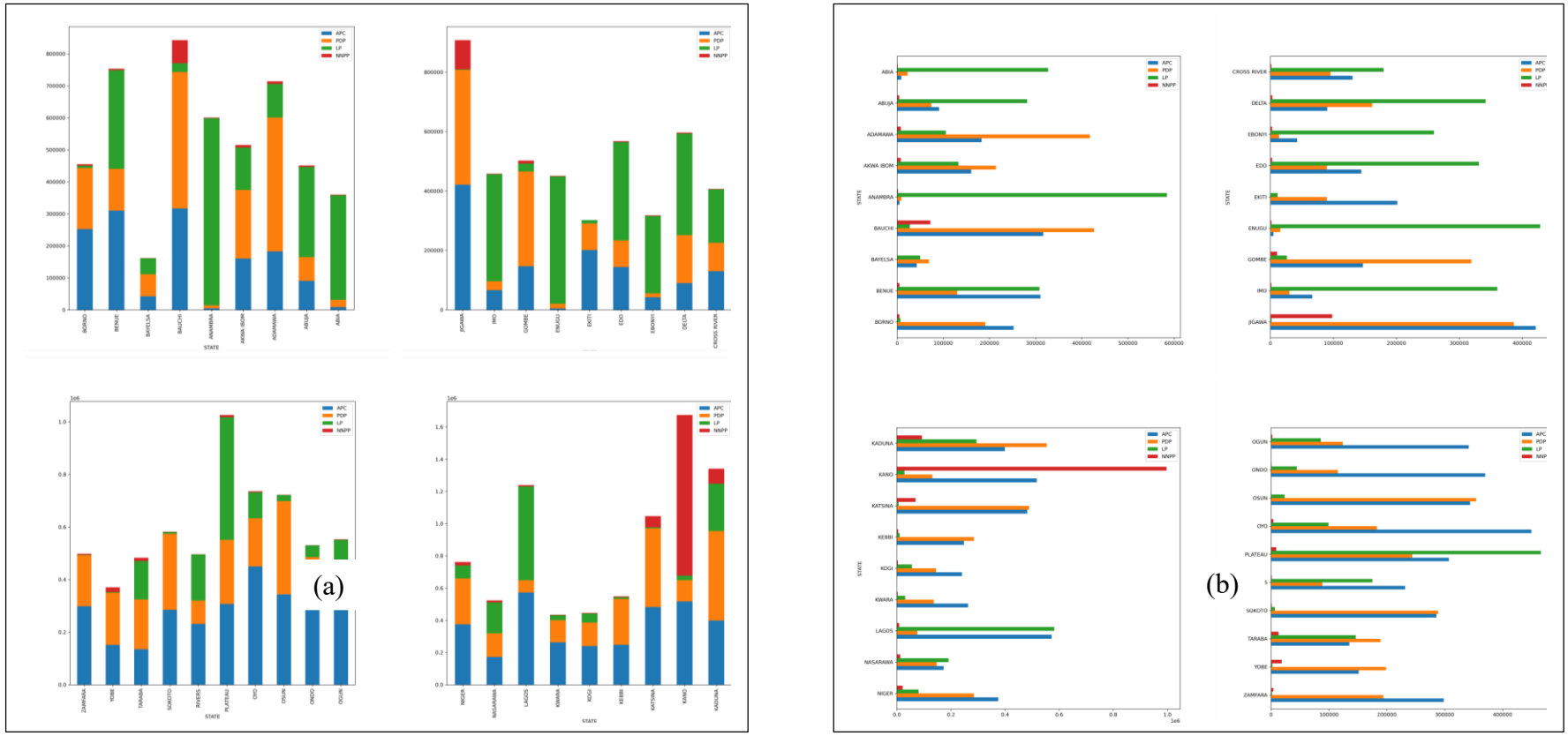

Figure 7: (a) Stacked bar charts and (b) Horizontal bar chart showing election results by state.

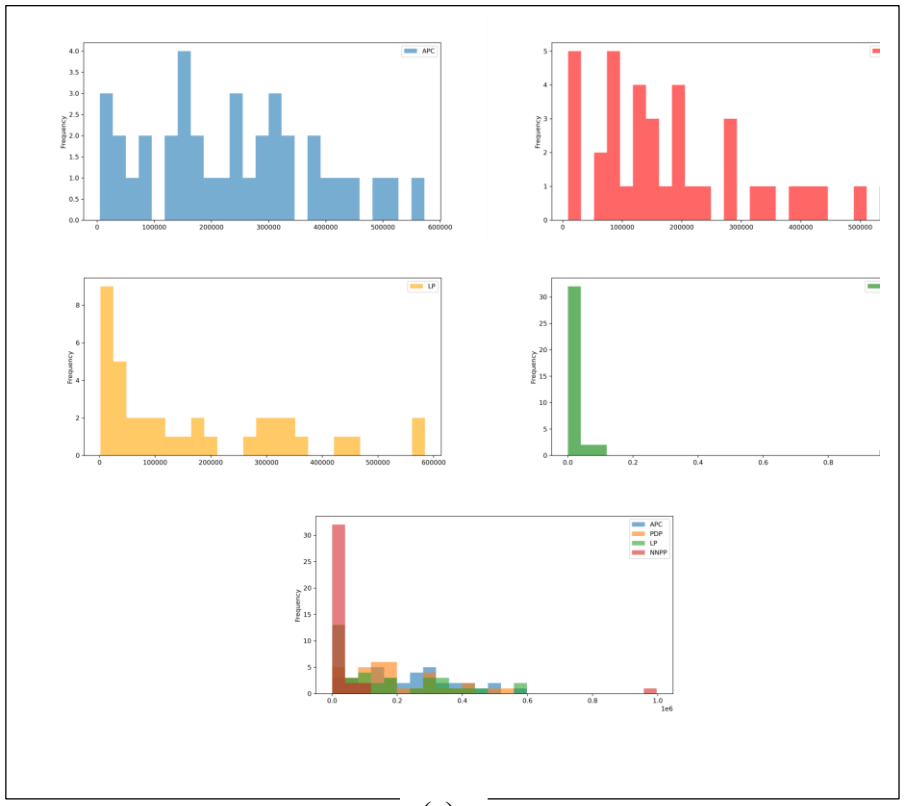

(a)

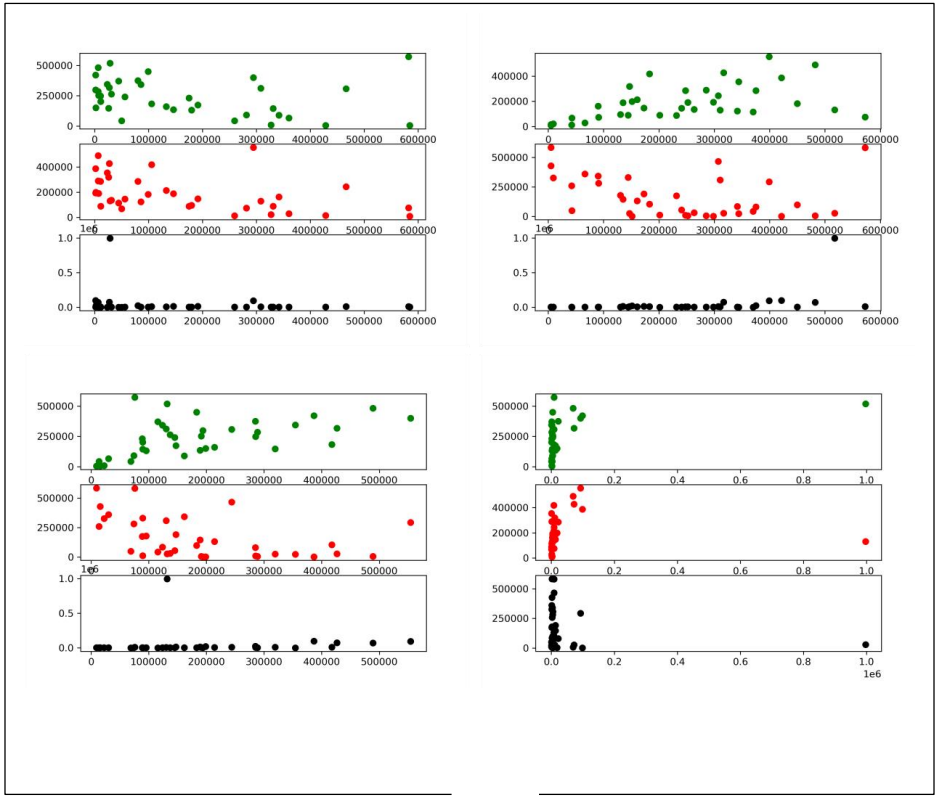

(b)

Figure 8: (a) Histogram charts and (b) Scatter plots

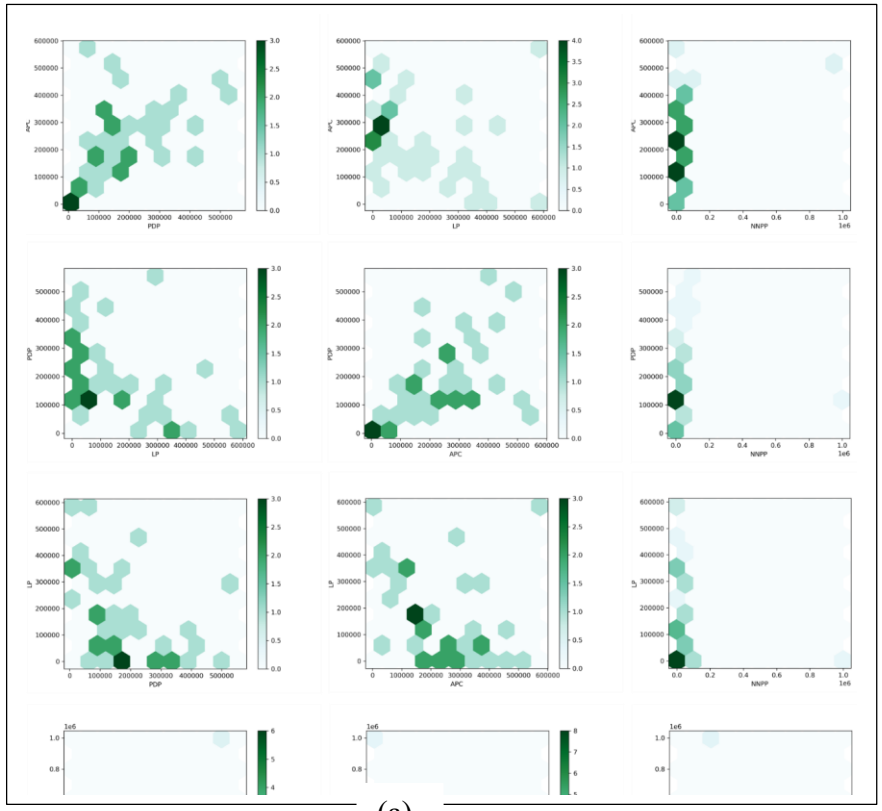

(a)

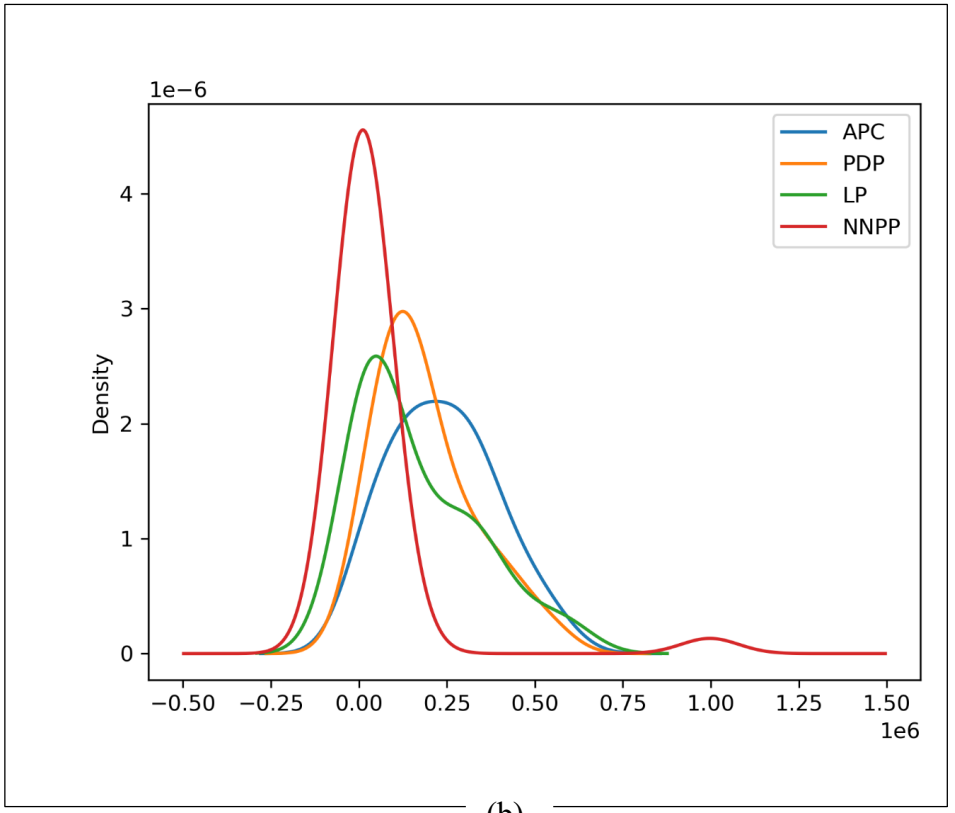

(b)

Figure 9: (a) Hexagon chart (b) Kernel Density Estimate (KDE) plot

4.0 RESULTS AND DISCUSSION

The results of this research are various visualizations of the 2023 presidential election result including choropleth maps in both color and gray (figure 4a and 4b), Numeric labeled map (figure 5a).

The colors of the choropleth maps are defined as follow: Blues for APC, Reds for PDP, Oranges for LP and Greens for NNPP.

```
#STEP 1: Import Libraries...
import pandas as pd
import geopandas as gpd
import matplotlib.pyplot as plt
from mpl_toolkits.axes_grid1 import make_axes_locatable



#STEP 2: Reading/Load Dataset
# Read Geospatial (GeoJSON) file and CSV files...
nig_states = gpd.read_file('NGA_adm1.geojson')
election_result = pd.read_csv('Presidential Election Results By States.csv')



#STEP 3: Clean & Transform Dataset
# Let do some data cleaning and merge the Geospatial to the CSV table...
# Note there should be a common column name on the two dataset, in this case state column
# Check column names...
print(nig_states.columns)
print(election_result.columns)
```

```
# Rename state column name to match on both datasets...
nig_states.rename(columns={'state_name':'STATE'}, inplace=True)

# Capitalize the state column on 'nig_states'...
nig_states['STATE'] = nig_states['STATE'].apply(lambda x: x.upper())

# Do more cleaning on the merged geodadaframe...
#1) Make sure numeric columns (such as party vote counts) are not read as string/object

# Check column types before conversion...
print('Before converting \n\n',merge_gdf.dtypes)

# Convert the columns... Alternatively, we could use the argument "thousands=',"' when reading the CSV file...
merge_gdf['APC'] = merge_gdf['APC'].str.replace(',', '').astype('int64')
merge_gdf['PDP'] = merge_gdf['PDP'].str.replace(',', '').astype('int64')
merge_gdf['LP'] = merge_gdf['LP'].str.replace(',', '').astype('int64')
merge_gdf['NNPP'] = merge_gdf['NNPP'].str.replace(',', '').astype('int64')

# Check column types after conversion...
print('\nAfter converting\n', merge_gdf.dtypes)



#STEP 4: Explore & Merge Dataset
# Do the merging...
```

```
merge_gdf = pd.merge(nig_states, election_result, how='inner', on='STATE')

merge_gdf.head()









#STEP 5: Plot Map/Chart


# Choropleth maps...

# Define the color map and column variables....

party_cmap =   'Greens' # 'Blues', 'Reds', 'Oranges'

party_column = 'NNPP'   # 'APC',   'PDP',  'LP'


# First create subplot and add the map layers on it

fig, ax = plt.subplots(1, figsize=(13, 13))

divider = make_axes_locatable(ax)

cax = divider.append_axes("bottom", size="2%", pad="5%")


# Add label to polygons...

merge_gdf.apply(lambda x: ax.annotate(text=x['STATE'], xy=x.geometry.centroid.coords[0], ha='center', color='gray'), axis=1)

# Set title for map

# fig.suptitle('CHOROPLETH MAP SHOWING HOW LP PERFORMED IN THE GENERAL ELECTION')

ax.set_title(f"CHOROPLETH MAP SHOWING HOW {party_column} PERFORMED IN THE GENERAL ELECTION")

# Plot the map...
```

```
merge_gdf.plot(ax=ax, cax=cax, cmap=party_cmap, column=party_column, edgecolor='gray', legend=True, legend_kwds={"label": "Vote Count Range", "orientation":"horizontal"})


# Save map to file...
fig.savefig(f'{party_column}.png', dpi=300)


# ----------------------
# Numeric Label maps...
# Define the color map and column variables....
party_color =   'Black'
party_column = 'PDP'   # 'APC',   'PDP',  'LP'


# First create subplot and add the map layers on it
fig, ax = plt.subplots(1, figsize=(15, 15))


# Add label to polygons...
merge_gdf.apply(lambda x: ax.annotate(text=x['STATE']+ "\n" + str(x[party_column]) ,
                            xy=x.geometry.centroid.coords[0],
                            ha='center', color='white'), axis=1)
# Set title for map
# fig.suptitle('CHOROPLETH MAP SHOWING HOW LP PERFORMED IN THE GENERAL ELECTION')
ax.set_title(f"NUMERIC LABEL MAP SHOWING HOW {party_column} PERFORMED IN THE GENERAL ELECTION")
# Plot the map...
merge_gdf.plot(ax=ax, color=party_color, edgecolor='white')
plt.grid()
# Save map to file...
```

```
# fig.savefig(f'{party_column}.png', dpi=300)


# ---------------------

# Interactive Locator map...

merge_gdf.explore('NNPP', cmap='Greens', height=550, width=850)


# ---------------------


# ---------------------

# Read in the 'Presidential Election Results' CSV table...

election_result = pd.read_csv('Presidential Election Results By States.csv', thousands=',', usecols = ['STATE', 'APC', 'PDP', 'LP', 'NNPP'])

election_result.sort_values('STATE', inplace=True, ascending=False)


# ---------------------


# Election Donut Chart

party_num_votes = [sum(election_result.APC), sum(election_result.PDP), sum(election_result.LP), sum(election_result.NNPP)]

parties = ['APC', 'PDP', 'LP', 'NNPP']

custom_colors = ["skyblue", "yellowgreen", 'tomato', 'gray']

# explosion

explode = (0.05, 0.05, 0.05, 0.05)



plt.figure(figsize=(5, 5))
```

```
plt.pie(party_num_votes, labels=parties, colors=custom_colors, autopct='%1.1f%%', pctdistance=0.85, explode=explode)

central_circle = plt.Circle((0, 0), 0.5, color='white')

fig = plt.gcf()

fig.gca().add_artist(central_circle)

plt.rc('font', size=12)

plt.title("Total Number of viotes for: APC, PDP, LP and NNPP", fontsize=14)

plt.show()


# Save map to file...

fig.savefig(f'DonutCahrt.png', dpi=300)

# ----------------------


# Horizontal Bar plot...

election_result[28:38].plot(x="STATE", kind='barh', figsize=(10,10)) # :12, 12:24, 24:

# Save map to file...

plt.savefig(f'set4.png', dpi=300)

# ----------------------


# Stacked Bar plot...

election_result[28:38].plot(x="STATE", kind='bar', stacked=True, figsize=(10,10)) # :10, 10:19, 19:28, 28:38

# Save map to file...

plt.savefig(f'stk4.png', dpi=300)


# ----------------------

# Histogram chart... Get an overview of your party’s vote distribution with a histogram
```

```
# election_result[['PDP']].plot(kind='hist', bins=25, alpha=0.6, color='red', figsize=(10,5)) # 'APC', 'PDP', 'LP', 'NNPP'


election_result[['APC', 'PDP', 'LP', 'NNPP']].plot(kind='hist', bins=25, alpha=0.6, figsize=(10,5)) #


# Save map to file...
plt.savefig(f'hist.png', dpi=300)



# ----------


plt.subplot(3, 1, 1)
plt.scatter(x=election_result['NNPP'], y=election_result['APC'], c='green')

plt.subplot(3, 1, 2)
plt.scatter(x=election_result['NNPP'], y=election_result['PDP'], c='red')

plt.subplot(3, 1, 3)
plt.scatter(x=election_result['NNPP'], y=election_result['LP'], c='black')


# Save map to file...
plt.savefig(f'nnpp_scatter.png', dpi=300)


# ----------
# Hexagon bin plot - data represented in the form of a honeycomb (alternative to scatter plot)
```

```
election_result.plot(kind='hexbin', x="APC", y="NNPP", gridsize=10)
# election_result.plot(kind='hexbin', x="APC", y="LP", gridsize=10)


# Save map to file...
plt.savefig(f'nnpp-hexagon1.png', dpi=300)
# ---------------------
# Kernel Density Estimate (KDE)
election_result.plot(kind='kde', bw_method=0.5)
# Save map to file...
plt.savefig(f'kde.png', dpi=300)
# ---------------------
```

Figure 10: Python code for this study (online version is at: https://tinyurl.com/nasgalpaper)

5.0 CONCLUSION

In conclusion, geospatial data visualization is an essential tool for effectively communicating insights and trends from election results. Python offers a wide range of libraries and tools for creating high-quality geospatial visualizations, from basic static charts to dynamic interactive dashboards that can be powered on the web, mobile and desktop platforms. In this paper, we have discussed, the different types of visualizations, and the techniques for creating effective election data visualizations. Although python geopandas is good geospatial analysis tool, future work may explore other geospatial visualization libraries as that will reinforce the accuracy of our work. This paper serves as a crucial resource that showcases transparency and effective governance to both the general public and decision makers. It allows them to swiftly understand and analyze election outcomes through visual representation. Moreover, it opens up opportunities for further research in the same or related areas. Researchers can explore alternative tools beyond Python-based libraries for visualizing and analyzing datasets, contributing to a broader spectrum of approaches in this field.

REFERENCES

[1] Gajalakshmi, K., & Thottolil, M. R., (2021). Dynamic Mapping of Covid-Outbreak in Karnataka Region Using Python-GIS. *International Journal of Current Engineering and Scientific*

Research (IJCESR). ISSN (PRINT): 2393-8374, (ONLINE): 2394-0697, VOLUME-8, ISSUE-3, 2021.

[2] Hadi, M. A., Fard, F. H., & Vrbik, I. (2020, August). Geo-Spatial Data Visualization and Critical Metrics Predictions for Canadian Elections. In 2020 IEEE Canadian Conference on Electrical and Computer Engineering (CCECE) (pp. 1-7). IEEE.

[3] Hamid, A. M., Sameer, M. K., & Mageed, N. N. (2020, March). Geo-database production of digital land use map using remote sensing and GIS techniques. In *AIP Conference Proceedings* (Vol. 2213, No. 1, p. 020024). AIP Publishing LLC.

[4] Hoffmann, L. K., & Patel, R. N. (2022). Vote-selling behaviour and democratic dissatisfaction in Nigeria.

[5] Jordahl, K. (2016). Geopandas documentation. URL: http://sethc23. github. io/wiki/Python/geopandas. pdf-Download vom, 26, 2022.

[6] Lavanya, A., Sindhuja, S., Gaurav, L., & Ali, W. (2023). A Comprehensive Review of Data Visualization Tools: Features, Strengths, and Weaknesses.

[7] Lemenkova, P. (2020). Python libraries matplotlib, seaborn and pandas for visualization geo-spatial datasets generated by QGIS. *Analele stiintifice ale Universitatii" Alexandru Ioan Cuza" din Iasi-seria Geografie*, 64(1), 13-32.

[8] Li, F., & Wang, L. (2022). Research on Data Visualization Technology Based on Python. *International Journal of Multidisciplinary Research and Analysis*, 5(5), 907-910.

[9] Moruzzi, G., & Moruzzi, G. (2020). Plotting with matplotlib. Essential Python for the Physicist, 53-69.

[10] Nkwunonwo, U. C., & Okeke, F. I. (2013). GIS-based production of digital soil map for Nigeria. *Ethiopian Journal of Environmental Studies and Management*, 6(5), 498-506.

[11] Odion, D., Shoji, K., Evangelista, R., Gajardo, J., Motmans, T., Defraeye, T., & Onwude, D. (2023). A GIS-based interactive map enabling data-driven decision-making in Nigeria's food supply chain. MethodsX, 10, 102047.

[12] Olabanjo, O., Wusu, A., Asokere, M., Padonu, R., Olabanjo, O., Ojo, O., ... & Aribisala, B. (2022). From Twitter to Aso-Rock: A Natural Language Processing Spotlight for Understanding Nigeria 2023 Presidential Election.

[13] Stojanović, M., Drobnjak, S., Jovanović, J. M., Galjak, N., & Vučićević, A. (2020). Analysis of Cartographic Generalization based on PYTHON Programming Language on Digital Topographic Maps. In GISTAM 2020-*Proceedings of the 6th International Conference on Geographical Information Systems* (pp. 191-198). SciTePress.

FAIR ELECTION: A REVIEW OF GEOSPATIAL TECHNIQUES AND FORENSIC GIS IN MONITORING ELECTION PROCESS IN NIGERIA

Morgan V. U, Francisca O. O, Johnson N. G, & Godwin S.

*Department of Geography, Faculty of Social Sciences, Federal University, Lokoja, Nigeria

Correspondence E-mail: morgan.victor@fulokoja.edu.ng

Abstract:

Election crimes are a major challenge facing Nigeria's democracy, with incidents of ballot box snatching, voter intimidation, and other forms of electoral malpractice occurring regularly. Investigating and prosecuting these crimes can be a daunting task, especially when they have a geographic component. However, geospatial technologies, specifically Forensic GIS, can play a critical role in providing evidence for prosecution. Additionally, applying the principles of FAIR data science can ensure that the evidence presented in court is reliable, trustworthy, and transparent. This study examines previous literature on the role of geospatial technologies and FAIR data science in investigating and prosecuting election crimes in Nigeria and its application. It also highlights the benefits of geospatial technologies in identifying and mapping the location of incidents, tracking the movement of suspects, and providing evidence for prosecution. Additionally, it discusses how applying the principles of FAIR data science can improve data quality, management, and sharing, leading to more reliable and transparent evidence in court. The study concludes by highlighting the need for capacity building and training for investigators and policymakers to maximize the benefits of these technologies and principles in the fight against election crimes in Nigeria and establish future research and practice as well as the need to enhance forensic GIS and FAIR data science use in the electioneering process.

Keywords: Election, Forensic GIS, Geospatial Techniques

1.0 INTRODUCTION

Election crimes present a significant threat to the integrity of Nigeria's democratic processes. Instances of ballot box snatching, voter intimidation, and other forms of electoral malpractice undermine the credibility and fairness of elections. Investigating and prosecuting these crimes is essential for maintaining a robust and transparent electoral system. However, the complex nature of election crimes, particularly those with a geographic component, poses numerous challenges for law enforcement agencies and the justice system.

Geospatial technologies, including Forensic Geographic Information Systems (GIS), offer promising solutions for addressing these challenges. By integrating geospatial data, such as maps, satellite imagery, and spatial analysis techniques, investigators can effectively identify and map the location of election-related incidents, track the movement of suspects, and gather crucial evidence for prosecution. Furthermore, the application of FAIR (Findable, Accessible,

Interoperable, and Reusable) data science principles ensures that the collected evidence is reliable, trustworthy, and transparent.

2.0 LITERATURE REVIEW

A comprehensive review of the existing literature reveals the growing recognition of the role that geospatial technologies and FAIR data science play in investigating and prosecuting election crimes. In a study by [3], the authors investigated the use of Geospatial Technology for Managing Elections in Nigeria. The study demonstrated that GIS can provide critical information for the management and monitoring of elections, including identifying and mapping the location of polling units, tracking the movement of electoral materials, and providing real-time information on election incidents.

Additionally, researchers have emphasized the importance of FAIR data science principles in ensuring the quality, management, and sharing of data used in criminal investigations.

Prof. Mark D. Wilkinson: Wilkinson is a bioinformatician and one of the co-authors of the original FAIR data principles. While his work primarily focuses on biological and life sciences, the FAIR principles he helped develop are widely applicable, including in criminal investigations.

Dr. Carole Goble: Goble is a Professor of Computer Science at the University of Manchester and has extensively worked on data management and FAIR principles. She emphasizes the importance of applying these principles to criminal investigations, ensuring that data collected and used in such cases can be easily discovered, accessed, and reused by others.

Prof. Paul Taylor: Taylor is a forensic statistician who has highlighted the importance of FAIR data principles in forensic science. His research focuses on developing statistical models and tools to support decision-making in criminal investigations, and he emphasizes the need for data quality and transparency.

These researchers, among others, have emphasized the significance of applying FAIR data science principles to ensure the quality, management, and sharing of data in criminal investigations, enabling transparency, reproducibility, and collaboration among investigators and stakeholders.

In the specific context of Nigeria, limited research has been conducted on the application of geospatial technologies and FAIR data science in combating election crimes. This study aims to fill this gap by examining the existing literature, assessing its relevance to Nigeria's election crime landscape, and identifying potential opportunities for implementing these technologies and principles.

3.0 METHODOLOGY

3.1 Geospatial Technologies in Investigating and Prosecuting Election Crimes

3.1.1 Identifying and mapping incidents

Geospatial technologies provide investigators with tools to identify and map the location of election-related incidents accurately. By integrating geospatial data and geocoding techniques, incidents such as ballot box snatching or voter intimidation can be precisely located on a map. This spatial visualization enhances situational awareness and enables targeted law enforcement responses.

3.1.2 Tracking suspect movement

Geospatial technologies facilitate the tracking of suspects involved in election crimes. Through the analysis of spatial trajectories, investigators can identify patterns, identify key individuals, and track their movements before, during, and after criminal activities. This information can serve as crucial evidence in establishing the involvement and culpability of suspects.

3.1.3 Remote sensing and evidence collection

Remote sensing technologies, such as satellite imagery, can provide valuable evidence for prosecuting election crimes. High-resolution satellite imagery can be employed to capture images of crime scenes, monitor electoral processes, and detect anomalies. These images can support the identification of irregularities, the assessment of the integrity of electoral procedures, and the validation of witness testimonies.

3.1.4 Integration with investigative workflows

Geospatial technologies should be integrated seamlessly into existing investigative workflows to maximize their effectiveness. Collaboration between law enforcement agencies, forensic experts, and GIS specialists is crucial to ensure the efficient use of geospatial tools and data. By aligning workflows and sharing information, investigators can generate comprehensive and persuasive evidence for successful prosecution.

3.2 FAIR Data Science Principles in Election Crime Investigations

.2.1 Introduction to FAIR data science principles

FAIR data science principles emphasize the importance of data being Findable, Accessible, Interoperable, and Reusable. By implementing these principles, investigators can enhance the quality, management, and sharing of data throughout the investigation process.

3.2.2 Improving data quality and management

FAIR data science principles promote standardized metadata and documentation, ensuring that data used in election crime investigations are well-described and have sufficient contextual

information. This facilitates data discovery, reduces ambiguity, and enhances the reliability of the evidence presented in court.

3.2.3 Enhancing data sharing and collaboration

Effective collaboration and data sharing among investigators, law enforcement agencies, and relevant stakeholders are crucial in combating election crimes. FAIR data science principles promote data sharing protocols, interoperability standards, and data governance frameworks. This enables the exchange of information, fosters transparency, and facilitates cross-agency collaboration.

3.2.4 Ensuring transparency and reproducibility

FAIR data science principles encourage transparency and reproducibility in data analysis. By utilizing open-source tools, documenting data processing steps, and ensuring proper version control, investigators can provide transparent and auditable evidence in court. This promotes trust in the investigative process and enhances the credibility of the evidence presented.

4.0 RESULT AND DISCUSSION

4.1 Benefit and Challenges

The application of geospatial technologies and FAIR data science in investigating and prosecuting election crimes offers several significant benefits. These include improved accuracy in identifying incident locations, enhanced investigative efficiency through suspect tracking, reliable evidence generation using remote sensing data, and increased transparency and trustworthiness through FAIR data science principles. However, several challenges must be addressed to maximize the potential of these technologies and principles. These challenges include the availability and accessibility of high-quality geospatial data, the need for technical expertise among investigators and policymakers, the establishment of data sharing mechanisms, and addressing privacy and ethical considerations associated with geospatial technologies.

4.2 Capacity Building and Training

To harness the full potential of geospatial technologies and FAIR data science in combating election crimes, capacity building and training initiatives are crucial. Investigators and policymakers should receive training on the acquisition, analysis, and interpretation of geospatial data, as well as the implementation of FAIR data science principles. Collaborations between academia, government agencies, and non-governmental organizations can facilitate the development of comprehensive training programs tailored to Nigeria's election crime context.

5.0 CONCLUSION AND RECOMMENDATION

This study has examined the role of geospatial technologies and FAIR data science in investigating and prosecuting election crimes in Nigeria. The findings highlight the potential benefits of utilizing geospatial technologies, such as Forensic GIS, in identifying incident locations, tracking suspect

movement, and collecting reliable evidence for prosecution. Additionally, the application of FAIR data science principles ensures data quality, management, and sharing, leading to more transparent and trustworthy evidence in court.

To fully leverage these technologies and principles, capacity building and training initiatives are necessary for investigators and policymakers. Training programs should focus on acquiring technical skills and knowledge required for effectively utilizing geospatial technologies and implementing FAIR data science principles in the election crime investigation process. Moreover, future research and practice should explore the integration of emerging technologies, such as artificial intelligence and machine learning, to further enhance the efficiency and effectiveness of geospatial technologies in combating election crimes. Collaborations among academia, government agencies, and non-governmental organizations are essential for developing best practices, guidelines, and policy frameworks that support the use of geospatial technologies and FAIR data science in election crime investigations.

By embracing geospatial technologies and FAIR data science, Nigeria can strengthen its ability to combat election crimes, protect its democratic processes, and ensure transparent and credible elections in the future.

This study highlights the importance of continued research and practice in the application of geospatial technologies and FAIR data science in Nigeria's fight against election crimes. Future research should focus on exploring novel approaches, such as the integration of artificial intelligence and machine learning techniques, to enhance the effectiveness and efficiency of these technologies. Additionally, establishing collaborations between academia, government agencies, and non-governmental organizations can facilitate the development of best practices, guidelines, and policy frameworks for the use of geospatial technologies and FAIR data science in election crime investigations.

Reference:

[1] ACLEDDATA. (2023, February 22). Political Violence and the 2023 Nigerian Election. ACLED. Retrieved from https://acleddata.com/2023/02/22/political-violence-and-the-2023-nigerian-election/.

[2] Adeshina, T. (2007, Summer). Nigerian Voting Systems. ESRI ArcNews. Retrieved from https://www.esri.com/news/arcnews/summer07articles/nigerian-voting.html

[3] Omoleke & Maduekwe. (2017). The Use of Geospatial Technology for Managing Elections in Nigeria: Issues and Challenges. International Journal of Innovation and Research in Educational Sciences, 4(4). ISSN (Online): 2349–5219.

[4] Wilkinson, M. D., et al. (2016). The FAIR Guiding Principles for scientific data management and stewardship. Sci. Data, 3, 160018. doi: 10.1038/sdata.2016.18

[5] Goble, C., Cohen-Boulakia, S., Soiland-Reyes, S., Garijo, D., Gil, Y., Crusoe, M. R., Peters, K., & Schober, D. (2020). FAIR computational workflows. Data Intelligence, 2, 108–121. doi: 10.1162/dint_a_00033

[6] Francisca O. O. (2022, November 16). "If you wish to go FAR, go FAIRy: Reconnoitering an Emerging Computing Paradigm." Inaugural Lecture, Federal University Lokoja, Kogi State.

SUB THEME 02

GEOSPATIAL Information for Ensuring Government Accountability

INTEGRATION OF GEOSPATIAL TECHNIQUES AND ARTIFICIAL INTELLIGENCE IN MAPPING MULTIDIMENSIONAL POVERTY IN AFRICA: A REVIEW

Ifechukwu Ugochukwu Nzelibe

Department of Surveying and Geoinformatics, Federal University of Technology, Akure, Ondo State, Nigeria.

Email: nzelibeifechukwu@gmail.com

Abstract

Multidimensional Poverty (MP) considers poverty in multiple dimensions of depravations such as health, education, energy, the standard of living and access to basic services. MP remains a major challenge in Africa, with a large proportion of the population living in MP. According to United Nations Development Programme (UNDP), Africa has shown the highest Multidimensional Poverty Index (MPI) having over 40% of its population living in MP. This paper is a review, aimed at assessing the potential of the integration of geospatial techniques and Artificial Intelligence (AI) in mapping MP, with a specific focus on Africa. Based on the reviews of past studies, the combination of satellite data such as nighttime light, daytime satellite imagery and high-resolution settlement data in combination with techniques such as Field surveys, Statistical correlation models (Transfer learning) and AI (deep learning) has been applied in mapping MP. The findings from studies show that the combination of geospatial and AI has the capability of providing more accurate and granular MP maps, compared to the traditional approach. Again, this paper explains the concept of MP with a specific focus on Africa and presents a map depicting the current MPI in African countries. Finally, pitfalls exist especially in the accuracy, granularity and frequency of MP data. Consequently, the geospatial and AI approaches are recommended for more accurate, frequent, cost-effective and granular data, required for mapping poverty and design of interventions that effectively address the needs of the most vulnerable populations in Africa.

Keywords: Africa; Artificial Intelligence (AI); Geospatial; Mapping; Multidimensional Poverty Index (MPI)

1.0 INTRODUCTION

Among the 17 Sustainable Development Goals (SDGs) officially launched in 2015, poverty eradication topped the list. Included in the Global Indicator Framework for monitoring progress on poverty reduction is the proportion of a country's population living below its national poverty line, which is typically sourced from household income and expenditure surveys. From the perspective of statisticians and other compilers of official poverty statistics, the SDGs' leave no one behind principle which requires data to be disaggregated by geographic location, ethnicity, gender, income class, and other relevant dimensions, presents several challenges. Conventionally, household income and expenditure surveys have sample sizes that are sufficient to provide

nationally representative poverty estimates, but not large enough to provide reliable estimates at levels granular enough to meet all disaggregated data requirements of SDG 1. Moreover, the sample sizes are inadequate in providing reliable estimates at levels granular enough to allow development planners efficiently target areas that need immediate poverty intervention [38].

The integration of geospatial techniques and artificial intelligence (AI) in mapping multidimensional poverty has the potential to provide more accurate and refined understandings of poverty, and to inform the development of effective poverty reduction strategies [64]. Geospatial approach in mapping multidimensional poverty involves the use of spatial data and mapping techniques to identify and visualize the spatial distribution of poverty across different dimensions. This approach combines geospatial data, such as satellite imagery and Geographical Information Systems (GIS), with multidimensional poverty measures to produce poverty maps that provide a more accurate and nuanced understanding of poverty. Artificial intelligence (AI) can be applied in mapping multidimensional poverty to improve the accuracy and efficiency of poverty measurement and analysis [37]. AI techniques such as machine learning, computer vision, and natural language processing is now being applied in analysing large amounts of data and to identify patterns and trends in multidimensional poverty.

Several of milestones have been achieved through the integration of satellite data and artificial intelligence in mapping poverty which could facilitate in understanding and addressing poverty. Mobile phone and geospatial data have been combined in the past to provide insight into the spatial distribution of poverty measurements [64], allowing for more frequent and granular datasets. Also, open-source satellite imagery features and machine learning has been incorporated to improve poverty mapping accuracy, making it more practical for most applications [37]. Convolutional Neural Networks has been applied on high-resolution satellite images of cities in Mozambique and combined their outputs with household level geo-referenced survey data to generate detailed neighbourhood-level poverty maps, providing key operational guidance for implementation of the urban social safety net [63]. Supplementing survey data with satellite data has proven an improved poverty estimate [45].

Satellite imagery can be used to identify features such as housing, infrastructure, and vegetation, which can be used as indicators of poverty. Machine learning algorithms can then be trained to analyse these features and to identify areas that are most likely to be affected by poverty [42]. Social media and survey data can provide valuable insights into the experiences of people living in poverty. Natural language processing techniques is applied to analyse these data sources and to identify indicators of poverty and the live experiences of those affected by poverty. GIS can be used to combine and visualize multiple data sources, such as satellite imagery, census data, and survey data, to create a more comprehensive understanding of poverty across different dimensions. Machine learning algorithms can be applied to develop predictive models that can forecast changes in poverty over time [45]. The study of [42]. demonstrated an accurate, inexpensive, and scalable method for estimating consumption expenditure and asset wealth from

high-resolution satellite imagery using a convolutional neural network, which could transform efforts to track and target poverty in developing countries.

Accuracy is germane in mapping multi-dimensional poverty, considering the limitations in the accuracy of satellite-based poverty maps. The accuracy of satellite-based poverty maps is limited by factors such as the quality of the satellite imagery and the availability of ground truth data [16]. An interpretable computational framework to accurately predict poverty has been demonstrated at a local level by applying object detectors to high-resolution satellite images [16]. An accuracy of 0.539 Pearson's R^2 was achieved in predicting village-level poverty in Uganda, which indicated a 31% improvement over existing benchmarks. Again, a global poverty map at 30 arcsec resolution using a poverty index calculated by dividing population count by the brightness of satellite observed lighting was produced [23].

Satellite-based poverty maps can be a useful tool for estimating poverty, especially in areas where traditional census data is unavailable or out-of-date. For instance, [41]. proposed a new methodology combining grid-cell selection and ensemble to improve poverty prediction. [23]. produced a global poverty map using a poverty index calculated from satellite observed lighting and population count, calibrated using national level poverty data. Furthermore, studies in metropolitan areas of North and South America have showcased the feasibility of estimating household income and socio-economic conditions, by applications of computer vision to satellite imagery [59]. It is clear that satellite-based poverty maps are of great benefit in complementing traditional poverty maps, especially in areas where census data is limited.

Even though the satellite and machine learning approach are of great benefit, there are limitations to its use. Considering the findings of [37], although incorporating open-source satellite data improved poverty mapping, proprietary imagery can be costly and infrequently acquired. Again, in the study involving the convolutional neural networks on high-resolution satellite images to generate neighbourhood-level poverty maps in Mozambique [63], an interpretable computational framework to predict poverty at a local level using object detectors on high-resolution satellite images, achieving improved accuracy and interpretability in poverty mapping in Uganda [6]. A lack of detailed data on poverty was observed to be common in many developing countries especially in Africa. Satellite data alone may not be sufficient for poverty mapping, as such incorporating survey-derived variables may improve model performance [37]. While satellite data can be a useful tool for poverty mapping, studies have suggested that it should be used in conjunction with other data sources, considering its limitations.

1.1 Theoretical Background

This paper focuses on review of the milestones achieved in integrating geospatial techniques and artificial intelligence in mapping multidimensional poverty in Africa for the purpose of proffering possible solutions in the challenges of lack of detailed data on poverty common to developing countries. This review will address the key concept of multidimensional poverty and world Bank measures of MP, poverty in Africa, Trends in the applications of satellite data and artificial

intelligence in mapping multidimensional poverty. Finally potential areas relevant for future research in the aspect of multidimensional poverty would be identified.

1.1.1 Poverty measures and concepts of multidimensional poverty

There are several measures and approaches used to measure poverty. Here are some commonly used poverty measures these include: Income Poverty; Multidimensional Poverty [4]; Human Development Index (HDI), proposed by the United Nations Development Programme (UNDP) [59]; Capability Approach, Proposed by Amartya Sen [26]; Subjective Poverty [3]; Absolute and Relative Poverty [25]. These measures vary in their focus, scope, and methodology, and are often used in combination to provide a more comprehensive understanding of poverty. Each measure has its strengths and limitations, and the choice of measure depends on the specific context and objectives of the analysis.

Multidimensional poverty is a concept that considers poverty not only in terms of income or consumption but also in terms of multiple dimensions of deprivation, such as health, education, and living standards [76]. It recognizes that poverty is not only about a lack of income or material resources but also about the inability to access basic services and opportunities that are necessary for a decent standard of living. The multidimensional poverty approach uses a set of indicators that capture different dimensions of poverty, such as health, education, housing, sanitation, and access to basic services. These indicators are combined to create a multidimensional poverty index (MPI) that measures the extent of poverty in a given population [74]. The MPI provides a more comprehensive and nuanced understanding of poverty than income-based measures alone. It enables policymakers to identify the specific dimensions of poverty that need to be addressed and to design targeted interventions that address the root causes of poverty[76]. The concept of multidimensional poverty has gained increasing recognition in recent years, with a growing number of countries adopting MPIs to measure and address poverty. The United Nations Development Programme (UNDP) and the Oxford Poverty and Human Development Initiative (OPHI) are among the organizations that have played a leading role in developing and promoting the use of MPIs [70] .

1.1.2 Multidimensional poverty measure (MPM)

The Multidimensional Poverty Measure (MPM) introduced by the World Bank has gained popularity as an indicator that gauges the proportion of households facing deprivation across three dimensions of well-being: monetary poverty, education, and basic infrastructure services. Its aim is to present a more comprehensive understanding of poverty. Although poverty is commonly associated with a lack of financial resources, focusing solely on income poverty fails to encompass a broader range of well-being indicators. In fact, the World Bank's Poverty and Shared Prosperity report [76] demonstrates that nearly 39 percent of individuals experiencing multidimensional poverty are not identified as poor based on income poverty alone.

Alkire and Foster proposed a comprehensive approach to measuring multidimensional poverty that goes beyond solely relying on income or consumption-based measures. Their methodology combines multiple indicators or dimensions of poverty, such as education, health, living standards, and social participation, into a single poverty index [4]. Since its introduction, the Alkire-Foster method has gained widespread recognition and has been applied in various studies and reports to provide a more nuanced understanding of poverty beyond income measures alone [2]; [8]. It has been used to measure multidimensional poverty at the national, regional, and global levels, contributing to policy discussions and interventions aimed at reducing poverty and improving well-being.

The World Bank developed its Multidimensional Poverty Measure (MPM) in 2018, drawing inspiration from other well-known multidimensional measures such as the Multidimensional Poverty Index (MPI) created by the UNDP and Oxford University. Unlike the MPI, the MPM includes the dimension of monetary poverty, which is measured as household income or consumption per capita falling below $2.15 per day based on the International Poverty Line established in 2017 [44]. By incorporating both monetary and non-monetary deprivations, the MPM highlights to policymakers the significance of addressing various aspects of human welfare beyond income poverty alone. It recognizes that households in rural areas of Sub-Saharan Africa, for instance, may have sufficient income to surpass monetary poverty but still lack access to vital services like healthcare, education, or reliable electricity. Conversely, households that are income poor but have access to basic services may experience better well-being than those deprived in non-monetary dimensions such as healthcare or education. The interaction and overlap of multiple dimensions can intensify poverty and inequality, perpetuating cycles of deprivation.

The Multidimensional Poverty Measure (MPM) encompasses three dimensions of well-being: monetary standard of living, education, and basic infrastructure services. Within these dimensions, six standardized indicators are considered: consumption- or income-based poverty, educational enrolment, educational attainment, access to drinking water, sanitation, and electricity. Each indicator is assigned a value of 0 or 1, with 1 indicating deprivation. To create a single index, the MPM combines the number of deprivations, requiring a decision on the weighting of each indicator. The World Bank's MPM assigns equal weight to dimensions and indicators within each dimension. Individuals are classified as multidimensionally deprived if they are lacking in at least one dimension or a combination of indicators that equals or exceeds one-third of the weight of a full dimension. Since the monetary dimension has only one indicator and there are three equally weighted dimensions, being income poor also indicates poverty in the broader multidimensional context. Selecting the dimensions, indicators, and thresholds for deprivation parameters is crucial. For instance, the educational enrolment indicator considers a child up to grade 8 who is not enrolled in school as deprived. Detailed indicators, weights, and thresholds for the MPM are presented in Table 1. While Table 2 presents the share of population deprived in each indicator, derived from 121 countries, around the world.

Table 1: Multidimensional Poverty Measure Indicators, Weights, and Thresholds [75]

Dimension	**Parameter**	**Weight**
Monetary	Daily consumption or income is less than US$ 2.15 per person.	1/3
Education	At least one school-age child up to the age of grade 8 is not enrolled in school.	1/6
	No adult in the household (age of grade 9 or above) has completed primary education.	1/6
Access to basic infrastructure	The household lacks access to limited-standard drinking water.	1/9
	The household lacks access to limited-standard sanitation.	1/9
	The household has no access to electricity.	1/9

Table 2: Share of population deprived in each indicator, around the world [75]

Region	Monetary (%)	Educational attainment (%)	Educational enrolment (%)	Electricity (%)	Sanitation (%)	Drinking water (%)	Multidimensional poverty, headcount ratio (%)
East Asia & Pacific	3.2	7.6	2.4	2.4	15.3	7.5	4.8
Europe & Central Asia	0.3	0.9	1.6	1.7	7.1	4.5	2.1
Latin America & Caribbean	3.8	9.4	1.6	1.0	16.6	3.0	4.6
Middle East & North Africa	1.2	8.2	2.6	0.3	2.7	1.1	1.8
South Asia	8.1	20.5	19.2	14.6	35.6	5.2	17.3
Sub-Saharan Africa	32.5	35.9	19.5	48.0	65.6	30.5	51.9
Rest of the World	0.7	0.9	0.3	0.0	0.2	0.2	1.4
All regions	8.8	12.7	8.9	12.1	23.1	10.5	14.5

3.0 METHODOLOGY

3.1 Satellite Data and Artificial Intelligence in Mapping Multidimensional Poverty

Poverty statistics are typically compiled based on data collected from household surveys. However, sample sizes of these surveys are typically not large enough to provide reliable estimates at more granular levels, and therefore resulting poverty estimates may not be reliable at very granular disaggregation levels. Increasing sample sizes is a way to enhance reliability of survey estimates, but it is often not practical as achieving such increases requires significant additional resources, which are not readily available to NSOs or the organizations that conduct these surveys [5]. An alternative method is the use small area estimation (SAE) techniques, in collaboration with development partners like the World Bank, by combining survey results with census and other auxiliary data to produce more granular data.

On the other hand, there have been attempts to integrate beyond traditional types of data such as those coming from surveys and censuses. A good example is the use of satellite imagery for various development indicators, and there are several reasons why its popularity is increasing. For one, advances in satellite-based socioeconomic measurements have led to an influx of high frequency data for both, data-rich and data-poor environments. One of these measurements is night-time light intensity which has been increasingly used following the initial works of [15] and [34]. This helped mitigate some of the known data shortcomings, including those of the SAE, if enhancing granularity is the main objective. Night-time light intensity can also be used to estimate values in between surveys and enable nowcasting as well as help illuminate areas that are less covered by surveys and censuses.

However, using data on nightlights alone have several drawbacks. The data produced by satellites are top-coded which makes highly developed, urbanized areas hard to differentiate. On the other side of the spectrum, the least developed areas often do not have measurable night-time lights, and this makes it difficult to obtain estimates for proxy measures of socioeconomic development in such areas. Building on these developments, the use of daytime satellite images has started to become an important focus of research. [77] showed that poverty mapping using satellite imagery in combination with transfer learning and convolutional neural networks (CNN) can lead to the predictive performance of survey data collected in the field. [42] trained a CNN to extract features in high-resolution daytime images using night time images as labels. The extracted features were used to predict asset wealth and consumption expenditure across five African countries.([42] were able to provide that such a model is strongly predictive of both average household consumption expenditure and asset wealth as measured at the cluster level for countries where recent survey data is available.

On the other hand, [33] has proven that this method does not generalize in the same way that other measures of development predict access to drinking water and a variety of health and education-related indicators. It is possible to apply this method in other countries and continents given certain limitations. The study presented in this manuscript serves as a proof of concept in

implementing the techniques used by [42] using only publicly available satellite data that have lower resolution and are readily available tools for data processing, akin to the objective of [79] which used the same kind of satellite imagery to examine spatial distribution of economic well-being in Africa.

There are many sources of nightlight intensity data. However, the best known and publicly published are datasets based on Defence Meteorological Satellite Program Operational Line-Scan System (DMSPOLS) and Suomi National Polar-Orbiting Partnership Visible Infrared Imaging Radiometer Suite (SNPPVIIRS) missions. Both were conducted by the National Oceanic and Atmospheric Administration (NOAA). It was decided that images from VIIRS will be used for this study because it offered a substantial number of improvements over Operational Line-Scan System as stated in the work of [22]. A cloud-free average radiance value was used to filter out the effects of fires and other transitory events as well as irrelevant background, while unlit areas were set to zero.

When combined with machine learning, high-resolution satellite imagery has proven broadly useful for a range of sustainability-related tasks, from poverty prediction; [16] to infrastructure measurement [13] to forest and water quality monitoring [24] to the mapping of informal settlements [53]. Compared to coarser (10-30m) publicly-available imagery [19], high-resolution (< 1m) imagery has proven particularly useful for these tasks because it is often able to resolve specific objects or features that are undetectable in coarser imagery. When combined with machine learning, recent work demonstrated an approach for predicting local-level consumption expenditure using object detection on high-resolution daytime satellite imagery [7]. showing how this approach can yield interpretable predictions and also outperform previous benchmarks that rely on lower-resolution, publicly-available satellite imagery [19].

3.2 Geospatial Data in Mapping Poverty

Since 1999 and 2013 respectively, Landsat 7 and 8 satellite series cover the entire Earth surface with a temporal resolution of 16 days and a spatial resolution of 15 to 30 meters depending on the spectral bands (8 for Landsat 7 and 11 for Landsat 8). Since 2014, Sentinel satellite series generate images with a spatial resolution of 10 meters. It is then possible to get remote-sensing data with a high time-frequency and a good spatial resolution [41]. Researchers are turning to volunteer-curated geographic information and open geospatial datasets to study socioeconomic development, social inequalities, and territorial conflicts [28]. One of the more popular geospatial data crowdsourcing platforms is OpenStreetMap (OSM), a global geospatial database containing billions of entries of volunteered geographic information, maintained by a massive community of mappers from around the world all working towards the goal of curating accurate and complete geospatial data. The community of OSM contributors typically consists of individual mappers, university researchers, volunteer communities, and non-profit organizations. Such organizations regularly organize field mapping activities, workshops, and events that promote geospatial data mapping and contribution.

The combined use of coarse and fine spatial resolution remote sensing data is utilized to gain a deeper understanding of human living conditions [50]. Coarse resolution satellite imagery, which is readily accessible, frequently updated, and often free, offers a broad overview for large-scale decision-making [50]. On the other hand, fine spatial resolution remote sensing data, although less common and more costly due to commercialization, play a crucial role in accurately identifying poverty [20]. Despite their scarcity and expense, high spatial resolution data remain a more cost-effective alternative compared to traditional surveying methods [85].

Remote sensing imagery classification, a popular technique in land use/land cover studies, has been integrated with local expert knowledge and ontology to enhance the accuracy of poverty identification using remote sensing images [46]. Adjusting thresholds for different study areas is often necessary to ensure meaningful results [46], and post-processing is required due to misclassifications [50]. Additional data layers from Geographic Information Systems (GIS) have been found to improve the performance of remote sensing-based poverty classification by incorporating local knowledge and supplementary information [48].

For informal settlements, characterized by lower socioeconomic status, poor living conditions, and unfavourable environments, the integration of remote sensing and GIS techniques has proven advantageous in identifying and understanding such communities [48]. The vegetation, impervious surface, bare soil method has been successfully applied to classify detailed urban land use using very high-resolution remote sensing data, both in developed and developing countries [35]. Combining GIS and remote sensing techniques can enhance the temporal and spatial resolution of poverty identification. For instance, the integration of remote sensing data with mobile operator Call Detail Records (CDRs) has shown potential in representing human living conditions, especially in urban areas [64]. Furthermore, the affordability of GIS and remote sensing-based informal settlement identification makes them invaluable tools in developing nations [48].

The Earth Observation (EO) satellite missions focusing on land have measured physical properties of the land surface as well as the use of the land in different forms. This includes generic land cover and land use, [30] or more thematic maps such as forest cover maps [32], surface water [57], and human settlements and their dynamics [55]. Nightlights recorded by satellites can now be used to complement the information provided by global built-up areas and population density used to address societal activities [21]. In recent times, common geospatial data applied in mapping poverty include: Nighttime Luminosity Data, Daytime Satellite Imagery and High-Resolution Settlement [21].

3.3 Poverty Identification with Machine Learning

With significant advancements in computer hardware and ongoing research, machine learning, including deep learning techniques like ImageNet, has emerged as a frontier in computer science [60]. Deep learning enables the extraction of meaningful features from remote sensing data through automatic learning and classification [42]. Numerous studies have successfully applied

deep learning methods to classify remote sensing images for poverty identification [85]. For instance, ImageNet has been used to predict poverty based on nighttime light intensity, leveraging the learned knowledge [56]. Nighttime light, which correlates with manufacturing, population, and socioeconomic patterns, has emerged as a valuable remote sensing data source for measuring human activities [14]. NTL data is commonly used to represent socioeconomic status [52], and its correlation with poverty has led to its adoption in poverty research in developing countries [23].

Transfer learning, which allows the transfer of knowledge learned by convolutional neural networks (CNN) to related problems, proves useful when limited labeled data is available [46]. Random Forest Regression (RFR), a popular machine learning method for handling multiple data sources, has been utilized in various applications [1]. For example, a study combined different data sources and employed RFR to develop a machine learning model for estimating regional poverty levels based on NTL data [85]. The integration of machine learning, remote sensing, and Geographic Information Systems (GIS) has demonstrated promising potential, surpassing traditional field surveys and standalone remote sensing classification methods in several research endeavours [49].

Table 3 is a summary of techniques adopted in mapping poverty including the advantages and challenges encountered in their applications as derived from [51].

Table 3: Summary of techniques for mapping poverty [51]

Techniques	**Advantage**	**Limitation and Challenge**
Field surveys and investigations; Evaluation of culture and history	Both methodologies and results are easy to understand	Require knowledgeful investigators; high financial cost; labour-intensive and low scalability
Statistical correlation models; Transfer learning	Models are easy to use and replicable; low financial cost	Too many algorithms; results are not reliable
Machine learning imagery classification; Time-series deep learning	Emerging technology and promising results; low financial cost	Require high quality labels and advancing algorithms; lack of research

4.0 Result and Discussion

4.1 Mapping Multidimensional Poverty in Africa

Multidimensional poverty remains a major challenge in Africa, with a large proportion of the population living in poverty across multiple dimensions such as health, education, living standards, and access to basic services. According to the United Nations Development Programme's (UNDP) Multidimensional Poverty Index (MPI), which measures poverty across

multiple dimensions, Africa has the highest level of multidimensional poverty in the world. In 2021, the MPI estimated that over 480 million people in Africa (around 40% of the population) live in MP. The drivers of multidimensional poverty in Africa are complex and multifaceted, with factors such as conflict, climate change, inequality, and weak governance contributing to the persistence of poverty in many countries. The COVID-19 pandemic has also had a significant impact on poverty in Africa, exacerbating existing vulnerabilities and pushing more people into poverty. Consequently, the need for mapping poverty still remains an issue. While most of the studies focused on African continent is still highly dependent on traditional approach, a number of studies have been seen to have adopted the geospatial and AI methodologies.

Several studies have been conducted involving the application of Geospatial and AI technologies in MP mapping in Africa. The challenges of designing poverty alleviation programs with tightening budgets was addressed by [11]. Geographical information systems (GIS) were highlighted for detailed poverty mapping, MP identification, and optimizing service delivery to the poor. Household survey data combined with environmental variables from satellite imagery was used to create poverty maps in Uganda, which reveals that combining household survey data with satellite imagery improves poverty predictions, highlighting the influence of environmental factors [8] applies the Alkire and Foster multidimensional poverty measures to estimate poverty among women in 14 Sub-Saharan African countries, revealing significant differences across dimensions. Including additional dimensions alters country rankings, with rural areas experiencing higher poverty rates and lack of schooling being a key contributor. [54] carried out a systematic review to examine the use of geoinformation analyses in studying malnutrition in Sub-Saharan Africa. The review suggests incorporating crowd-sourced geodata collection and spatial health data infrastructures to deepen understanding of this complex issue. Remote sensing and household surveys was applied to link agro-ecological factors with poverty patterns in Burkina Faso, revealing strong spatial dependency and validating the approach [40]. Geospatial visualizations of poverty deprivation were created as a contextual baseline for future evaluation by [72]. The MPI of water poverty is applied to show the impact of water scarcity on African populations [43]. The findings reveal disparities in water poverty between developed but water-scarce countries and lower-income water-rich countries.

This study demonstrates the use of multidimensional poverty measures and geospatial maps to evaluate public health interventions, highlighting the prevalence and determinants of poverty in Mozambique. Geospatial analysis of Nigeria's MP, focusing on Jigawa State reveals a dynamic poverty pattern and highlight the role of physical and natural resources in contributing to the state's high poverty rate [27], [10] examines poverty levels and trends in Malawi, Mozambique, Tanzania, and Zimbabwe using various poverty measures. The findings emphasize the importance of considering both breadth and inequality components in multidimensional poverty analysis. [2], examines multidimensional poverty in three drought-prone agro-ecological settings in Ethiopia. The Alkire-Foster method and Correlation Sensitive Poverty Index (CSPI) are used to analyse poverty. The study emphasizes the need for contextualized indicators and location-specific

approaches in poverty research and policy design. Based on the study of [42], involving the application of the transfer learning approach within 5 African countries, Malawi, Tanzania, Nigeria, Uganda, and Rwanda the out-of-sample R2 accuracies obtained are 0.55, 0.57, 0.68, 0.69 and 0.75 respectively. [17], proposes a reinforcement learning approach that combines low-resolution imagery with high-resolution imagery to predict poverty in Uganda, achieving improved performance with fewer high-resolution images. However, a call for validation of the outputs over the African continent still remains a bone of contention. Using remotely sensed data to illustrate the nature of poverty in Africa based on the night light emission as a poverty indicator, Figure 1 shows the Niger River Delta between Lagos (Nigeria) in the West and Doula (Cameroon) in the East. Highlighting the statement of [21] based on this figure "Both major cities exhibit the expected features of large well-lit metropolitan areas. The secondary cities and rural areas are represented by yellow reddish colours representing diffuse settlement infrastructure with little or no public illumination.

There is however a number of blue dots, which map the oil extraction sites in the delta. They can be seen as an allegory of inequality. The oil revenues generated by the oil extraction a largely disconnected from the local population. From the current global MP database [76], the information for Africa were extracted and presented on Table 4 and mapped in Figure 2. The database has revealed that MP data in Africa are limited and outdated. For instance, from the global MP database, the 2019 data is the latest data in Africa, which is found in only 3 countries in Africa (Malawi, Uganda and Zimbabwe). While Congo in Central Africa has its latest MP data in 2011. Also, some countries in Africa such as Tanzania, Eritrea, Central African Republic, Western Sahara, Algeria and Libya were completely missing on the global MP databased.

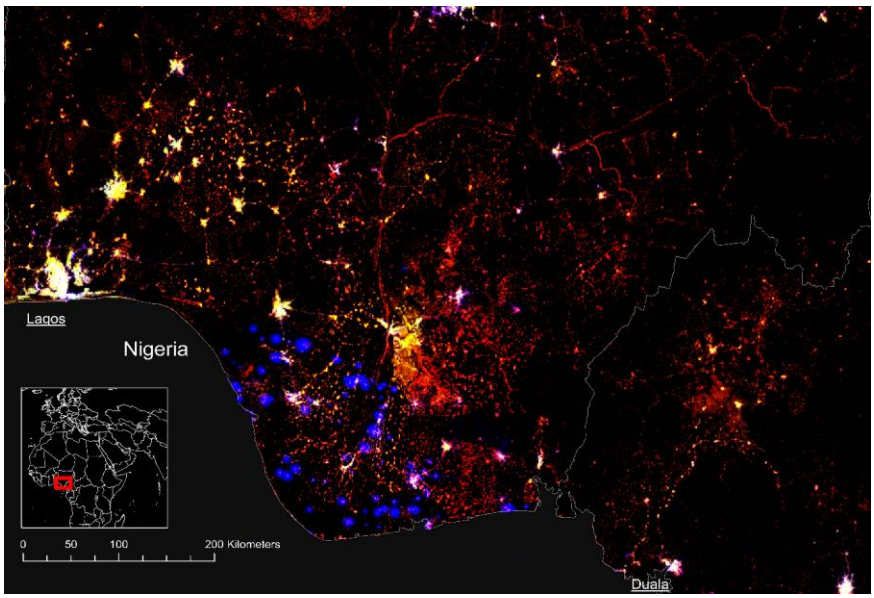

Figure 1: Typical example of night time light illustrating the well-lit oil extraction sites in the midst of highly populated settlements deprived of nightlights [21]

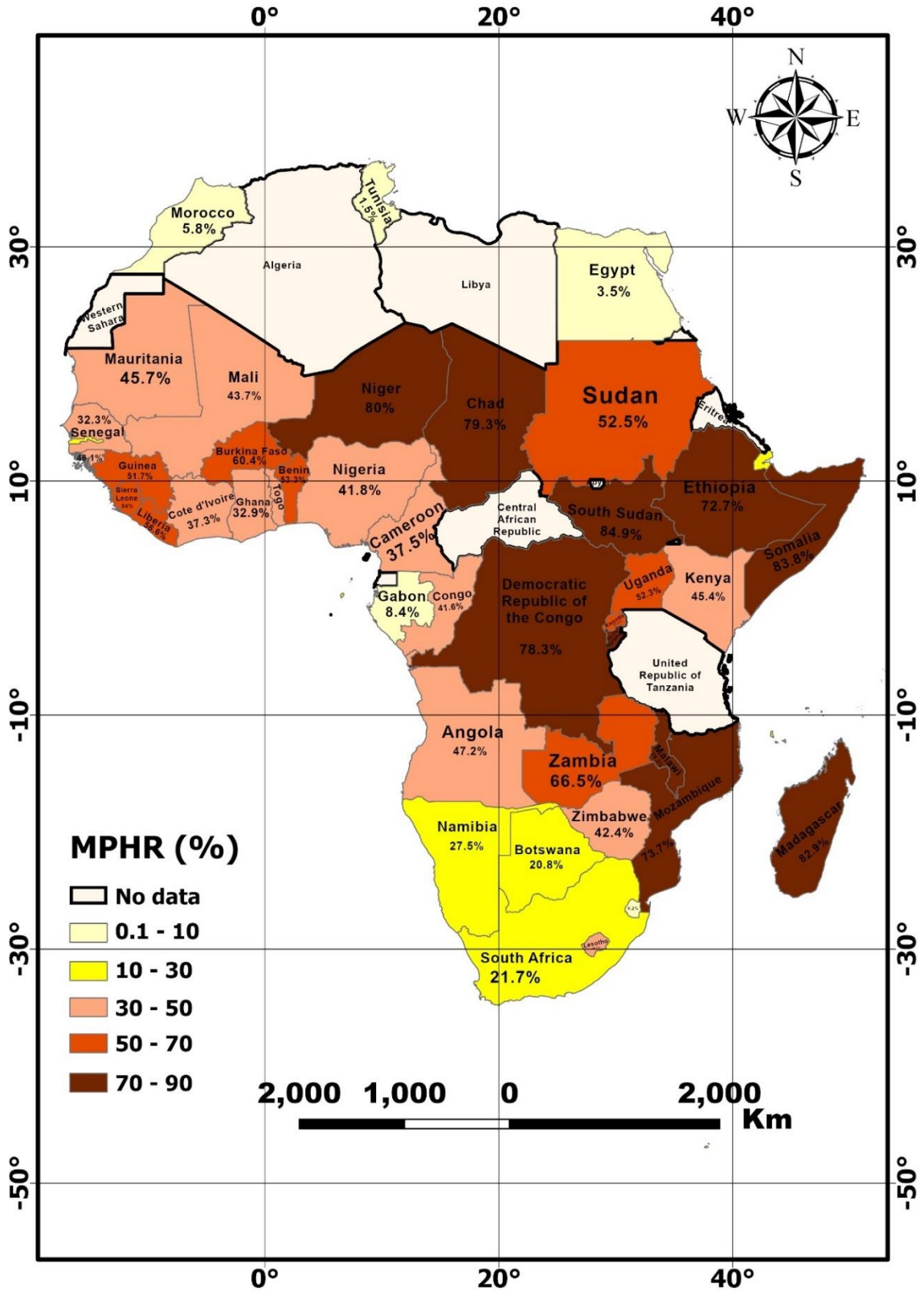

Figure 2: Multidimensional poverty headcount ratio in Africa [76]

Table 4: Individuals in households deprived in each indicator, African, (for 2009 and later; with 2017 ICP) [76]

		Deprivation rate (share of population)						
Country NAME	Survey Year	Monetary (%)	Educational attainment (%)	Educational enrollment (%)	Electricity (%)	Sanitation (%)	Drinking water (%)	Multidimensional poverty headcount ratio (%)
Angola	2018	31.1	29.8	27.4	52.6	53.6	32.1	47.2
Benin	2018	19.9	50.2	31.5	54.3	80.0	22.1	53.3
Botswana	2015	15.0	8.2	4.2	35.5	52.0	3.7	20.8
Burkina Faso	2018	30.5	56.4	50.9	47.2	69.6	19.7	60.4
Burundi	2013	65.1	66.3	18.9	91.8	94.3	20.6	85.2
Cape Verde	2015	4.6	11.7	2.7	9.9	30.2	11.1	7.6
Cameroon	2014	25.7	24.4	15.9	1.2	38.9	23.2	37.5
Chad	2018	30.9	69.0	34.9	90.0	87.0	34.8	79.3
Comoros	2014	18.6	15.3	7.3	28.5	67.2	6.4	26.3
DR Congo	2012	69.7	22.5	8.0	83.0	80.0	47.9	78.3
Congo	2011	35.4	13.4	2.3	29.9	47.3	23.4	41.6
Cote d'Ivoire	2018	11.4	48.6	30.4	18.1	64.4	20.7	37.3
Djibouti	2017	19.1	30.1	18.0	34.2	45.4	7.1	29.3
Egypt	2017	2.5	10.6	4.2	0.5	3.2	0.8	3.5
Ethiopia	2015	27.0	66.7	31.2	64.1	95.9	42.7	72.7
Gabon	2017	2.5	11.3	7.9	8.6	68.2	11.5	8.4
Gambia	2015	13.4	29.9	6.1	8.0	58.2	8.2	18.3
Ghana	2016	25.3	15.1	9.0	19.5	79.9	40.8	32.9
Guinea	2018	13.8	61.3	25.0	56.4	71.1	21.0	51.7
Guinea-Bissau	2018	21.7	41.0	30.1	42.1	63.0	21.6	46.1
Kenya	2015	29.4	22.5	6.1	56.9	69.0	32.2	45.4
Lesotho	2017	32.4	18.1	4.8	58.7	55.1	13.7	40.7
Liberia	2016	27.6	30.5	54.1	79.7	61.8	25.7	56.6
Madagascar	2012	80.7	49.0	34.7	13.0	76.9	59.9	82.9
Malawi	2019	70.1	54.3	3.7	88.8	75.1	11.4	78.3
Mali	2018	14.8	66.6	28.2	23.9	51.9	23.8	43.7
Mauritania	2014	6.5	54.3	8.3	54.1	49.3	38.6	45.7
Mauritius	2017	0.1	7.2	0.2	0.2	-	-	0.4
Morocco	2013	1.4	12.7	6.8	2.4	12.9	8.7	5.8
Mozambique	2014	64.6	54.9	33.3	14.6	71.3	41.1	73.7
Namibia	2015	15.6	11.3	6.1	53.8	68.3	9.2	27.5
Niger	2018	50.6	79.7	28.0	78.7	85.2	37.5	80.0
Nigeria	2018	30.9	17.6	20.3	39.4	44.9	27.5	41.8
Rwanda	2016	52.0	36.9	4.3	64.0	28.1	24.5	57.4
Sao Tome and Principe	2017	15.6	19.5	4.3	31.2	62.0	8.2	24.9
Senegal	2018	9.3	42.0	31.9	26.6	37.4	15.2	32.3
Seychelles	2018	0.5	0.4	-	0.0	0.2	5.5	0.9
Sierra Leone	2018	26.0	28.7	18.7	68.7	87.2	33.8	54.0
Somalia	2017	70.7	59.2	56.3	50.6	39.4	11.8	83.8
South Africa	2014	20.5	2.3	2.3	4.1	35.2	10.4	21.7
South Sudan	2016	67.3	39.3	62.2	-	88.1	13.9	84.9
Sudan	2014	15.3	40.2	22.7	48.5	92.9	44.9	52.5
Swaziland	2018	0.2	0.0	-	0.0	0.1	0.1	0.2
Togo	2018	28.1	32.7	14.0	47.4	83.7	25.3	46.4
Tunisia	2015	0.1	20.2	2.1	0.2	6.5	2.1	1.5
Uganda	2019	42.2	31.4	11.8	41.3	71.1	23.7	52.3
Zambia	2015	61.4	24.4	30.4	69.2	60.0	34.4	66.5
Zimbabwe	2019	39.8	0.9	6.0	38.0	38.3	19.3	42.4

4.2 Potential Pitfalls in Mapping Multidimensional Poverty in Africa

The gaps identified from review of studies in mapping multidimensional poverty using geospatial techniques and artificial intelligence (AI) in Africa, including:

i. Lack of high-quality, spatially disaggregated data: Mapping multidimensional poverty using geospatial techniques and AI requires high-quality data that are spatially disaggregated. However, in many African countries, data are often limited, outdated, or not disaggregated at the local level, making it challenging to accurately map poverty across different dimensions.

ii. Limited understanding of the social and cultural context: Poverty is not only an economic phenomenon, but also a social and cultural one. To accurately map multidimensional poverty, it is important to understand the social and cultural context in which poverty occurs. However, there is limited research on how social and cultural factors influence poverty in different regions of Africa.

iii. Ethical and legal considerations: The use of geospatial techniques and AI raises ethical and legal concerns related to privacy, data ownership, and informed consent. More research is needed to understand how to ensure that the use of these techniques is ethical, transparent, and inclusive.

iv. Limited focus on vulnerable populations: Mapping multidimensional poverty using geospatial techniques and AI should prioritize the needs of vulnerable populations such as women, children, and ethnic minorities. However, there is limited research on how to effectively capture the experiences of these populations and to design interventions that are inclusive and equitable.

v. Limited consideration of the intersectionality of poverty: Poverty is not experienced in isolation, but rather intersects with other social identities and experiences such as gender, race, and disability. Mapping multidimensional poverty using geospatial techniques and AI should consider the intersectionality of poverty, but there is limited research on how to effectively do so.

5.0 CONCLUSION AND RECOMMENDATION

Geospatial mapping of poverty can be used to identify areas and populations that are most affected by poverty, and to target resources and interventions where they are most needed. Poverty maps can be used to identify areas with high levels of multidimensional poverty and to prioritize the allocation of resources and development projects to these areas. Geospatial mapping can also be used to identify the spatial patterns of poverty, such as the spatial concentration of poverty in certain regions, urban-rural disparities in poverty, and the links between poverty and environmental factors such as land use and climate change. Furthermore,

geospatial mapping can provide a valuable tool for monitoring and evaluating poverty reduction programs and policies. By tracking changes in poverty over time, geospatial mapping can help to assess the impact of poverty reduction programs and to identify areas where further interventions may be needed. Application of satellite data can provide a cost-effective and automatic way to estimate and monitor poverty rates at high spatial resolution, especially in countries with limited capacity to support traditional methods of data collection.

Application of AI in mapping MP can be seen is in the analysis of satellite imagery. Satellite imagery can be used to identify features such as housing, infrastructure, and vegetation, which can be used as indicators of poverty. Machine learning algorithms can be trained to analyse these features and to identify areas that are most likely to be affected by poverty. Natural language processing techniques can also be used to analyse text data, such as survey responses or social media posts, to identify indicators of poverty and to better understand the lived experiences of those affected by poverty. By analysing these data sources, AI can provide a more refined understanding of poverty and its drivers. Another application of AI in mapping MP is in the development of predictive models that can forecast changes in poverty over time. By analysing historical data and identifying patterns and trends, these models can provide insights into the future trajectory of poverty and can inform the development of poverty reduction strategies.

The integration of geospatial techniques and AI in mapping MP in Africa has the potential to provide more accurate and timely information for policymakers and development practitioners, and to inform the development of effective poverty reduction strategies. However, it is important to ensure that these techniques are developed and used in an ethical and transparent manner, and that they do not perpetuate or exacerbate existing inequalities. There is also need for more research that addresses gaps in mapping MP using geospatial techniques and AI in Africa, in order to provide more accurate and detailed understandings of poverty and to design interventions that effectively address the needs of the most vulnerable populations.

References

[1] Abdel-Rahman, E. M., Ahmed, F. B., & Ismail, R. (2013). Random forest regression and spectral band selection for estimating sugarcane leaf nitrogen concentration using EO-1 Hyperion hyperspectral data. *International Journal of Remote Sensing*, *34*(2), 712–728. https://doi.org/10.1080/01431161.2012.713142

[2] Abeje, M. T., Tsunekawa, A., Haregeweyn, N., Ayalew, Z., Nigussie, Z., Berihun, D., Adgo, E., & Elias, A. (2020). Multidimensional Poverty and Inequality: Insights from the Upper Blue Nile Basin, Ethiopia. *Social Indicators Research*, *149*(2), 585–611. https://doi.org/10.1007/s11205-019-02257-y

[3] Achdut, N., Refaeli, T., & Schwartz Tayri, T. M. (2021). Subjective Poverty, Material Deprivation Indices and Psychological Distress Among Young Adults: The Mediating Role of Social

Capital and Usage of Online Social Networks. *Social Indicators Research*, *158*(3), 863–887. https://doi.org/10.1007/s11205-021-02729-0

[4] Alkire, S., & Foster, J. E. (2011). Counting and Multidimensional Poverty Measurement. *Journal of Public Economics*, *95*(7–8).

[5] Asian Development Bank (ADB). (2020). *Mapping Poverty through Data Integration and Artificial Intelligence:* https://doi.org/10.22617/FLS200215-3

[6] Ayush, K., Uzkent, B., Burke, M., Lobell, D., & Ermon, S. (2020). Generating interpretable poverty maps using object detection in satellite images. *Twenty-Ninth International Joint Conference on Artificial Intelligence (IJCAI-20) Special Track on AI for Computational Sustainability and Human Well-Being*, 4410–4416.

[7] Ayush, K., Uzkent, B., Tanmay, K., Burke, M., Lobell, D., & Ermon, S. (2021). Efficient Poverty Mapping from High Resolution Remote Sensing Images. *Proceedings of the AAAI Conference on Artificial Intelligence*, *35*(1), 12–20. https://doi.org/10.1609/aaai.v35i1.16072

[8] Batana, Y. M. (2013). Multidimensional Measurement of Poverty Among Women in Sub-Saharan Africa. *Social Indicators Research*, *112*(2), 337–362. https://doi.org/10.1007/s11205-013-0251-9

[9] Belgiu, M., & Drăguţ, L. (2016). Random forest in remote sensing: A review of applications and future directions. *ISPRS Journal of Photogrammetry and Remote Sensing*, *114*, 24–31. https://doi.org/10.1016/j.isprsjprs.2016.01.011

[10] Berenger, V. (2019). The counting approach to multidimensional poverty. The case of four African countries. *South African Journal of Economics*, *87*(2), 200–227. https://doi.org/10.1111/saje.12217

[11] Bigman, D., & Fofack, H. (2000). *Geographical Targeting for Poverty Alleviation*. The World Bank. https://doi.org/10.1596/0-8213-4625-3

[12] Blumenstock, J., Cadamuro, G., & On, R. (2015). Predicting poverty and wealth from mobile phone metadata. *Science*, *350*(6264), 1073–1076. https://doi.org/10.1126/science.aac4420

[13] Cadamuro, G., Muhebwa, A., & Taneja, J. (2018). *Assigning a Grade: Accurate Measurement of Road Quality Using Satellite Imagery*.

[14] Chand, T. R. K., Badarinath, K. V. S., Elvidge, C. D., & Tuttle, B. T. (2009). Spatial characterization of electrical power consumption patterns over India using temporal DMSP-OLS night-time satellite data. *International Journal of Remote Sensing*, *30*(3), 647–661. https://doi.org/10.1080/01431160802345685

[15] Chen, X., & Nordhaus, W. D. (2011). Using luminosity data as a proxy for economic statistics. *Proceedings of the National Academy of Sciences*, *108*(21), 8589–8594. https://doi.org/10.1073/pnas.1017031108

[16] Chen, Z., Yu, B., Hu, Y., Huang, C., Shi, K., & Wu, J. (2015). Estimating House Vacancy Rate in Metropolitan Areas Using NPP-VIIRS Nighttime Light Composite Data. *IEEE Journal of Selected Topics in Applied Earth Observations and Remote Sensing*, *8*(5), 2188–2197. https://doi.org/10.1109/JSTARS.2015.2418201

[17] Chen, Z., Yu, B., Song, W., Liu, H., Wu, Q., Shi, K., & Wu, J. (2017). A New Approach for Detecting Urban Centers and Their Spatial Structure with Nighttime Light Remote Sensing. *IEEE Transactions on Geoscience and Remote Sensing*, *55*(11), 6305–6319. https://doi.org/10.1109/TGRS.2017.2725917

[18] David J. Rogers, Thomas Emwanu, & Timothy P. Robinson. (2006). Poverty Mapping in Uganda: An Analysis Using Remotely Sensed and Other Environmental Data. *Rogers2006PovertyMI*.

[19] Drusch, M., Del Bello, U., Carlier, S., Colin, O., Fernandez, V., Gascon, F., Hoersch, B., Isola, C., Laberinti, P., Martimort, P., Meygret, A., Spoto, F., Sy, O., Marchese, F., & Bargellini, P. (2012). Sentinel-2: ESA's Optical High-Resolution Mission for GMES Operational Services. *Remote Sensing of Environment*, *120*, 25–36. https://doi.org/10.1016/j.rse.2011.11.026

[20] Duque, J. C., Patino, J. E., Ruiz, L. A., & Pardo-Pascual, J. E. (2015). Measuring intra-urban poverty using land cover and texture metrics derived from remote sensing data. *Landscape and Urban Planning*, *135*, 11–21. https://doi.org/10.1016/j.landurbplan.2014.11.009

[21] Ehrlich D., Schiavina M., Pesaresi M., & Kemper, T. (2018). *Detecting spatial pattern of inequalities from remote sensing Towards mapping of deprived communities and poverty*.

[22] Elvidge, C. D., Baugh, K. E., Zhizhin, M., & Hsu, F.-C. (2013). Why VIIRS data are superior to DMSP for mapping nighttime lights. *Proceedings of the Asia-Pacific Advanced Network*, *35*(0), 62. https://doi.org/10.7125/APAN.35.7

[23] Elvidge, C. D., Sutton, P. C., Ghosh, T., Tuttle, B. T., Baugh, K. E., Bhaduri, B., & Bright, E. (2009). A global poverty map derived from satellite data. *Computers & Geosciences*, *35*(8), 1652–1660. https://doi.org/10.1016/j.cageo.2009.01.009

[24] Fisher, J. R. B., Acosta, E. A., Dennedy-Frank, P. J., Kroeger, T., & Boucher, T. M. (2018). Impact of satellite imagery spatial resolution on land use classification accuracy and modeled

water quality. *Remote Sensing in Ecology and Conservation*, *4*(2), 137–149. https://doi.org/10.1002/rse2.61

[25] Foster, J. E. (1998). Absolute versus Relative Poverty. *The American Economic Review*, *88*, 335–341.

[26] Frediani, A. A. (2010). Sen's Capability Approach as a framework to the practice of development. *Development in Practice*, *20*(2), 173–187. https://doi.org/10.1080/09614520903564181

[27] Gambo, J., Shafri, H. Z. M., & Yusuf, Y. A. (2022). An analysis of multidimensional poverty in Nigeria using statistical and geospatial modelling: A case study of Jigawa state. *IOP Conference Series: Earth and Environmental Science*, *1064*(1), 012047. https://doi.org/10.1088/1755-1315/1064/1/012047

[28] Gervasoni, L., Fenet, S., Perrier, R., & Sturm, P. (2018). Convolutional neural networks for disaggregated population mapping using open data. *5th IEEE International Conference on Data Science and Advanced Analytics (DSAA), IEEE,* , 594–603.

[29] Ghosh, T., Anderson, S., Elvidge, C., & Sutton, P. (2013). Using Nighttime Satellite Imagery as a Proxy Measure of Human Well-Being. *Sustainability*, *5*(12), 4988–5019. https://doi.org/10.3390/su5124988

[30] Gong, P., Wang, J., Yu, L., Zhao, Y., Zhao, Y., Liang, L., Niu, Z., Huang, X., Fu, H., Liu, S., Li, C., Li, X., Fu, W., Liu, C., Xu, Y., Wang, X., Cheng, Q., Hu, L., Yao, W., … Chen, J. (2013). Finer resolution observation and monitoring of global land cover: first mapping results with Landsat TM and ETM+ data. *International Journal of Remote Sensing*, *34*(7), 2607–2654. https://doi.org/10.1080/01431161.2012.748992

[31] Grippa, T., Georganos, S., Zarougui, S., Bognounou, P., Diboulo, E., Forget, Y., Lennert, M., Vanhuysse, S., Mboga, N., & Wolff, E. (2018). Mapping Urban Land Use at Street Block Level Using OpenStreetMap, Remote Sensing Data, and Spatial Metrics. *ISPRS International Journal of Geo-Information*, *7*(7), 246. https://doi.org/10.3390/ijgi7070246

[32] Hansen, M. C., Potapov, P. V., Moore, R., Hancher, M., Turubanova, S. A., Tyukavina, A., Thau, D., Stehman, S. V., Goetz, S. J., Loveland, T. R., Kommareddy, A., Egorov, A., Chini, L., Justice, C. O., & Townshend, J. R. G. (2013). High-Resolution Global Maps of 21st-Century Forest Cover Change. *Science*, *342*(6160), 850–853. https://doi.org/10.1126/science.1244693

[33] Head, A., Manguin, M., Tran, N., & Blumenstock, J. E. (2017). Can Human Development be Measured with Satellite Imagery? *Proceedings of the Ninth International Conference on*

Information and Communication Technologies and Development, 1–11. https://doi.org/10.1145/3136560.3136576

[34] Henderson, J. V., Storeygard, A., & Weil, D. N. (2012). Measuring Economic Growth from Outer Space. *American Economic Review*, *102*(2), 994–1028. https://doi.org/10.1257/aer.102.2.994

[35] Herold, M., Liu, X., & Clarke, K. C. (2003). Spatial Metrics and Image Texture for Mapping Urban Land Use. *Photogrammetric Engineering & Remote Sensing*, *69*(9), 991–1001. https://doi.org/10.14358/PERS.69.9.991

[36] Herold, M., Scepan, J., & Clarke, K. C. (2002). The Use of Remote Sensing and Landscape Metrics to Describe Structures and Changes in Urban Land Uses. *Environment and Planning A: Economy and Space*, *34*(8), 1443–1458. https://doi.org/10.1068/a3496

[37] Hersh, J., Engstrom, R., & Mann, M. (2021). Open data for algorithms: mapping poverty in Belize using open satellite derived features and machine learning. *Information Technology for Development*, *27*(2), 263–292. https://doi.org/10.1080/02681102.2020.1811945

[38] Hofer, M., Sako, T., Martinez Jr., A., Addawe, M., Bulan, J., Durante, R. L., & Martillan, M. (2020). *Applying Artificial Intelligence on Satellite Imagery to Compile Granular Poverty Statistics*. https://doi.org/10.22617/WPS200432-2

[39] Immitzer, M., Atzberger, C., & Koukal, T. (2012). Tree Species Classification with Random Forest Using Very High Spatial Resolution 8-Band WorldView-2 Satellite Data. *Remote Sensing*, *4*(9), 2661–2693. https://doi.org/10.3390/rs4092661

[40] Imran, M., Stein, A., & Zurita-Milla, R. (2014). Investigating rural poverty and marginality in Burkina Faso using remote sensing-based products. *International Journal of Applied Earth Observation and Geoinformation*, *26*, 322–334. https://doi.org/10.1016/j.jag.2013.08.012

[41] Jarry, R., Chaumont, M., Berti-Équille, L., & Subsol, G. (2021). *Assessment of CNN-Based Methods for Poverty Estimation from Satellite Images* (pp. 550–565). https://doi.org/10.1007/978-3-030-68787-8_40

[42] Jean, N., Burke, M., Xie, M., Davis, W. M., Lobell, D. B., & Ermon, S. (2016). Combining satellite imagery and machine learning to predict poverty. *Science*, *353*(6301), 790–794. https://doi.org/10.1126/science.aaf7894

[43] Jemmali, H. (2017). Mapping water poverty in Africa using the improved Multidimensional Index of Water Poverty. *International Journal of Water Resources Development*, *33*(4), 649–666. https://doi.org/10.1080/07900627.2016.1219941

[44] Jolliffe, D. M., Mahler, D. G., Lakner, C., Atamanov, A., & Tetteh Baah, S. Kofi. (2017). *Assessing the Impact of the 2017 PPPs on the International Poverty Line and Global Poverty* (WPS 9941). http://documents.worldbank.org/curated/en/353811645450974574/Assessing-the-Impactof-the-2017-PPPs-on-the-International-Poverty-Line-and-Global-Poverty

[45] Klemens, B., Coppola, A., & Shron, M. (2015). *Estimating Local Poverty Measures Using Satellite Images: A Pilot Application to Central America*. The World Bank. https://doi.org/10.1596/1813-9450-7329

[46] Kohli, D., Sliuzas, R., & Stein, A. (2016). Urban slum detection using texture and spatial metrics derived from satellite imagery. *Journal of Spatial Science*, *61*(2), 405–426. https://doi.org/10.1080/14498596.2016.1138247

[47] Kohli, D., Stein, A., Sliuzas, R., & Kerle, N. (2015). *Identifying and Classifying Slum Areas Using Remote Sensing*.

[48] Kohli, D., Warwadekar, P., Kerle, N., Sliuzas, R., & Stein, A. (2013). Transferability of Object-Oriented Image Analysis Methods for Slum Identification. *Remote Sensing*, *5*(9), 4209–4228. https://doi.org/10.3390/rs5094209

[49] Lin, L., Di, L., Tang, J., Yu, E., Zhang, C., Rahman, Md., Shrestha, R., & Kang, L. (2019). Improvement and Validation of NASA/MODIS NRT Global Flood Mapping. *Remote Sensing*, *11*(2), 205. https://doi.org/10.3390/rs11020205

[50] Lin, L., Di, L., Yang, R., Zhang, C., Yu, E., Rahman, M. S., Sun, Z., & Tang, J. (2018). Using Machine Learning Approach to Evaluate the PM2.5 Concentrations in China from 1998 to 2016. *Proceedings of the 2018 7th International Conference on Agro-Geoinformatics (Agro-Geoinformatics)*, 1–5.

[51] Lin, L., Di, L., Zhang, C., Guo, L., & Di, Y. (2021). Remote Sensing of Urban Poverty and Gentrification. *Remote Sensing*, *13*(20), 4022. https://doi.org/10.3390/rs13204022

[52] Ma, T., Zhou, C., Pei, T., Haynie, S., & Fan, J. (2014). Responses of Suomi-NPP VIIRS-derived nighttime lights to socioeconomic activity in China's cities. *Remote Sensing Letters*, *5*(2), 165–174. https://doi.org/10.1080/2150704X.2014.890758

[53] Mahabir, R., Croitoru, A., Crooks, A., Agouris, P., & Stefanidis, A. (2018). A Critical Review of High and Very High-Resolution Remote Sensing Approaches for Detecting and Mapping Slums: Trends, Challenges and Emerging Opportunities. *Urban Science*, *2*(1), 8. https://doi.org/10.3390/urbansci2010008

[54] Marx, S., Phalkey, R., Aranda-Jan, C. B., Profe, J., Sauerborn, R., & Höfle, B. (2014). Geographic information analysis and web-based geoportals to explore malnutrition in Sub-Saharan

Africa: a systematic review of approaches. *BMC Public Health*, *14*(1), 1189. https://doi.org/10.1186/1471-2458-14-1189

[55] Melchiorri, M., Florczyk, A., Freire, S., Schiavina, M., Pesaresi, M., & Kemper, T. (2018). Unveiling 25 Years of Planetary Urbanization with Remote Sensing: Perspectives from the Global Human Settlement Layer. *Remote Sensing*, *10*(5), 768. https://doi.org/10.3390/rs10050768

[56] Noor, A. M., Alegana, V. A., Gething, P. W., Tatem, A. J., & Snow, R. W. (2008). Using remotely sensed night-time light as a proxy for poverty in Africa. *Population Health Metrics*, *6*(1), 5. https://doi.org/10.1186/1478-7954-6-5

[57] Pekel, J.-F., Cottam, A., Gorelick, N., & Belward, A. S. (2016). High-resolution mapping of global surface water and its long-term changes. *Nature*, *540*(7633), 418–422. https://doi.org/10.1038/nature20584

[58] Pesaresi, M., Syrris, V., & Julea, A. (2016). A New Method for Earth Observation Data Analytics Based on Symbolic Machine Learning. *Remote Sensing*, *8*(5), 399. https://doi.org/10.3390/rs8050399

[59] Piaggesi, S., Gauvin, L., Tizzoni, M., Cattuto, C., Adler, N., Verhulst, S. G., Young, A., Price, R., Ferres, L., & Panisson, A. (2019). Predicting City Poverty Using Satellite Imagery. . *Proceedings of the IEEE/CVF Conference on Computer Vision and Pattern Recognition Workshops*, 90–96.

[59] Priambodo, A. (2021). The impact of unemployment and poverty on economic growth and the human development index (HDI). *Perwira International Journal of Economics & Business*, *1*(1), 29–36. https://doi.org/10.54199/pijeb.v1i1.43

[60] Russakovsky, O., Deng, J., Su, H., Krause, J., Satheesh, S., Ma, S., Huang, Z., Karpathy, A., Khosla, A., Bernstein, M., Berg, A. C., & Fei-Fei, L. (2015). ImageNet Large Scale Visual Recognition Challenge. *International Journal of Computer Vision*, *115*(3), 211–252. https://doi.org/10.1007/s11263-015-0816-y

[61] Sheehan, E., Meng, C., Tan, M., Uzkent, B., Jean, N., Burke, M., Lobell, D., & Ermon, S. (2019). Predicting economic development using geolocated wikipedia articles. , 2698–2706. *In Proceedings of the 25th ACM SIGKDD International Conference on Knowledge Discovery & Data Mining*, 2698–2706.

[62] Shi, K., Yang, Q., Fang, G., Yu, B., Chen, Z., Yang, C., & Wu, J. (2019). Evaluating spatiotemporal patterns of urban electricity consumption within different spatial boundaries: A case study of Chongqing, China. *Energy*, *167*, 641–653. https://doi.org/10.1016/j.energy.2018.11.022

[63] Sohnesen, T. P., Fisker, P., & Malmgren-Hansen, D. (2022). Using Satellite Data to Guide Urban Poverty Reduction. *Review of Income and Wealth*, *68*(S2). https://doi.org/10.1111/roiw.12552

[64] Steele, J. E., Sundsøy, P. R., Pezzulo, C., Alegana, V. A., Bird, T. J., Blumenstock, J., Bjelland, J., Engø-Monsen, K., de Montjoye, Y.-A., Iqbal, A. M., Hadiuzzaman, K. N., Lu, X., Wetter, E., Tatem, A. J., & Bengtsson, L. (2017). Mapping poverty using mobile phone and satellite data. *Journal of The Royal Society Interface*, *14*(127), 20160690. https://doi.org/10.1098/rsif.2016.0690

[65] Stevens, F. R., Gaughan, A. E., Linard, C., & Tatem, A. J. (2015). Disaggregating Census Data for Population Mapping Using Random Forests with Remotely-Sensed and Ancillary Data. *PLOS ONE*, *10*(2), e0107042. https://doi.org/10.1371/journal.pone.0107042

[66] Stoler, J., Daniels, D., Weeks, J. R., Stow, D. A., Coulter, L. L., & Finch, B. K. (2012). Assessing the Utility of Satellite Imagery with Differing Spatial Resolutions for Deriving Proxy Measures of Slum Presence in Accra, Ghana. *GIScience & Remote Sensing*, *49*(1), 31–52. https://doi.org/10.2747/1548-1603.49.1.31

[67] Stow, D. A., Lippitt, C. D., & Weeks, J. R. (2010). Geographic Object-based Delineation of Neighborhoods of Accra, Ghana Using QuickBird Satellite Imagery. *Photogrammetric Engineering & Remote Sensing*, *76*(8), 907–914. https://doi.org/10.14358/PERS.76.8.907

[68] Stow, D., Lopez, A., Lippitt, C., Hinton, S., & Weeks, J. (2007). Object-based classification of residential land use within Accra, Ghana based on QuickBird satellite data. *International Journal of Remote Sensing*, *28*(22), 5167–5173. https://doi.org/10.1080/01431160701604703

[69] Tingzon, I., Orden, A., Go, K. T., Sy, S., Sekara, V., Weber, I., Fatehkia, M., García-Herranz, M., & Kim, D. (2019). Mapping poverty in the philippines using machine learning, satellite imagery, and crowd-sourced geospatial information. *The International Archives of the Photogrammetry, Remote Sensing and Spatial Information Sciences*, *XLII-4/W19*, 425–431. https://doi.org/10.5194/isprs-archives-XLII-4-W19-425-2019

[70] United Nations General Assembly. (2015). *Transforming Our World: The 2030 Agenda for Sustainable Development*.

[71] van Beijma, S., Comber, A., & Lamb, A. (2014). Random forest classification of salt marsh vegetation habitats using quad-polarimetric airborne SAR, elevation and optical RS data. *Remote Sensing of Environment*, *149*, 118–129. https://doi.org/10.1016/j.rse.2014.04.010

[71] Varshney, K. R., Chen, G. H., Abelson, B., Nowocin, K., Sakhrani, V., Xu, L., & Spatocco, B. L. (2015). Targeting Villages for Rural Development Using Satellite Image Analysis. *Big Data*, *3*(1), 41–53. https://doi.org/10.1089/big.2014.0061

[72] Victor, B., Blevins, M., Green, A. F., Ndatimana, E., González-Calvo, L., Fischer, E. F., Vergara, A. E., Vermund, S. H., Olupona, O., & Moon, T. D. (2014). Multidimensional Poverty in Rural Mozambique: A New Metric for Evaluating Public Health Interventions. *PLoS ONE*, *9*(9), e108654. https://doi.org/10.1371/journal.pone.0108654

[73] Weeks, J. R., Hill, A., Stow, D., Getis, A., & Fugate, D. (2007). Can we spot a neighbourhood from the air? Defining neighbourhood structure in Accra, Ghana. *GeoJournal*, *69*(1–2), 9–22. https://doi.org/10.1007/s10708-007-9098-4

[74] World Bank. (2018). *Poverty and Shared Prosperity 2018: Piecing Together the Poverty Puzzle*. https://www.worldbank.org/en/publication/poverty-and-shared-prosperity-2018

[75] World Bank. (2020). *Poverty and Shared Prosperity 2020: Reversals of Fortune.* https://openknowledge.worldbank.org/handle/10986/34496

[76] World Bank. (2022). *Poverty and Shared Prosperity 2022: Correcting Course*. https://www.worldbank.org/en/publication/poverty-and-shared-prosperity

[77] Xie, M., Jean, N., Burke, M., Lobell, D., & Ermon, S. (2016). Transfer Learning from Deep Features for Remote Sensing and Poverty Mapping. *Proceedings of the AAAI Conference on Artificial Intelligence*, *30*(1). https://doi.org/10.1609/aaai.v30i1.9906

[78] Yao, Y., Liu, X., Li, X., Zhang, J., Liang, Z., Mai, K., & Zhang, Y. (2017). Mapping fine-scale population distributions at the building level by integrating multisource geospatial big data. *International Journal of Geographical Information Science*, 1–25. https://doi.org/10.1080/13658816.2017.1290252

[79] Yeh, C., Perez, A., Driscoll, A., Azzari, G., Tang, Z., Lobell, D., Ermon, S., & Burke, M. (2020). Using publicly available satellite imagery and deep learning to understand economic well-being in Africa. *Nature Communications*, *11*(1), 2583. https://doi.org/10.1038/s41467-020-16185-w

[80] Yu, B., Shi, K., Hu, Y., Huang, C., Chen, Z., & Wu, J. (2015). Poverty Evaluation Using NPP-VIIRS Nighttime Light Composite Data at the County Level in China. *IEEE Journal of Selected Topics in Applied Earth Observations and Remote Sensing*, *8*(3), 1217–1229. https://doi.org/10.1109/JSTARS.2015.2399416

[81] Yu, B., Tang, M., Wu, Q., Yang, C., Deng, S., Shi, K., Peng, C., Wu, J., & Chen, Z. (2018). Urban Built-Up Area Extraction from Log- Transformed NPP-VIIRS Nighttime Light Composite Data. *IEEE Geoscience and Remote Sensing Letters*, *15*(8), 1279–1283. https://doi.org/10.1109/LGRS.2018.2830797

[82] Zhang, C., Yang, Z., Di, L., Lin, L., & Hao, P. (2020). Refinement of cropland data layer using machine learning. *The International Archives of the Photogrammetry, Remote Sensing and Spatial Information Sciences*, *XLII-3/W11*, 161–164. https://doi.org/10.5194/isprs-archives-XLII-3-W11-161-2020

[83] Zhao, N., Liu, Y., Cao, G., Samson, E. L., & Zhang, J. (2017). Forecasting China's GDP at the pixel level using nighttime lights time series and population images. *GIScience & Remote Sensing*, *54*(3), 407–425. https://doi.org/10.1080/15481603.2016.1276705

[84] Zhao, X., Yu, B., Liu, Y., Chen, Z., Li, Q., Wang, C., & Wu, J. (2019). Estimation of Poverty Using Random Forest Regression with Multi-Source Data: A Case Study in Bangladesh. *Remote Sensing*, *11*(4), 375. https://doi.org/10.3390/rs11040375

[85] Zhou, Y., Ma, T., Zhou, C., & Xu, T. (2015). Nighttime Light Derived Assessment of Regional Inequality of Socioeconomic Development in China. *Remote Sensing*, *7*(2), 1242–1262. https://doi.org/10.3390/rs70201242

SUB THEME 05

Emerging Geospatial Data Acquisition Techniques that Support Good Governance

EVALUATION OF SPECTRAL DISTANCE FOR EFFECTIVE FEATURE MAPPING IN A MULTICLASS PROBLEM

Zitta, N[1*]., Adeniyi, G[2]. & Fimba, E. D[3]

[1]Department of Surveying & Geoinformatics, Federal University of Technology Minna

[2]Department of Surveying and Geoinformatics University of Abuja

[3]Department of Surveying and Geoinformatics, Modibbo Adama University Yola

Corresponding author *bawazitta@gmail.com

Abstract

Mapping of land surface features through satellite images is one important aspect of Remote sensing applications. The accuracy of this process depends on how the feature selection is carried out. In a multispectral satellite image, the separability of the features depends on the band combinations used. The Landsat image was considered in this study and the Histogram minimum method of atmospheric correction which is suitable for cloud free images. The image autocorrelation reveals that the Moran's I obtained for the three LULC images are all positive values as 0.6368, 0.6167 and 0.8073 for the year 1986, 2000 and 2019 respectively which indicates tendency towards clustering. Using sample of training areas, Jeffries-Matusita distance was computed as a measure to check the degree of spectral separability on the bands used. This is to investigate if any pairs of land cover (LC) class consistently show similar spectral signature. This study presents a spectral separability analysis for LC features using Landsat-8 OLI/TIRS of 2019, Landsat 5 Thematic Mapper (TM) of 1986 and Enhanced Thematic Mapper (ETM) of the year 2000. This measurement reveals spectral overlapping between selected LC features and for the discrimination, statistical comparisons such as calculating the means of digital numbers (DNs), standard deviation of single band reflectance values and plotting the standard errors on all classes used. LTM 1986 shows pretty good separation in bands 3, 4, 5 & 7 while 1, 2 & 6 did not. Bands 3, 4, 5 & 7 in ETM 2000 also indicated good separability while 1, 2 & 6 clearly show poor spectral separability. Finally, L8 OLI returned bands 5, 6 & 7 with appreciable separation while bands 1, 2, 3, 4, & 8 did show good separation. These statistical results were proven to be good indicators of spectral similarity because the heterogeneity measure makes it more effective and objective.

Keywords: Multiclass Mapping, Multispectral, Remote Sensing, Spectral Separability

1.0 INTRODUCTION

The mapping of earth's features using satellite remote sensing technique is one significant facet of Remote sensing applications [8]. The accuracy of this process depends on the feature selection. In a multispectral satellite image, the separability of the features depends on the band combinations used [2]. Separability is a measure of the spectral distance between two signatures, and helps you to decide how different the signatures are. There are several ways of defining

"distance" [14]. This separability depends on how far apart the spectral signatures are placed in an N-dimensional space. Here, N denotes the number of bands under consideration. The spectral distance or the separability of the classes can be evaluated by a variety of distance measures, such as Euclidean distance, spectral angle, and the Jeffries Matusita distance [8]. When the spectral signature information is available, it can be exploited to discriminate between the classes [9]. Separability which measures looking at the distance between class means are: Euclidean Distance and Divergence while those who measure looking at both the differences between class means and the distribution of the values about those means are: M statistic, J-M Distance, Bhattacharyya Distance etc. likewise, some methods only work with one band at a time (e.g. Euclidean Distance, M statistic); while some can work on any number of bands (e.g. J-M Distance).

Generally, a land cover classification problem deals with the semantic segmentation of the raw satellite images. The first step in this kind of semantic segmentation is the preparation of labelled training samples [10]; [4]. The characterization and classification of different surfaces using remote sensing are usually based on multi-spectral, multi-polarized data or even derived parameters such as texture [2]. These classes are labelled depending on their separability index [1]; [5]. This index is a discriminating factor, which is helpful in classifying the class of a pixel. Machine learning algorithms for this classification can be unsupervised when there is no spectral information available [1]. The separability measures can be parametric or nonparametric [7]. The Transformed Divergence method can also be used for the separability analysis [3]. Rather than evaluating the spectral separability, the spectral similarity can be measured using the indices [13]. The simplest is the Euclidean distance, which is the square root of the sum of the squares of the distances between each pair of band mean values.

Note: In this case we are extending the definition "distance" to the n-dimensions of n bands, and using spectral space rather than spatial space. The fundamental Problem is before using collected pixels or classes in remote sensing, researchers barely do the needful by first answering the following questions:

i. What type of distribution do you have?

ii. Do the classes have a good separability?

iii. Is the separability statistically significant?

Therefore, the main purpose of this work is testing the discriminative ability of an index or technique at detecting between two distinct classes (e.g., say grass and trees) and also testing how 'good' the training data is before used in a classification. This separability criterion can be used to pairwise measure the separability between classes, allowing the assessment of the quality of the selected class samples in the available feature space [6]. The JM separability criterion was also applied to hyperspectral remote-sensing imagery. [12] opined that, the most distinct hyperspectral bands are selected through an unsupervised band selection technique for the hyperspectral image analysis using the JM separability criterion. In this case, the JM

separability is integrated during a band selection process so that only the most distinct bands are selected for data classification. As stated in [11], the JM criterion was used to evaluate the performance of a genetic algorithm developed to select the optimal bands of hyperspectral data capable of discriminating between various broadleaved vegetation species. Several measures of spectral separability have been developed to statistically measure the distance between pairs of signature with Transformed Divergence and Jeffries-Matusita (JM) Distance being more popular and available in commercial and open source remote sensing packages. For this study, JM Distance is used which is defined as:

1.1 Theoretical Background of Jeffries-Matusita (JM) Distance

1.1.1 Assessment of similarity of spectral signature

It is useful to evaluate the spectral distance or separability between training signatures or pixels. This was carried out in order to assess if different classes that are too similar could cause classification errors. A *Jeffries-Matusita's* separability check was used in confirming the degree of spectral separation acceptability of the bands used for each of the land use and land cover classes. It is a function of separability that directly relates to the probability of how good a resultant classification will be. The JM distance is represented by:

$$JM_{ij} = \sqrt{2(1 - \exp(-B))} \quad . \tag{1}$$

Where,

$$B = \frac{1}{8}\left(\mu_i - \mu_j\right)^T \left(\frac{c_i + c_j}{2}\right)^{-1} \left(\mu_i - \mu_j\right) + \frac{1}{2} In\left(\frac{|c_i + c_j|/2}{\sqrt{|c_i| \times |c_j|}}\right) \tag{2}$$

Where i and j are the two classes being compared, μ_i and μ_j are the mean vectors, c_i and c_j are the covariance matrices, and are the determinants of classes i and j while T is the transposition function. The JM distance has a maximum value of 2 which indicates 100% classification accuracy between two classes or complete separability. This algorithm is particularly meaningful for evaluating the result of maximum likelihood classification [8].

2.0 STUDY AREA

The study area (see Fig. 1.) is Jos metropolis, the capital city of Plateau state which lies between longitude 8° 40' 47.15"E and 9° 8' 13.20"E, latitude 9° 36' 11.54"N and 10° 2' 20.51"N. the study area coverage: is 18,423.00 Ha with temperature range of 11°C- 18°C in Nov to Jan and March to April is about 22°C averagely. The vegetation cover is northern guinea savannah zone characterized with short trees and grasses. Relief/Topography is on an average height of 1,200m. Extinct volcanoes and crater lakes are the source of great rivers; Kaduna, Gongola, Hadeja and Yobe.

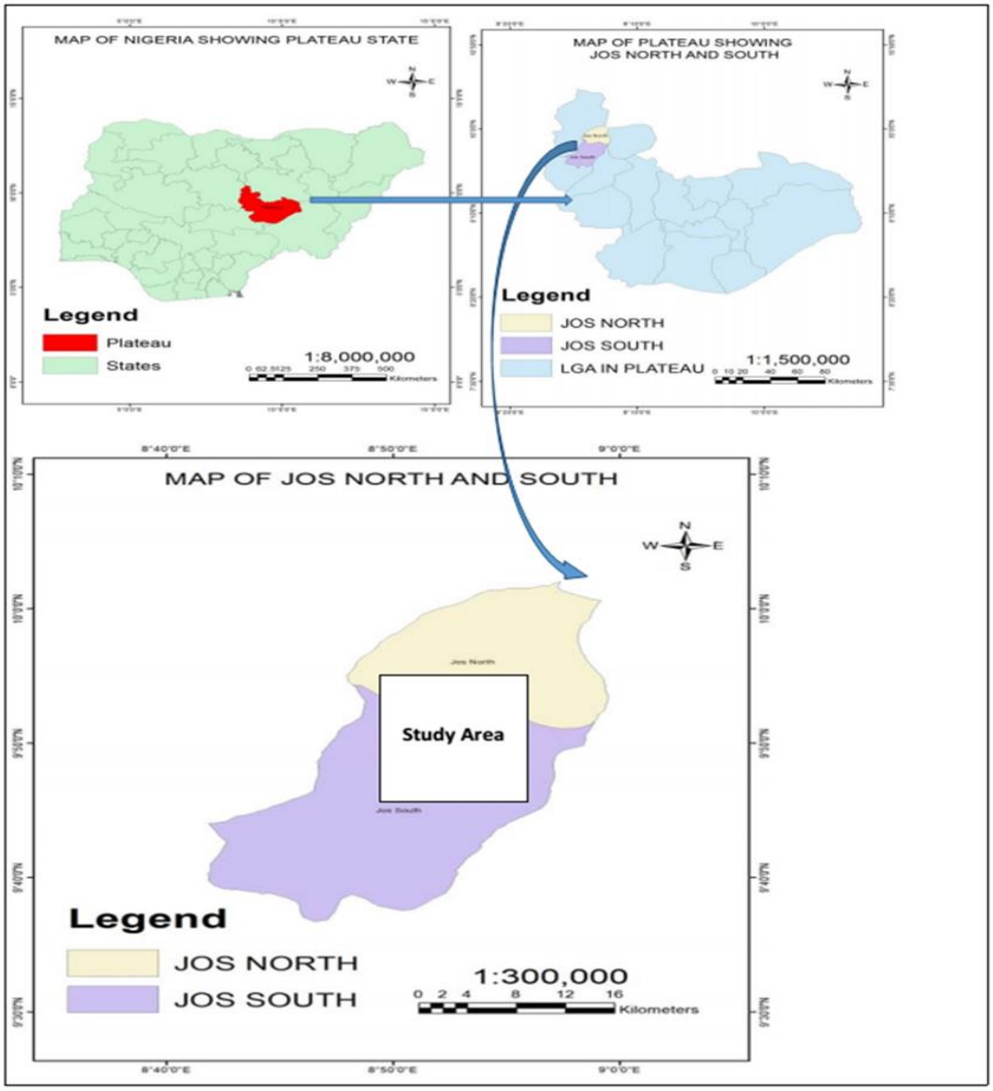

Figure 1. Map of study area

3.0 METHODOLOGY

The methodology entails the satellite image pre-processing and auto-correlation, and pixel training selection stages as shown in the flowchart methodology (see Fig. 2).

3.1 Materials

The hardware used consisted of Hp Laptop computer with 2.00 GB of RAM, 500 GB HARD disk and Laserjet 2055c printer. Three different software packages were also used – Envi 5.0, ESRI's ArcMap 10 and Microsoft Excel 2010. Landsat satellite images downloaded were: Landsat 5 TM 1986, Landsat L7 ETM+SLC-on 2000 and Landsat L8 OLI 2019 (30m spatial resolution).

3.1.1 Satellite image pre-processing. The first step after downloading the required dataset is correcting the raw images for the atmospheric defects. This constitutes the pre-processing step.

Dark Object Subtraction is a standard algorithm used for atmospheric correction. One more important reason for the atmospheric correction is that the separability between the classes is enhanced after the procedure, because of which histogram equalization will not be necessary.

3.1.2 Satellite image autocorrelation: This describes the degree to which values in a cell are similar to the cells immediately surrounding it. This was performed on the three Landsat images to give meaningful description of the various cell values particularly their spatial pattern. The King's Case procedure examines the cells diagonally connected to each cell as well as those normally examined for the Rook's Case. The summary of AUTOCORR can be seen in the Table 1 below where No of cells, Mean of cells, Standard deviation of cells and Moran's I values using the King's case are displayed. No of cells is the sum of cells in the entire Landsat image used as research area, mean of cell is the average of the cells used. Std deviation of cells is a measure of the amount of variation or dispersion of a set of values. A low std deviation indicates that the values tend to be close to the mean of the set while a high std deviation shows that the values are spread out over a wider range. Moran's I is a measure of spatial autocorrelation. It is a tool which measures spatial autocorrelation based on both feature locations and values simultaneously and evaluates whether the pattern expressed is clustered, dispersed or random. The king's case is a combination of both bishop and rook's case where neighbouring cells are considered normally and diagonally, it is also referred to as Queen's case**.**

3.1.3 Pixel training selection

The samples of earth surface features selected for this exercise were: built up, vegetation, water body, mining area, rock and open space as shown in Figure 3**.**

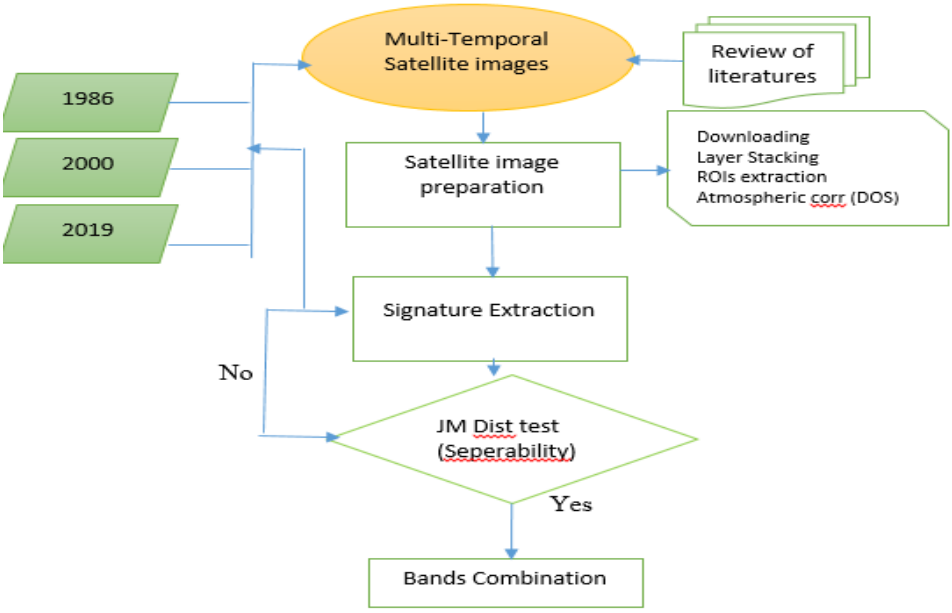

Figure 2. Flowchart of methodology

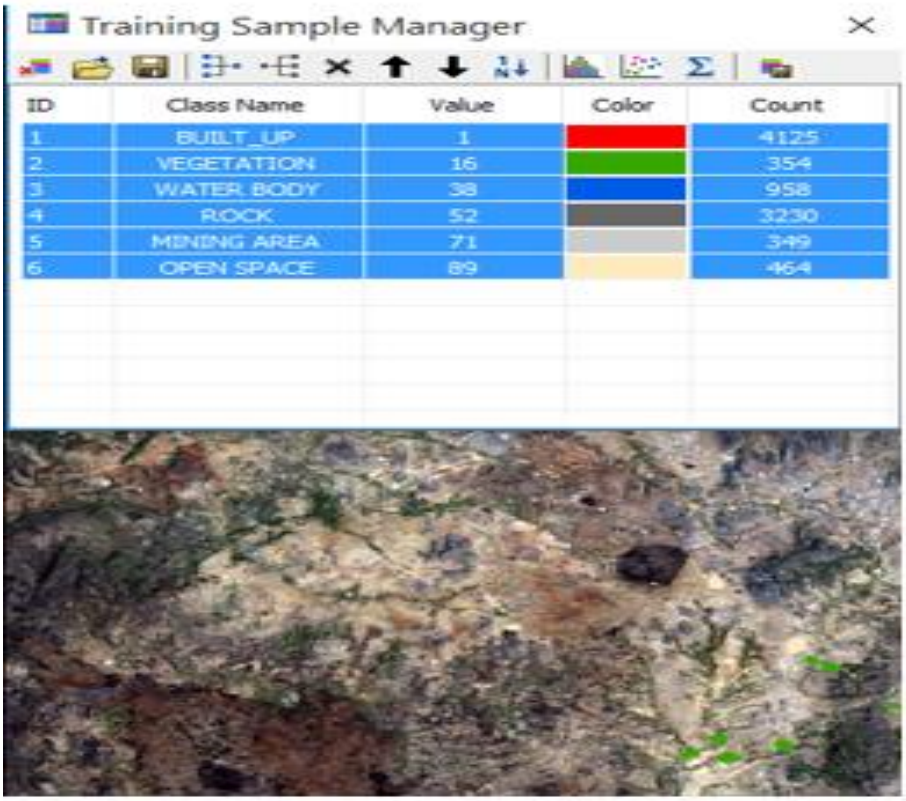

Figure 3. Pixel training sample manager of Landsat image

4.0 RESULTS AND DISCUSSION

Table 1 presents the results of the satellite image autocorrelation for the study epochs. Meanwhile, Figures 4, 5 and 6 show the spectral separability plots of the study epochs.

Table 1. Satellite image autocorrelation

	Landsat image	**1986**	**2000**	**2019**
King's case	Area (ha)	18423	18423	18423
	Mean of cells	4.5326	3.8487	3.4661
	Std of cells	0.0038	0.0036	0.0035
	Moran's I	0.6041	0.5813	0.8073

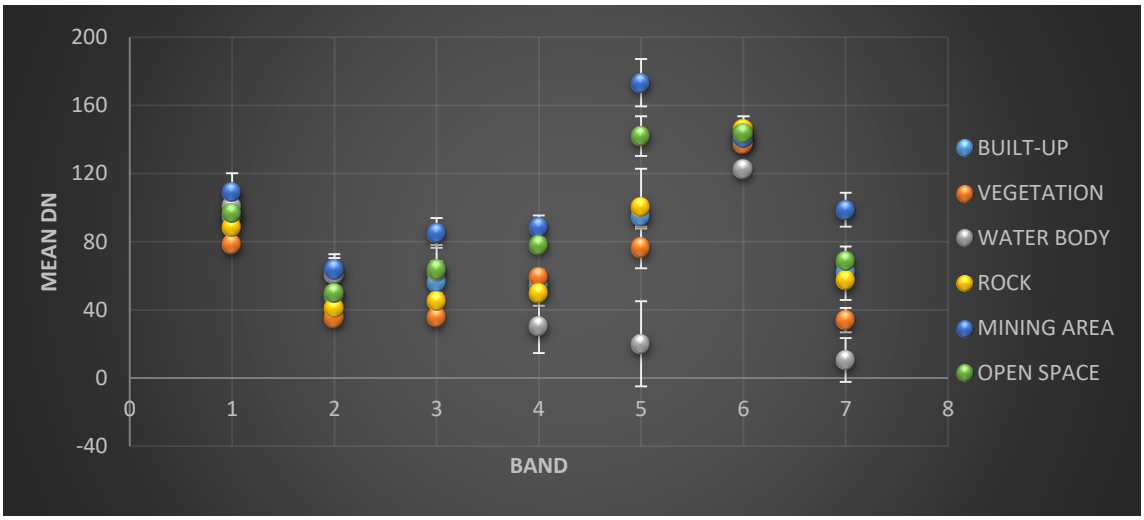

Figure 4. Spectral separability plots of 1986

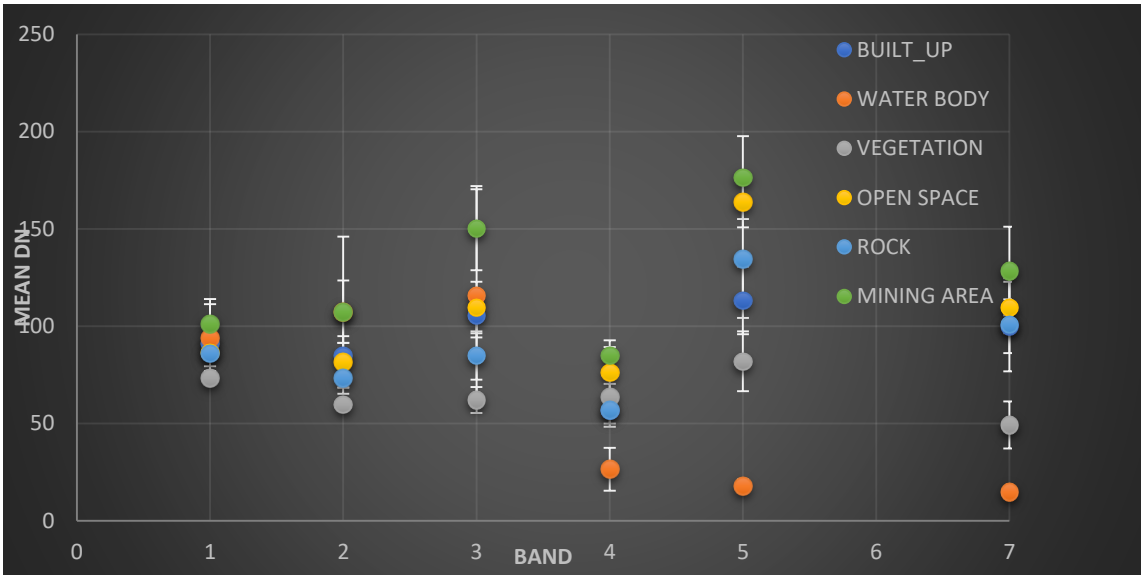

Figure 5. Spectral separability plots of 2000

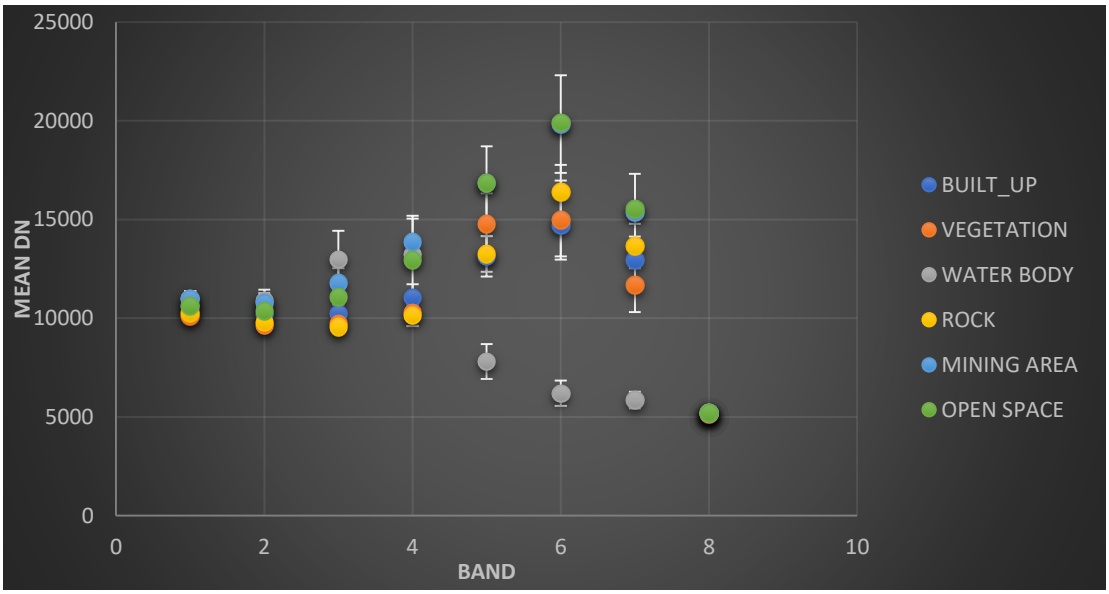

Figure 6. Spectral separability plots of 2019

The satellite images used in this study are Landsat Thematic Mapper (TM) of 1986, Enhanced Thematic Mapper (ETM) for the year 2000 and Operational Land Imager (OLI) of 2019 displayed under true color composite RGB (432) band combination to generate the respective LULC images. The image autocorrelation result shows that all the three LULC images have a total area coverage of 18,423 Ha which means they have the same area coverage. The LULC of 1986 has standard deviation (std) of cells as 0.0038 while the LULC of year 2000 has 0.0036 and that of 2019 LULC has 0.0044. All the values of std deviation obtained are low (small) which indicates that the data are tightly clustered around the mean of the set as 4.5326, 3.8487 and 3.4661 respectively. The std deviations returned are all positive therefore, they are all on the right-hand side of the normal curve. The Moran's I obtained for the three LULC images are all positive values as 0.6368, 0.6167 and 0.8073 respectively which indicates tendency towards clustering. That is, high values clustered near other high values and low values clustered around other low values. Even though this research is concern with only clustering and not which type of clustering that exist. The Moran's I defines the degree to which values of a cell are similar to that of other cells surrounding it. The three LULC images exhibited strong positive autocorrelation under the King's case since all the values of Moran's I index returned are near or close to +1**.**

Figure 4 shows that the separability in LTM 1986 which can be clearly seen as pretty good separation in bands 3, 4, 5 & 7 while 1, 2 & 6 did not exhibit any good separation. In Figure 1.5 that is the landsat image of year 2000, bands 3, 4, 5 & 7 also indicated good separability while 1, 2 & 6 clearly show poor spectral separability. Finally, L8 OLI returned bands 5, 6 & 7 with appreciable separation while bands 1, 2, 3, 4, & 8 did show good separation as shown in Figure 6.

5.0 CONCLUSION AND RECOMMENDATION

This measurement reveals spectral overlapping and separation between selected LC features and statistical comparisons such as calculating the means of digital numbers (DNs), standard deviation of single band reflectance values and plotting the standard errors on all classes was carried out. The statistical results reveal to be good indicators of spectral similarity because the heterogeneity measure makes it more effective and objective. This work therefore recommends that, first a separability test using pixels training samples be carried out on multispectral satellite images before any further usages to ascertain the reliability of data to be used

References

[1] Congalton, R.G & K. Green. (2008). Assessing the accuracy of remotely sensed data: principles and practices, CRC press, Kulkarni K & Vijaya, P. A (2019). Parametric Approaches to Multispectral Image Classification using Normalized Difference Vegetation Index, *International Journal of Innovative Technology and Exploring Engineering*, 9(2S) (2019) DOI: 10.35940/ijitee.B1061.1292S19, pp 611-615.

[2] Dabboor, M, Howella, S., Shokra, H & Yackel, J (2014). The Jeffries–Matusita distance for the case of complex Wishart distribution as a separability criterion for fully polarimetric SAR data. *International Journal of Remote Sensing*, 2014 Vol. 35, No. 19, 6859–6873, http://dx.doi.org/10.1080/01431161.2014.960614

[3] Dhaka, S., Shankar, H., Roy, P. S., Kiran, R (2016). IRS P6 LISS-IV Image Classification using Simple, Fuzzy Logic and Artificial Neural Network Techniques: A Comparison Study, *International Journal of Technical Research & Science*, 1(2) (2016)

[4] Elhag, M., Psilovikos, A & Sakellariou, M (2013). Detection of land cover changes for water recourses management using remote sensing data over the Nile Delta Region, *Environment, Development and Sustainability*, 15(5) (2013)1189-1204

[5] Friedl, M.A (2010), MODIS Collection 5 global land cover: Algorithm refinements and characterization of new datasets. *Remote Sensing of the Environment*, 114(1) (2010) 168-182.

[6] Ghoggali, N. & Melgani, F (2009). Automatic Ground-Truth Validation with Genetic Algorithms for Multispectral Image Classification. *IEEE Transactions on Geoscience and Remote Sensing* ,47 (7): 2172–2181. doi:10.1109/TGRS.2009.2013693

[7] Huang, H (2016). Separability Analysis of Sentinel-2A Multi-Spectral Instrument (MSI) Data for Burned Area Discrimination, *Remote Sensing,* 8(10) (2016) 873 https://doi.org/10.3390/rs8100873

[8] Keerti, K & Vijaya, P. A. (2021). Separability Analysis of the Band Combinations for Land Cover Classification of Satellite Images. *International Journal of Engineering Trends and*

Technology, Volume 69 Issue 8, 138-144, ISSN: 2231 – 5381 /doi:10.14445/22315381/IJETT-V69I8P217

[9] Kulkarni K & P. A. Vijaya. (2019). Experiment of Multispectral Images using Spectral Angle Mapper Algorithm for Land Cover Classification, *International Journal of Innovative Technology and Exploring Engineering*, 8(6S4) 96-99

[10] Rogan, J (2003). Land-cover change monitoring with classification trees using Landsat TM and ancillary data, *Photogrammetric Engineering & Remote Sensing*, 69(7) (2003) 793-804

[11] Ullah, S., Groen, T. A., Schlerf M., Skidmore, A. K., Nieuwenhuis W., & Vaiphasa C. (2012). Using a Genetic Algorithm as an Optimal Band Selector in the mid and Thermal Infrared (2.5– 14 µm) to Discriminate Vegetation Species. *Sensors*, 12 (7): 8755–8769. doi:10.3390/ s120708755.

[12] Venkataraman, S., Bjerke H., Copenhaver K., & Glaser, J. (2006). Optimal Band Selection of Hyperspectral Data for Transgenic Corn Identification. Paper presented in *MAPPS/ASPRS 200 Fall Conference*, San Antonio, TX, November 6–10

[13] Ye, Chul-Soo (2020). Evaluating the Contribution of Spectral Features to Image Classification Using Class Separability, *Korean Journal of Remote Sensing*, 36(1) 55-65, https://doi.org/10.7780/kjrs.2020.36.1.5

[14] Yongji, W., Qingwen, Q & Ying, L (2018). Unsupervised Segmentation Evaluation Using Area-Weighted Variance and Jeffries-Matusita Distance for Remote Sensing Images. *Remote Sens*, 10, 1193; doi: 10.3390/rs10081193

SUB THEME 06

Geospatial Sciences for Effective Public Infrastructure Projects

THE COMPARATIVE TEMPORAL VARIATION EVALUATION OF KAINJI AND SHIRORO HYDROPOWER PLANT RESERVOIRS STORAGE WATER LEVEL IN NIGER STATE, NIGERIA

[1]Akinwale, A. S. & [2]Musa, A. A.

[1]Department of Surveying and Geoinformatics, The Federal Polytechnic, School of Environmental Studies Bida, Niger State. Nigeria

[2] Department of Surveying and Geoinformatics, School of Environmental Sciences Madibbo Adama University Technology Yola, Adamawa State. Nigeria

Corresponding author: akin4shot@gmail.com

Abstract

The temporal fluctuation variations in the reservoir water storage of any hydropower plants often affect the output power generation and supply. This paper therefore, aimed at evaluating the statistical comparative evaluation of the effect of rainfalls, evaporations, temperatures and water surface level (elevation) variations at the Kainji and Shiroro hydropower plants in Niger State, Nigeria. This was to assess; the monthly, annually and each ten years intervals of epochs of the variations between 1990 to 2022. The methods used includes generation of both previous and current meteorological and tide gauge data from their respective dam sites. Some basic mathematical algorithms, and statistical manipulation were used for the processed, analysis and presentation of the results. The results obtained for the Kainji Hydropower plant (KHPP) includes, average 141.83m maximum water elevation surface level (MWES) as against 141.72m for designed specifications and 136.7m minimum as against the 132m for designed. While at the Shiroro station, the maximum of 381m as against 382.6 for designed m and 360m as against 371.7m computed. The months of January, February and March been the peak of the evaporation from the reservoir across the four epochs on the reservoirs. The climax of the rainfall at the two station that often resulted into occasional excessive erosions and floods, (i. e. 2012 flooding) ranges between July, August and September with the temperature rising between $38^0 – 41^0$ C aiding evaporation respectively. Conclusively, significant water was lost due unprecedented evaporation, high temperature and flooding variations experiences and affection the surfaces water level with irrational rainfalls and drought Recommendations, since all the temporal variation studied here do contribute in negatively to water lost in the storge capacity. Efforts should be made toward continues use of both the previous and current data to monitor the reservoir storage capacity in and around the dam alongside with power generation to maintain water balance and stable power supply.

Keywords: Analysis of Variance, Comparative Evaluation, Epochs, Surface Elevation, Variations

1.0 INTRODUCTION

Tide a periodic vertical movement in the level of the sea, often affect the horizontal movement along the stream likewise and so called “tidal stream” [10]. Though all resulting from tide

consequence to the solar cycle at times of new and full moon at a place of highest high waters (HHW) [10]. The lowest low waters (LLW) of a tide cycle known as spring tides will always experience 7-¼ days after [10]. The first and last quarters of the moon, the lowest high waters and the highest low waters of a tide cycle often results into neap tides [10]. The effect is the variations in water depth and the vertical ocean and sea movement from place to place and often triggered up by strong water waves pushing materials such as; sediments, silts, hydrological debris, garbage off and on the shorelines constituting depths and vertical water movements [9] and [6]. In addition, the influence of thunderstorm and persistence days of heavy rainfalls often increases the volume of water, tides and strong waves. All the above always accompanied with ocean erosion manifesting and rapid rise and fall enveloping water into both vertical and horizontal movement across the shore [11]. In contract, the results from global warming with increase evidence of climate change and high rise of temperature has been steering up high evaporation with steady fluctuation diminishes in the water bodies and in particular dam's reservoirs across the globe [11].

Furthermore, the frequent entrance of water into the bodies of water such; reservoirs, lakes, seas, oceans etc., are visibly noticed from either the running rivers, streams and rainfalls. [5]. According to [6], that the gradual disappearances, reduction and fluctuation in the storage capacities sizes of water bodies are usually cause by the combination of tides and waves (i. e. rise and fall). The accompanied high temperature and evaporation gradually drying water from the surface as a result of intense heat directly from the sun are quietly invisible until the water disappears completely. On the other hand, sediments, silts, hydrological debris, garbage etc., are often gain assess into the water bottom floor from; rivers, seas, ocean etc., erosion and floods are particles that often decreases the size from the bottom of water upwardly [1]. This frequent occurrences on the surface and the entire water body leading to a significant lost in its storage throughout the seasons often affects the output performances of the power generation and supply of the dam to communities and the entire nation.

The Hypsographic Chart are therefore prepared in advance to continue checking and monitoring the reservoir's surface fluctuation monitoring with the tide gauge, while the depth is always been checked with the sounding operation [10]. There are however two separate tide cycles responsible for the rise and fall surface water bodies; height fluctuations from SPRINGS to NEAPS twice each in a lunar month (29 days) and height oscillations of each tide from high water to low water twice each in each lunar day [10]. Therefore, the principal focus is the to Comparatively study the Temporal Variation and Evaluation of Kainji and Shiroro Hydropower Plant Reservoirs Storage Water Level in Niger State, Nigeria.

2.0 STUDY AREA

The study area comprises of Kainji and Shiroro Hydropower Plants, both located in Niger State of Nigeria, and built in 1968 and 1990 respectively [8]. Constructed on separate rivers of Niger and Kaduna, Kainji is between latitudes 9°50' N and 10°35'N and longitudes 4°26'E and 4°40'E, while

Shiroro is precisely located between the gorge in Longitudes 06° 48′ 30″ and Longitude 07° 08′ 30″ and Latitudes 10° 11′ 00′ and 09° 44′00″ N [2]. The water was harvested into the reservoirs through both the primary (rivers) and secondary (rainfalls) sources, the reservoirs were designed to take 15 x 10^9 and 6 x 10^9Mm water respectively [14]. The state experiences distinct dry and wet seasons with annual rain fall varying between 1,100mm in the northern part to 1,600 mm in the southern parts. The two dams were meant to generate a combined hydropower output of 12,000 megawatts (MW), which is supposed to provide a huge amount of electricity to Nigerians and more than one billion people around her neighborhood uninterrupted. The Mainstream Energy Solutions Limited (MESL) and the North South Company as a power generating companies in 2011 acquired both power dams through the governmental policies of privatization, they were formerly of the Nigeria Electricity Power Authority (NEPA), later changed to Power Holding Company of Nigeria (PHCN) (Mainstream Energy Solutions Limited [13]. The below Figure1 shows the case study areas of the two power stations.

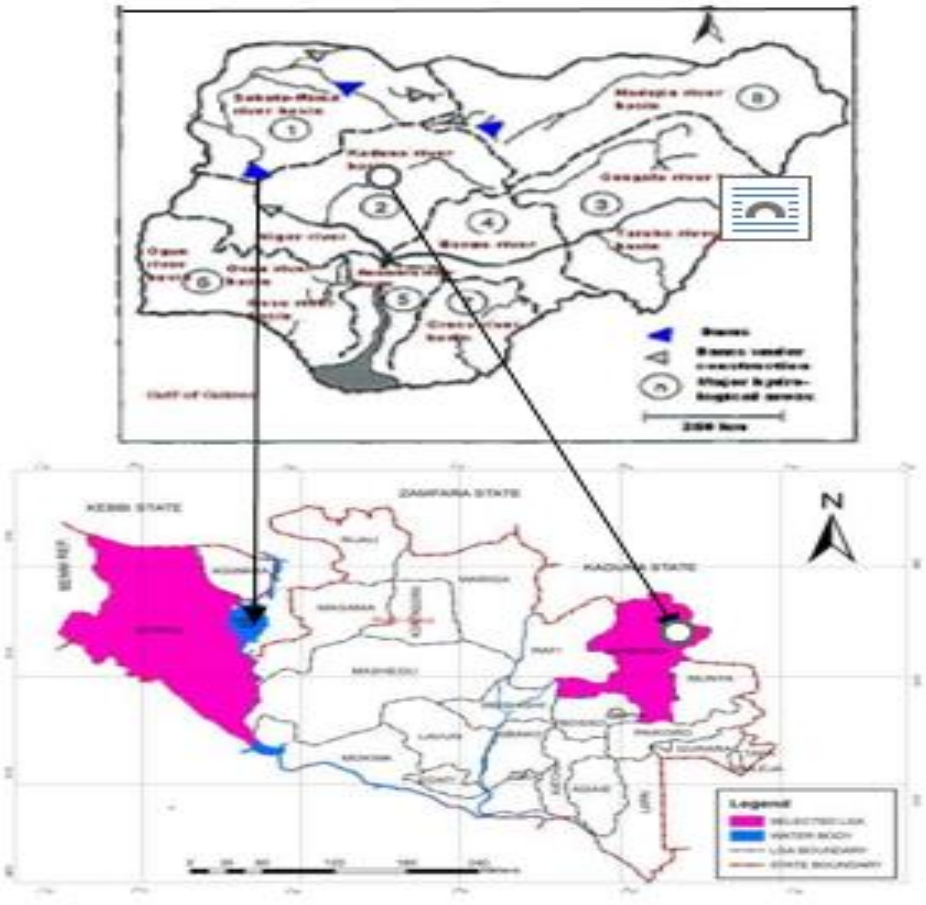

Figure 1: The Map of Nigeria Showing Niger State, Kainji and Shiroro Hydropower Plants

Source: Modified by Ministry of Land and Housing, Minna (2019)

3.0 METHOD AND MATERIAL

The methods used includes generation of both previous and current meteorological data from their respective dam station sites; such as; rainfalls, evaporations and temperatures records. Others are the tide gauge records of about 30 selected each of the fixed tide point around the Kainji and Shiroro hydropower plants to determines the water surface elevation variation across the reservoirs. The dailies records were mathematically processed into months, yearly and into the epochs of ten years intervals covering between 1990 to 2022 on both site stations. Some basic mathematical algorithms, statistical analysis of variance (ANOVA) were further used for the processing, analysis, observations variations and presentation of the results. The comparative studies of the rise and fall of the water surface level follows

Height Difference Method consisting of a very simple procedure for determining mean high water with required water level observations from 30 high tides and mean the high tide was computed for the 30 high tides observations at the control and at the subordinate stations with;

$$MHWs = HWs - (HWc - MHWc) \quad \ldots\ldots (1)$$

MHWs = Computed mean high water at subordinate tide station HWs = Observed high water at subordinate tide station HWc = Observed high water at control tide station MHWC = Published (by NOS) mean high water at control tide station. Previous data of temperature, evaporation and rainfalls were extracted from 1990 to 2022 in same epochs to observe their impact on the fluctuation sizes and shape of the water in the reservoir viz and viz the surface tide gauge elevation measurements. Table 1 below shows the dam's construction specification parameters used as a comparative parameter with the ones observed and computed from the field.

Table 1: Silent Feature / Design Parameter Specification of Kainji and Shiroro dams

Kainji HEP Dam		**Shiroro HEP Dam**	
Reservoir Variable	Value	Reservoir Variable	Value
FYOP	1968	FYOP	1990
RFSC (Mm^3)	15,0 x 10^9	R. Total Storage Cap. (m^3)	6.00 x10^9
Max Reservoir flood level (m)	143.50	Maxi Oper Reservoir Elevation (m)	382.0
Min Reservoir flood level	132.00	Min Reservoir flood level	360.00
Mx HE (m)	141.7	Dam width at its Roe (m)	300
Latitude	9°50' N	06° 48' 30" N and 07° 08' 30" N	17
Longitude	4°40'E	10° 11' 00"E and 09° 44' 00" E	32

Source: Collected from the two-dam sites 2020

3.1 Field Data Capturing Procedure and Tide Guage Measurements

Table 2 and 3 below shows the various data extracted from the dam's sites meteorological and hydrological data centers which includes; previous and current dailies observations and measurements as computed into different table rows and columns into monthly, annual and epochs. The data include the tide gauges, the temperature, rainfalls and evaporations, the water inflow and the turbine water usage were also considered. For example, the maximum tide gauge of the reservoir elevation water top surface level at the KHPP should not go beyond 141.7(m), while that of SHPP should not be more than 382.0m. The minimum from the tail race should not below 132.00m and 360.00 for the both dams respectively.

4.0 RESULTS AND DISCUSSION

Table 2 below shows the results of the data obtained and processed from Kainji Hydropower plant in their different rows and columns as followed; Column 1 represents the years of occurrences, columns 2 and 10 indicates the tide gauge mean measurements for the beginnings and ends of the daily, monthly and annual readings. The columns 3 and 4 showing the mean water inflow from the primary(river) and secondary (rainfalls) sources into the reservoir respectively. Others includes columns 5 the summations of the water from the primary and secondary sources together, while the columns 6 and 7 and 8 stands for the average turbine usage across the periods under review, the average evaporation and the temperature occurrences throughout the study period. While the column 9 constitute the water retains after the turbine usage, evaporation and the temperature actions respectively. The rows 2002, 2012 and 2022 on the table in red colour shows the performances of all the variables at the ends of each of the ten years intervals of the epochs.

Table 3 however indicates the summary results in epochs of all the variables in 1993 as only 7.5% of water that enters the reservoir was retained. Likewise in 2002, 2012 and 2022 the retained water was 5.7%, 29.5% and 19.9% respectively. The results shows that huge amount of water often disappeared via different factors ranging from evaporation deus to intense heat (temperature) Climate Change probably and including the usage by the turbine that generate power. The variation implication shows that in 1993

Table 2: The Rainfall, Temperature and Evaporation data Processed and computed form the extracted ones from 1993 to 2022 for Kainji Hydropower Dam

Year	Res Elev Lev(m)	Inflow m^3/s	Rainfall(mm)	Total / Sum (m^3/s)	T/Dis (m^3/s)	Evap (m^3/s)	Temp (^oC)	Retention in Reservoir (m^3/s)	Res E Lev(m)
1	2	3	4	5	6	7	8	9	10
1993	141.51	8741	1015.48	9,756.48	8395	627	37.5	734.48	140.89
1994	140.72	14108	1227.59	15,335.59	7385	568	37.7	7,382.5	141.56
1995	141.71	14336	1098	15,434.00	7275	617	38.2	7,542.0	137.81
1996	138.8	12584	813.25	13,397.25	7470	629	38.9	5,298.25	140.71
1997	141.27	11394	1117.29	12,511.29	5049	652	38.8	6,810.29	140.41
1998	141.49	16287	1249.36	17,536.36	**7740**	**665**	39.4	9,131.36	141.37
1999	141.62	17134	1295.17	18,429.17	8715	636	38.5	9,078.17	141.3
2000	141.15	14193	971	15,164.00	7325	698	38.5	7,141.00	140.81
2001	140.46	14837	982.47	15,819.47	10288	682	39.7	4,849.47	141.6
2002	**141.48**	**12824**	**735.33**	13,559.33	**12099**	**690**	**38.9**	**770.30**	**141.27**
2003	141.28	15506	846.93	16,352.93	9390	674	37.1	6,288.93	141.01
2004	141.64	13722	1183.06	14,905.06	8155	694	36.8	6,055.06	139.44
2005	140.01	12360	1024.43	13,384.43	10093	631	37.3	2,660.43	140.19
2006	140.71	12378	1140.59	13,518.59	10499	647	37.3	2,372.59	141.64
2007	141.66	15335	939.6	16,274.60	9529	630	37.7	6,115.6	139.43
2008	139.3	15940	1078.68	17,018.68	7143	601	36.4	9,274.68	141.04
2009	141.09	14462	1142.44	15,604.44	9338	616	36.1	5,650.40	141.33
2010	141.39	17178	1323.51	18,501.51	11511	645	36.4	6,345.51	140.94
2011	141	15312	1182.55	16,494.55	11730	586	37.3	4,178.55	139.5
2012	**139.79**	**15076**	**1090.74**	16,166.74	**10779**	**612**	**36.3**	**4,775.74**	**140.8**
2013	141.12	16465	783.67	17,248.67	9356	670	35.9	7,222.67	141.43
2014	140.98	12288	1082.8	13,370.80	12103	597	33.6	670.80	140.7
2015	140.29	13968	1053.12	15,021.12	11922	629	33.3	2,470.12	141.2
2016	140.83	16536	1084.56	17,620.56	10810	618	32.7	6,192.56	141.64
2017	141.52	16897	1537.59	18,434.59	10116	624	32.7	7,694.50	141.38
2018	141.52	17225	1242.2	18,467.20	7931	583	32.7	9,953.20	141.38
2019	141.51	17161	1818.95	18,979.95	6563	606	32.4	11,810.95	141.58
2020	138.74	19296	3223.2	22,519.20	4116	689	32.7	17,714.2	141.72

2021	141.12	16128	1113.68	17,241.68	12422	700	33.4	4,119.68	140.94
2022	140.98	17917	1168.59	19,085.59	14604	685	32.8	3,796.59	139.5

Source: Author's Field Work 2022

(a) Formulars Used

Total Sum Water into Reservoir (5) (m^3/s = Inflow (3)(r) (m^3/s) + Rainfall (4) (mm)…….. (2)

Retention in the reservoir (9) = Tootal Sum (5) (m^3/s) – (Turb Disch (6) (m^3/s) + Evapo (7) (m^3/s) ……..…….. (3)

Percentage Retained (%) = $\frac{\text{Retention in the reservoir (9) (m3/s)}}{\text{Total Sum (3) (m3/s)}}$ *100……. (4)

Variant in Res Water Surf Elev (11) = Tide Guage @ Beg (2) – Tide Guage @ the end of Period (10) ……..... (5)

(b) Summary Results in Epochs

Table 3 below however indicates the summary the results in epochs of all the variables in 1993, 2002, 2012 and 2022. In 1993, only 7.5% of water that enters the reservoir was retained. Likewise, in the in 2002, 2012 and 2022 the retained water between the inflow and outflow varies with 5.7%, 29.5% and 19.9% in the reservoir respectively. This result shows that huge amount of water often disappeared via different factors ranging from evaporation due to intense heat (temperature) Climate Change, turbine use, flood, spillages etc. But been replaced unequally through the continues inflow and annual rainfalls in the cycle other.

Table 3: Summary Results in Epochs

Year	**Res Elev Lev**	**Inflow m^3/s**	**Rainfall(mm)**	**Total / Sum (m^3/s)**	**T/Dis (m^3/s)**	**Evap (m^3/s)**	**Temp (°C)**	**Retention in Reservoir.**	**Res E Lev**	**Variation in Elev**
1	2	3	4	**5**	6	7	8	9	10	11
1993	141.51	8741	1015.48	9,756.48	8395	627	37.5	734.48	140.89	0.62
2002	141.48	12824	735.33	13,559.33	12099	690	38.9	770.30	141.27	0.21
2012	139.79	15076	1090.74	16,166.74	10779	612	36.3	4,775.74	140.8	-1.01
2022	140.98	17917	1168.59	19,085.59	14604	685	36.8	3,796.59	139.5	1.48

Source: Author's Field Work 2022

4.1 Kainji HPP Sample Results of Variations in Epochs in Charts Format

The below figures are the effects of difference factors responsible for various variations in the study in different epochs Figures 2, 3 & 4 below shows samples of sea wave in various fluctuation mode on the surface of the KHPP reservoir's first, second and third epochs; 1993 – 2002, 2003 – 2012 and 2013 – 2022 respectively. Figure 4 shows monthly effect of evaporation on the reservoir surface throughout the study periods. Figure 5 shows effect of rise and fall on the reservoir water body due temperature and evaporation and in turn causing increases and decreases variation in storage capacity in 30-month under study.

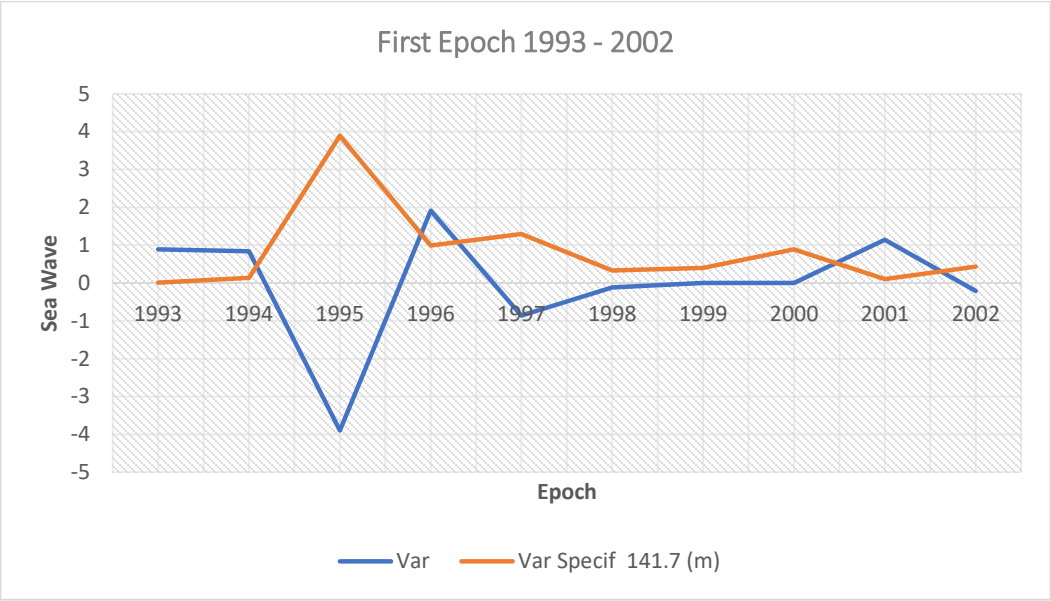

Figure 2. Sample of Sea Wave in the First Epoch 1993 - 2002

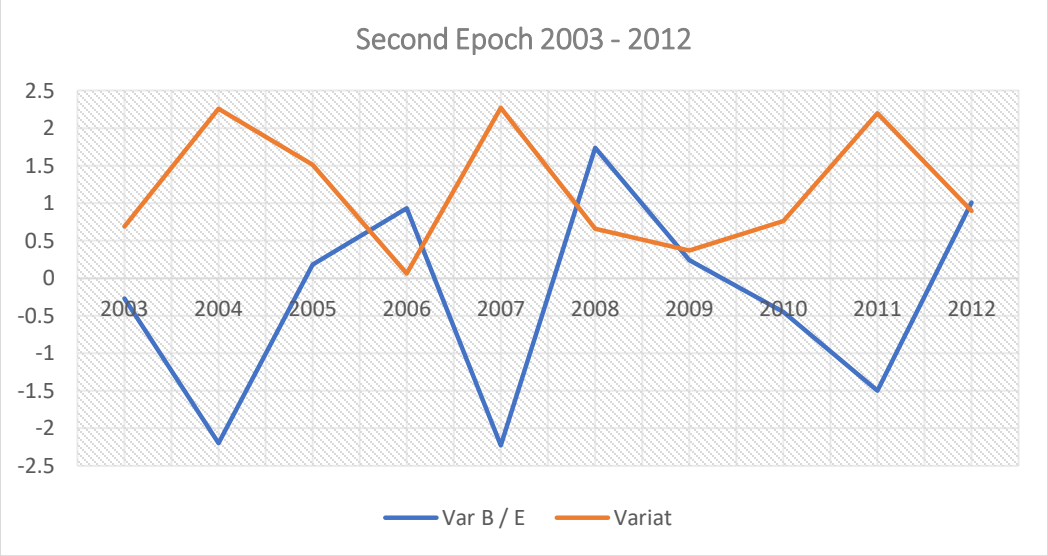

Figure 3. Sample of Sea Wave in the First Epoch 2003 - 2012

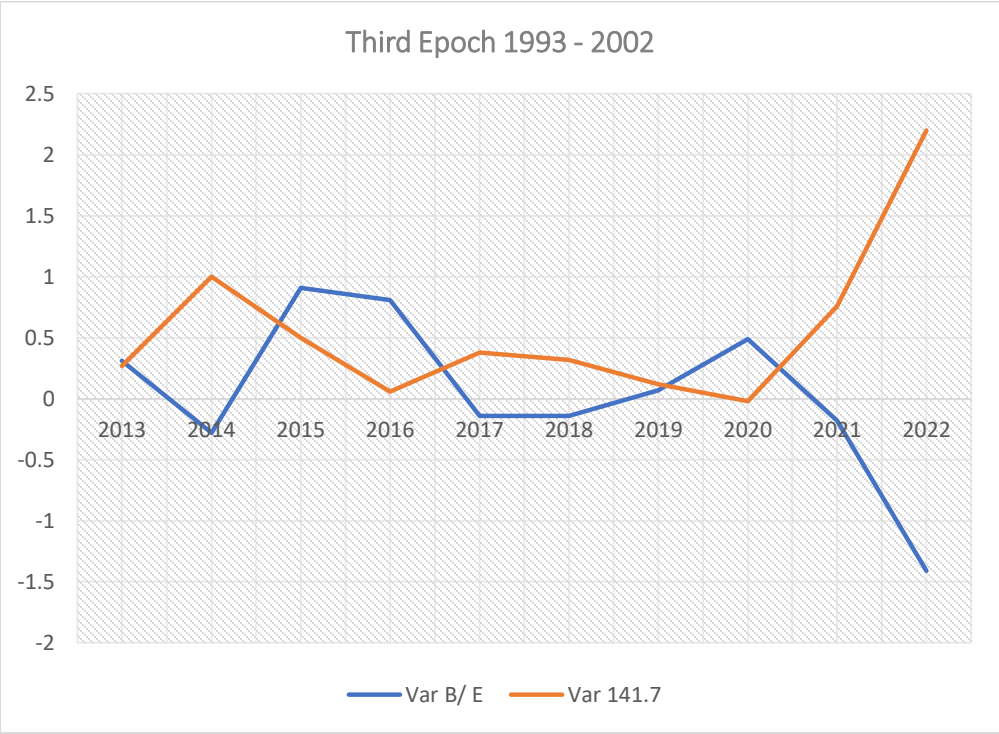

Figure 4. Sample of Sea Wave in the First Epoch 1993 – 2002

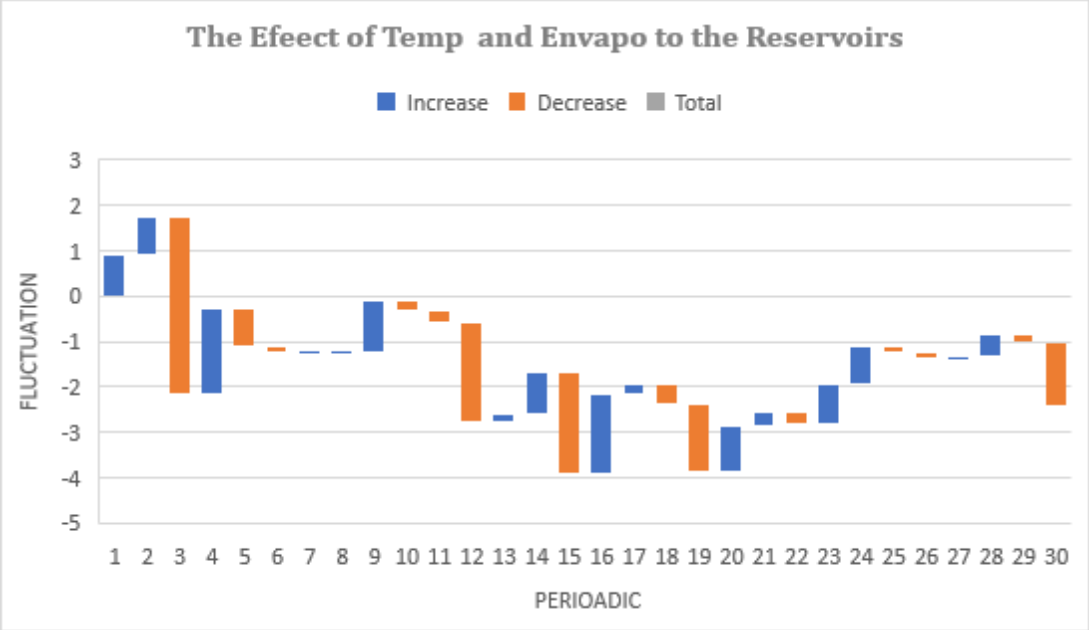

Figure 5. The Effect of Temperature and Evaporation in 30-month Temperature

4.2 Shiroro Hydropower Plants

Table 4 below shows similar results for similar procedure but for the Shiroro hydropower plant data station with the same manner of entries into row and column with the same types of

headings. Column 4 and 7 has some few no records (NRC) data for the rainfalls and evaporation measurements. The rows 2002, 2012 and 2022 on the table are in red colour to indicates the ends of each epoch. The Table 5 represents the summary of results for the three epochs for Shiroro Station with additional column 11 for the mean variations in tide measurements at the ends of the each of the epochs similar to Table 3.

Table 4. The Rainfall, Temperature and Evaporation data Processed and computed from the Extracted ones from 1993 to 2022 for Shiroro Hydropower Dam

Year	B of RSML (m)	S/T Inflow Primary Source	Rainfall Secondary Source (mm)	Turbine Disch (m^3s)	Sum/Total outflow m^3/s)	Evapo (m^3s)	Tempe ^oC	Retention	E of RSL (m)
1	**2**	**3**	**4**	5	**6**	7	**8**	**9**	**10**
1993	377.3	2,600.734	771.74	7,200	3,372.47	NRC	22.27	3,827.53	378.5
1994	374.2	109,366	732.17	4208	110,098.17	NRC	22.27	105,890.17	380.4
1995	377.4	86,948.5	739.57	12,511	87,688.07	NRC	26.40	75,177.07	379.4
1996	375.2	112,756	733.15	5,573	113,489.15	NRC	22.32	107,916.15	379.7
1997	375.4	90,437	NRC	5616	90,437	NRC	22.56	84,821	381
1998	377.7	104363	NRC	12632	104363	NRC	22.83	91,731	376.3
1999	371.9	89626	NRC	5436	89626	NRC	22.73	84,190	378.7
2000	373.4	99657	NRC	6499	99657	NRC	22.27	93,127	379.5
2001	370.6	105978	NRC	7544	105978	NRC	26.4	98,434	379.0
2002	379.2	117638	NRC	7235	90,437	3713.057	26.33	83,202	378.9
2003	375.5	105137.1	715.03	9024	105,852.13	24454.31	23.59	96,828.13	378.8
2004	373.5	114374.3	734.43	6989	115,108.73	3129.15	27.79	108,119.73	374.5
2005	378.4	113,235.2	717.56	2787	113,952.76	3214.52	28.37	111,165.76	377.1
2006	372.2	109734.3	131.90	1113	109,866.2	3037.77	28.51	108,753.2	378.9
2007	375	143783	101.48	6763	143,884.48	2823.39	27.98	137,121.48	372.9
2008	379.2	97631	705.94	7786	168,225.00	5618.38	24.94	160,439	378.6
2009	374.4	79861.5	755.48	7054	80616.98	3571.36	25.03	73,562.98	377.8
2010	372.1	125042.4	742.4	5489	125,784.8	3676.06	27.7	120,295.8	374.7
2011	370.3	94410	739.52	5654	95,149.52	7479.14	25.67	89,495.52	376.6
2012	378.7	95747.3	739.29	7944	96,486.59	3769.02	28.12	88,542.59	378.5
2013	374.6	133885.2	724.59	3167	134,609.79	3530.99	27.46	131,442.79	380.3
2014	375.7	134633.2	726.95	8597	135.360.15	3338.78	27.36	126,763.15	378.5
2015	378.2	119171.6	769.58	1864	119,941.18	3464.647	27.01	118,077.18	376.5
2016	373.3	160621	707.81	6484	161,328.81	3249.16	25.73	155,457.18	377.2
2017	379.5	103665.5	749.29	6330	104,414.79	3640.24	25.78	98,084.79	377.5
2018	378.7	93589.2	726.46	790	94,315.66	3915.05	27.48	93,525.66	374.4
2019	371.9	144126.4	753.53	3237	144,879.93	3741.31	25.68	141,642.93	375.0
2020	371.5	129485.2	722.79	4085	130,207.99	4540.13	25.3	126,122.99	378.5
2021	371.7	111955.6	763.37	12597	112,718.97	4588.81	26.8	100,121.97	373.8
2022	**375.9**	**165936.2**	**827.51**	**7200**	**166,763.71**	**3945.12**	**31.51**	**101,525.66**	**374.8**

Source: Author's Field Work 2023

Table 5: Summary of Results

Year	B of RSML (m)	S/T Inflow Primary Source	Rainfall Secondary Source (mm)	Turbine Disch (m^3s)	Sum/Total outflow m^3/s)	Evapo (m^3s)	Tempe °C	Retention	E of RSL (m)	Variation in Elev (m)
1	**2**	**3**	**4**	5	**6**	7	**8**	**9**	**10**	11
1993	377.3	2,600.734	771.74	7,200	3,372.47	NRC	22.27	3,827.53	378.5	-1.2
2002	379.2	117638	NRC	7235	90,437	3713.057	26.33	83,202	378.9	0.3
2012	378.7	95747.3	739.29	7944	96,486.59	3769.02	28.12	88,542.59	378.5	0.2
2022	375.9	165936.2	827.51	7200	128264.9	3754.057	31.51	38,498.81	374.8	1.1

Source: Author's Field Work 2023

Shiroro HPP Reservoir Water Variation Evaluation in Chart Format

Figure 6, 7 and 8, shows the effect of rise and falls of sea wave on the Shiroro reservoir water body. The variation between given specification parameter and the measured, the leading to increasing and decreasing in the water storage capacity of the reservoir. Figure 9 and 10 represents sample of the second and third epochs on Shiroro HPP reservoir water body fluctuation leading to increasing and decreasing in the storage capacity.

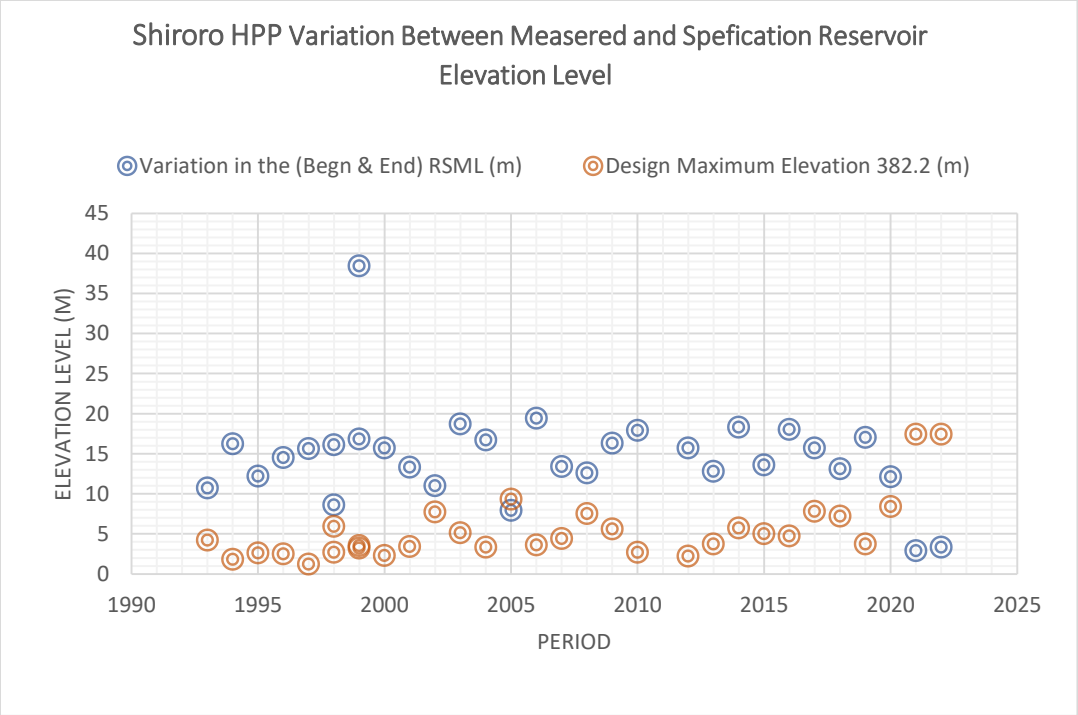

Figure 6: Shiroro HPP Variation Between Measured and Speciation Reservoir Elevation Level

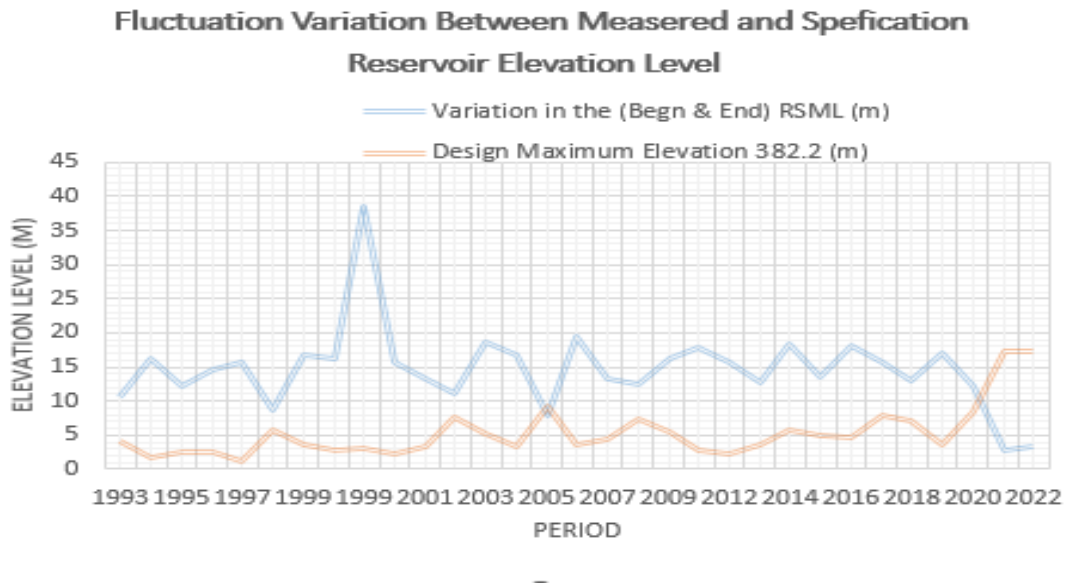

Figure 7: The Effect of Rise and Falls of Sea Wave on the Shiroro Reservoir Water Body

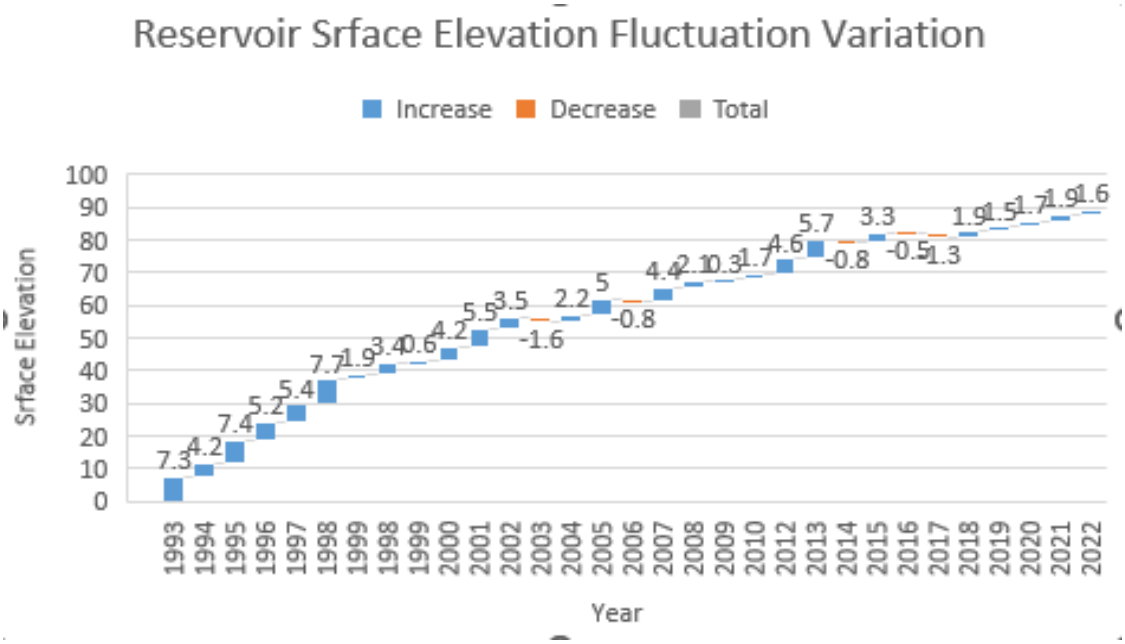

Figure 8: The Effect of Rise and Falls of Sea Wave on the Shiroro Reservoir Water Body Leading to increasing and decreasing in the Storage Capacity

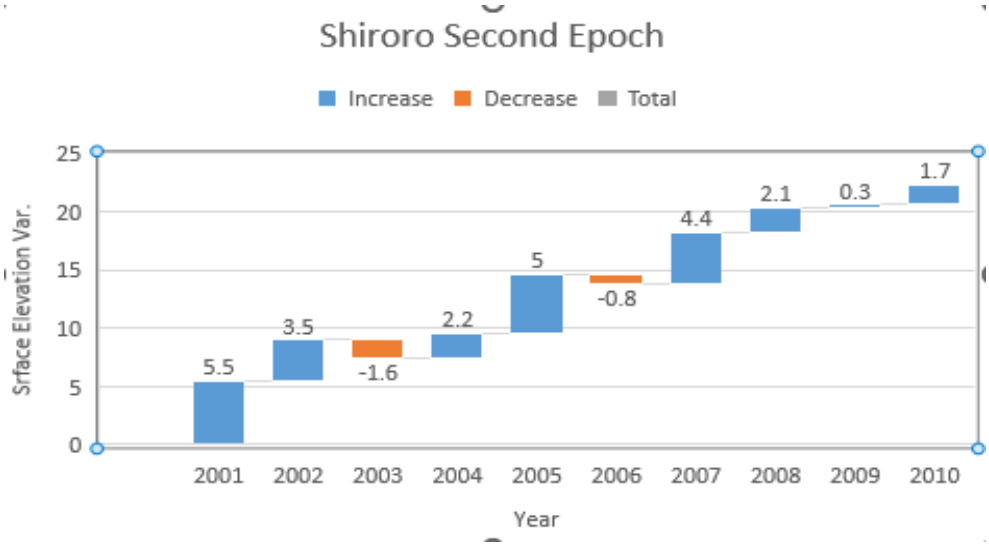

Figure 9: The Sample of the Second Epoch on Shiroro Reservoir Water Body Leading to increasing and decreasing in the Storage Capacity

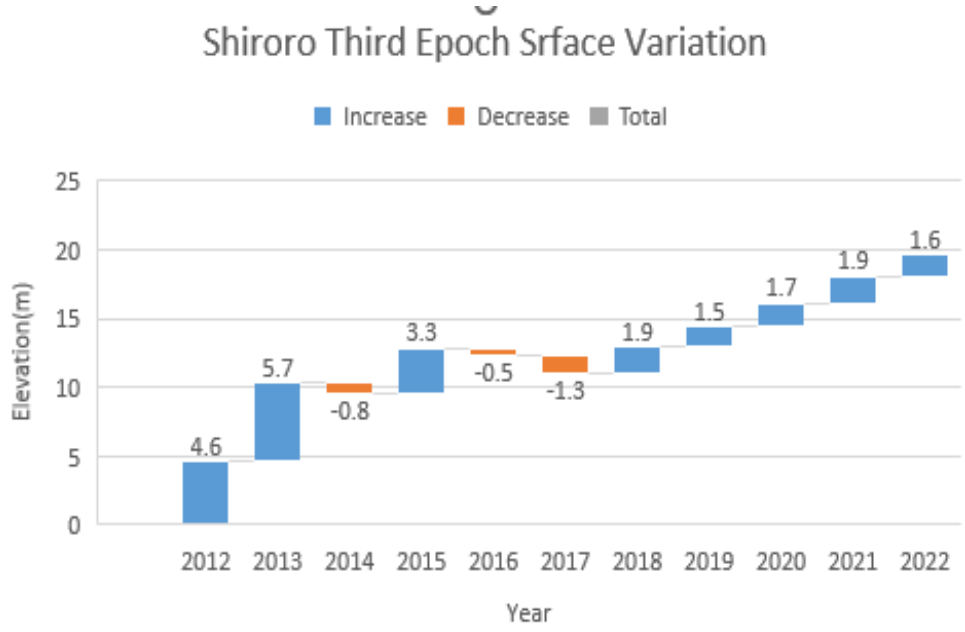

Figure 10: The Sample of the Second Epoch on Shiroro Reservoir Water Body Leading to increasing and decreasing in the Storage Capacity

5.0 CONCLUSION AND RECOMMENDATION

The comparative temporal variation evaluation study of Kainji and Shiroro hydropower plant reservoirs actually shows how the primary (river) and the secondary (rainfalls) water sources influence the quantities (increases) of water that goes into the reservoirs. On the other hand, evaporation tend to gradually drain the water at the surface via intense heat from temperature through the global climate change. Though the rate of the water moving into the pool of the

reservoir continuously is inconsistently constant to completely compensate the loss of water throughout the season. As the annual rainfalls often increase the quantity of water and even increasingly overwhelmed the reservoir to the brim at some instant with long protracted heavy rainfall leading to excessive erosion, flooding and with abnormal spillages on the dam. The overwhelmingness of the rainfall often attracts sediment, silts and other hydrological debris into the bottom of the reservoir and reducing the storage from the bottom while the evaporation does dry water from the surface.

The two selected dams are however victims of all the above scenario and irregular retention and retraction of water in and out of the reservoir. The fluctuation experience through the rises and fall continue to impact the increasing and decreasing experience in the body of water. Tide gauges are them used for the measurement of the water level daily at the strategically locations. The two-reservoir evaluated shows significant loss of water into evaporation in the three epochs that made up the thirty (30) months investigated. The average tide observed at the end of the first (2002) epoch shows the variation as 0.21m, temperature 38.9^{o}C and evaporation 690m^{3}s, the second epoch (2012) shows -1.01m as the average tide, the temperature 36.30^{o}C and evaporation 612m^{3}/s. While the third and the last epoch (2022) indicates; the average tide of the water level as 1.48m with the temperature and evaporation mean of 36.8^{o}C and 685m^{3}/s respectively. The overall cumulative effects of all the above was a significant rise and fall in the reservoir's water surface level and in turn responsible for the inconsistence between the water inflow and outflow quantity producing the power in the turbine. Samples of graphical charts and bar charts are also used to show the different variations as it affects mean; months, annual and ten years intervals of epochs. The average of 141.83m maximum water elevation surface level (MWES) as against 141.72m for designed specifications was observed, 136.7m minimum as against the 132m from the designed specification. The climax temperatures at the two station that often resulted into occasional excessive evaporation ranges between months of February, March, April and part of May leading the temperature to rise between 38^{0} – 41^{0} C and aiding the drain of water from the reservoir.

5.1 Recommendations

Recommendations, since all the temporal variation studied here do contribute negatively and increasing water lost from reservoirs. Efforts should be made toward continues use of both the previous and current data to monitor the reservoir stream wave throughout the season. More tide gauges should be constructed from the entrance (intake of the reservoir) upstream. Since the turbine generating power dependent practically on water, active measure should be put place to guide against low lowest water (LLW), and high highest water (HHW) to also safe the dam from frequent spillages.

References

[1] Agbonkhese, O (2014), Flood Menace in Nigeria: Impacts, Remedial and Management Strategies; Nigerian Building and Road Research Institute. *Civil and Environmental.org Research*. Vol.6, No.4, 2014.

[2] Akanmu J. O., (2007), Model for the optimal operation of shiroro reservoir, PhD thesis University of Lagos, Akoka. Nigeria. * Management at Shiroro hydropower dam, Nigeria. *An International Journal of Science and Technology*. Vol. 3(2), No 7, pp. 18-30

[3] Akinwale A. S. & Thompson A. D., (2020). Geospatial Analysis of Shiroro Dam Reservoir Water Storage, *Journal of Science & Technology*, Publisher: National Science & Technology Forum College of Science and Technology (CST) Karma Polytechnic (pp 41-51). JOS & T VOL, 1 No 5 2020 ISSN: 1595 – 0311.

[4] Akinwale A. S., Musa A. A., and Ibrahim M. (2021). Determination of the Approximate WaterDepth Variation (WDV) between the Reservoir Bed Floor (RBF) and the Water Surface Area (WSA); A Case Study of Kainji Hydropower Dam Kainji, Niger State. Nigeria - *LASU Journal of Engineering, Science and Technology* 2 (3), Jan. 2021 ISSN: 2734-2204.

[5] Akinwale, Akinsola Solomon and Maikano Samson (2019). Geospatial Evaluation of the Nigeria Dam Reservoirs Water Storage Capacity and Optima Power Generation, Presented at 54th annual general meeting and conference Nigeria Institution of Surveyors (NIS) / Annual. Theme: "National Mapping Infrastructure and Geospatial Technologies in Monitoring Disasters for Sustainable Development" 17th – 21nd June, 2019. Anambra State. Nigeria

[6] Akinwale, Akinsola Solomon, Aleem K.F. and Ibrahim Mohammed (2016). Nigeria Drying Water Bodies: A Case study of Kiri Dam Shelleng Local Government Area Adamawa State. Presented at 51st Nigerian Institutions of Surveyor Annual General Meeting (AGM) 2016, Oshogbo, Osun State. Nigeria. www.agm2016.nisagm.net Theme: "Beyond Mapping" Integrating Geospatial Solution for Sustainable Urban and Rural Development in Nigeria. 23 - 27 May, 2016.

[7] Al-Ansari, N. A. and Knutsson, S. (2012). Reduction of the Storage Capacity of two Small Reservoirs in Jordan. *Journal of Earth Sciences and Geotechnical Engineering*, vol. 2, no. 1, 2012, 17-37, pp18- 19 International Scientific Pres. Accessed 04/04/2015. *

[8] BRLi & DHI (2007), Establishment of a water management model for the Niger River Basin. Final Report (= document Rapport_final_Corps-rapport_anglais.pdf)

[9] Ehigiator, M. O, Oladosu O. S, and Ehigiator – Irughe I. R., (2017), Determination of volume and direction of flow of kainji reservoir using hydro-geomatics techniques Nigerian Journal of Technology (NIJOTECH) Vol. 36, No. 4, October 2017, pp. 1010 – 1015

Copyright© Faculty of Engineering, University of Nigeria, Nsukka, Print ISSN: 0331-8443, Electronic ISSN: 2467-8821 www.nijotech.com http://dx.doi.org/10.4314/njt.v36i4.3 Access Date: 04/03/19

[10] International hydrographic Organization (IHO) (2005), Manual on Hydrographic Publication M- 13 1st Edition Published by the International Hydrographic Bureau 4, Quai Antoine 1er B.P. 445 - MC 98011 MONACO Cedex Principauté de Monaco Telefax: (377) 93 10 81 40 E-mail: info@ihb.mc Web: www.iho.shom.fr http://www.africasia.com/archive/na/99_01/naam0101.htm Installed capacity: www.livingproofbiblechurch.org 2009-07-25. Retrieved 2009-08-01.

[11] Lawson S (2014): Coastal Erosion Nigeria Africa Urban Development Planning Residential Land Development. Edited By: C. Wilborn and Last Modified Date: 28 July 2014

[13] Mainstream Energy Solutions Limited (MSESL), (2019), Mainstream Energy to hit 1,300 Mw for Direct supply https://www.hydropower.org/companies/mainstream-energy-solutions-limited

[14] Mohammed J Mamman1, Otache Y Matins and Jibril Ibrahim (2018), Analysis and Characterization of Kanji Reservoir Inflow System, CRIMSON Publishers, http://www.cimsonpublishers.com. Access date 05/11/19. Discharge and water intake of River Niger https://www.nigerianstat.gov.ng/ and http://int.search.myway.com/search/GGmain.jhtml?searchfor=Bureau+of

[15] NOAA (2014): National Ocean and Atmospheric Studies USA, Office of Ocean and Coastal Resource Management. http://oceanservice.noaa.gov/tools/czm/welcome.html

GEOSPATIAL MAPPING FOR EFFECTIVE PUBLIC INFRASTRUCTURE: A SCENARIO OF BUS STOPS IN AKURE SOUTH, ONDO STATE, NIGERIA

Tata H[1]., Olaoye C. A[2].

[1]Department of Surveying and Geoinformatics, Federal University of Technology Akure, Ondo State Nigeria.

[2]Department of Surveying and Geoinformatics Leadcity University Tollgate, Ibadan, Oyo State

Corresponding author: htata@futa.edu.ng

Abstract

The bus stop is a designated place where buses stop for passengers to board and alight from. This study aims to carry out geospatial mapping of bus stops for effective public infrastructure: a scenario of bus stops within the study area. The study employs the method of Geographic Information Systems (GIS) as a tool to determine the spatial distribution pattern. A total of 73 bus stops were located within the study area. The hand-held GPS map 76 CSX was used to acquire data (coordinates) for all the bus stops. Attribute data used in the study were collected from the Ministry of Transportation, while the base map was downloaded from Google Earth. ArcGIS 10.3 software was used for the study, and a database was created while different types of queries were performed based on the attribute data obtained. Two different methods were used for spatial distribution: the Quadrat method and the nearest neighbour method. The result of the spatial distribution performed on the quadrat method gives a mean of 0.081111, a variance of 2.78145, and a variance/mean of 3.432507, while that of the nearest neighbour gives a z-score of -9.84310 and a p-value of 0.00000. Furthermore, proximity between the bus stops, buffer at 300 m, and density analysis were carried out. The result obtained from the two methods shows that the bus stops located within the study area were clustered. Therefore, it is concluded that the mapping and spatial distribution of bus stops should always be carried out.

Keywords: Bus Stops, Geospatial Mapping, Infrastructure

1.0 INTRODUCTION

A bus stop is a designated place where buses stop for passengers to board or alight from and is a vital component of a successful transportation system [4]. Bus stops play an important role as they serve as transit service points of contact between the passenger and the bus [10]. These are normally positioned on the highway and are distinct from off-highway facilities such as bus stations. The construction of bus stops tends to reflect the level of usage. Stops at busy locations may have shelters, seating, and possibly electronic passenger information systems; less busy stops may use a simple pole and flag to mark the location [4]. Bus stop design and location are recognized as crucial elements in the drive to improve the quality of bus services and public transport in general and also to meet the required convenience and comfort of bus stops, just as the [2] stressed their high level of importance. Any urban area must have effective and well-

planned public infrastructure to operate efficiently. An efficient public infrastructure system is essential for ensuring commuters' accessibility, connectivity, and comfort in the context of transportation. An effective tool for improving public infrastructure, such as bus stops, is provided by geospatial mapping in conjunction with data analysis.

The process of geospatial mapping entails the gathering of pertinent information on current bus stops, the examination of spatial patterns and variables affecting their placement, and the visualization of this data on maps to aid in comprehension and decision-making. Key information on the distribution of bus stops, their closeness to population centres, the demand for transportation, and accessibility to significant facilities like schools, hospitals, and commercial districts can be obtained by geospatial analysis. The management of traffic and congestion depends heavily on bus stops, which are an essential part of the transportation infrastructure [1]. The design and placement of bus stops are acknowledged as key components in the effort to enhance the quality of bus services and public transportation in general. The term "Total Journey Quality" refers to the idea that all parts of the journey must be taken into account, including the fact that bus passengers are also pedestrians at both ends of the bus trip. It is important to consider the comfort and convenience of bus stops [2]. However, the difficulties that make bus use in Nigeria ineffective include illegal parking, abandoned vehicles, and cramped bus stops [11], as well as the un-spacious nature of bus stops in Nigeria, which impedes traffic flow along them. These challenges are more prevalent within the city of Lagos [8].

In Nigeria and the world over, there is no denying the fact that transportation is essential to the fabric of urban life, as it enhances the quality of life of the citizens and delivers dividends to the entire populace. The basis of this assertion is not farfetched, as the study conducted in this context by [7], affirms that the quality of life of its citizens is heavily dependent on the efficiency and effectiveness of its transportation system. As good as the system is, there are also some identified menaces to it. As such, public transportation is regarded as an essential system that helps curb the menace of transportation. The latter is diversified, and each of its components is highly pertinent to the delivery of a sustainable transport system. Among the components or factors that need to be considered for the proper implementation of the public transport system are bus stops and bus stations.

Further study by, [5] stated that to increase urban mobility, bus stops and articulated bus services must be placed in the best possible locations. By doing so, both those who utilize public transportation and those who own private vehicles will be encouraged to do so. As a result, there may be fewer private vehicles on the road, which would ease traffic and delay. In addition, research done in this area by [9], showed that the demise of established public transportation networks has sparked a rapid rise in non-traditional modes of transportation, originally provided by minibuses, shared taxis, and vans, and more recently by commercial motorcyclists.

It is important to keep in mind that bus stops are geographically positioned in various places for various reasons; as a result, using spatial optimization to support strategic planning can help

improve current service. Given precise restrictions on the number of stops to be located, choosing new service stops that will allow access to places that do not already have enough access to a facility for servicing vehicles. The location of a bus stop is heavily influenced by the volume of traffic in a particular area. This study intends to utilize the proper tools to evaluate the spatial distribution and mapping out of bus stops in the study region. The problem of the spatial distribution of bus stops necessitates the use of digital mapping and Geographic Information Systems (GIS). To evaluate policy objectives and make future improvement plans, it is essential to measure the performance and efficacy of public bus transportation [6].

2.0 STUDY AREA

The study area selected for this research is Akure Environs in Ondo State, in the South-Western part of Nigeria. The geographic location is approximately between Latitudes 07°15'N to 07°30'N and Longitude 05°15'E to 05°25'E. The topography of the Basement Complex terrain of Akure is generally undulating with a virtually rugged terrain consisting of hills and valleys, with field recorded elevation varying between 330m above mean sea level in the south-western border (Nigeria Army barracks) and 399 m in the north-eastern border (Shagari Estate) [12].

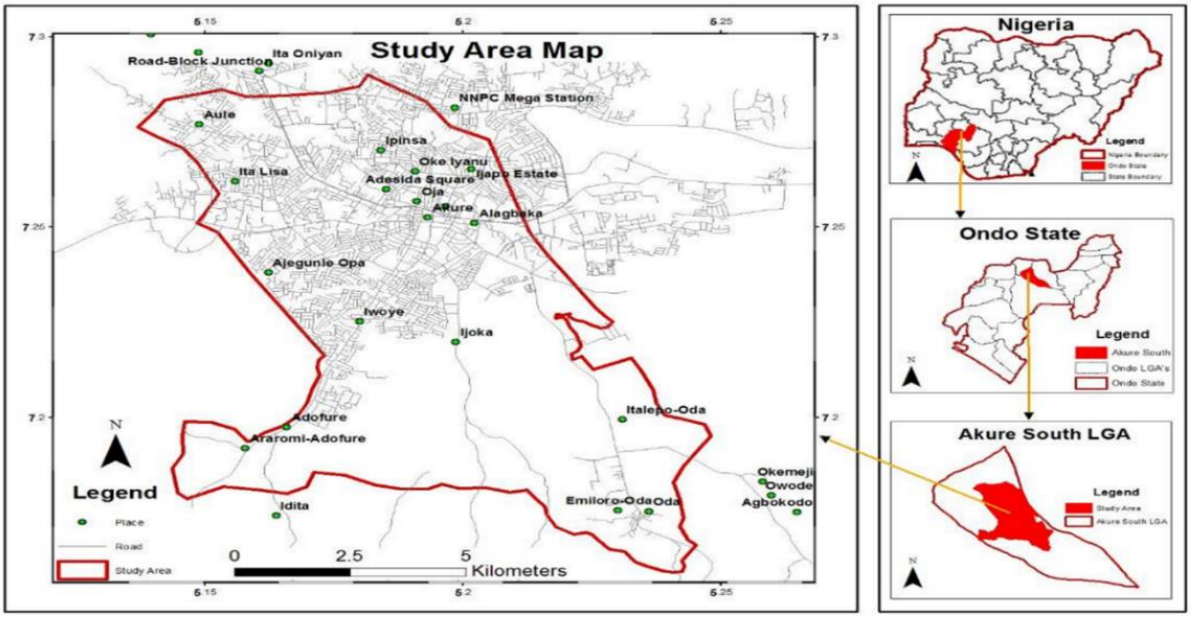

Figure 1: Study area map of Akure environs

Source: (Tata and Ono, 2018)

3.0 METHODOLOGY

The attribute data (names and locations of the existing bus stops) were obtained from the Ondo State Ministry of Transportation. The Google Earth Imagery of the study area was clipped out of Google Earth to derive the base map through the digitizing process. The geographic coordinates

of the existing bus stops were picked primarily from the field, geocoded, and integrated into the base map using ArcGIS Pro. A GIS database was created, and the spatial and attribute data were encoded and queried (selection by Location and Attributes). Quadrat and Nearest Neighbour using Microsoft Excel 2010 and Arc ArcGIS Pro software, respectively, were used to determine the spatial distribution of the bus stops.

Quadrat analysis is used to estimate how the intensity of a point pattern varies over an area. It is a method suited for investigating first-order effects. The region was partitioned into sub-regions using AutoCAD software of equal area, or quadrats of 1000m by 1000m, and superimposed on the bus stops in ArcGIS. The number of events in each quadrat was used to summarize the spatial pattern.

$$\lambda = {}^{N}/_{A} \quad (1)$$

where,

λ = intensity

N = number of bus stops

A = area

To describe the degree of spatial clustering of point distribution, the nearest neighbour distance method uses the average distance from every point to its nearest neighbour point. Nearest neighbour distances provide an estimate of the presence of spatial dependence among events.

4.0 RESULTS AND DISCUSSION

The variance-to-mean ratio of the event counts in the quadrats was used as a test static for randomness based upon the chi-square frequency distribution. We had a total of 90 quadrats. The test statistic is given by: (sum of squared differences)/Mean

$$\frac{\sum_{i=1}^{n}\left(X_i-\bar{X}\right)^2}{\bar{X}} = \frac{\sum_{i=1}^{n} X_i^2-\left[\frac{(\sum X_i)^2}{N}\right]}{\bar{X}} \quad (2)$$

The values of the test statistics in our cases would be:

$$\frac{307-59.21111111}{0.8111111} = 319.2820914$$

For degrees of freedom: N - 1 = 90 - 1 = 89

Confidence interval 95% = 0.95 = 1- 0.95 = 0.05

The value of the chi-square at the 0.95 level is 79.08.

If the variance-mean ratio is above 1 it is a clustered distribution therefore we conclude that the bus stops are clustered.

Table 1: Bus stops in each quadrat and the intensity

0	2	0	0	0	0	0	0	0
0	2	0	0	0	0	0	3	0
0	0	4	0	0	0	1	0	2
0	0	0	4	5	2	1	1	1
1	2	0	3	5	11	4	2	0
0	0	2	0	1	3	0	0	0
0	0	0	0	0	2	0	0	0
0	0	0	0	0	4	0	0	0
0	0	2	1	0	1	0	0	0
0	0	1	0	0	0	0	0	0
		intensity λ = number of events/Area						
0	0.000002	0	0	0	0	0	0	0
0	0.000002	0	0	0	0	0	0.000003	0
0	0	0.000004	0	0	0	0.000001	0	0.000002
0	0	0	0.000004	0.000005	0.000002	0.000001	0.000001	0.000001
0.000001	0.000002	0	0.000003	0.000005	0.000011	0.000004	0.000002	0
0	0	0.000002	0	0.000001	0.000003	0	0	0
0	0	0	0	0	0.000002	0	0	0
0	0	0	0	0	0.000004	0	0	0
0	0	0.000002	0.000001	0	0.000001	0	0	0
0	0	0.000001	0	0	0	0	0	0
	area = l^2	area = 1000000M^2						

The spatial distribution of bus stops as determined by nearest neighbour analysis shows that it is clustered Figure 2 and the p-value is less than the significance level and the z – score is negative, the bus stops are clustered. The result of both methods shows that the bus stops are clustered.

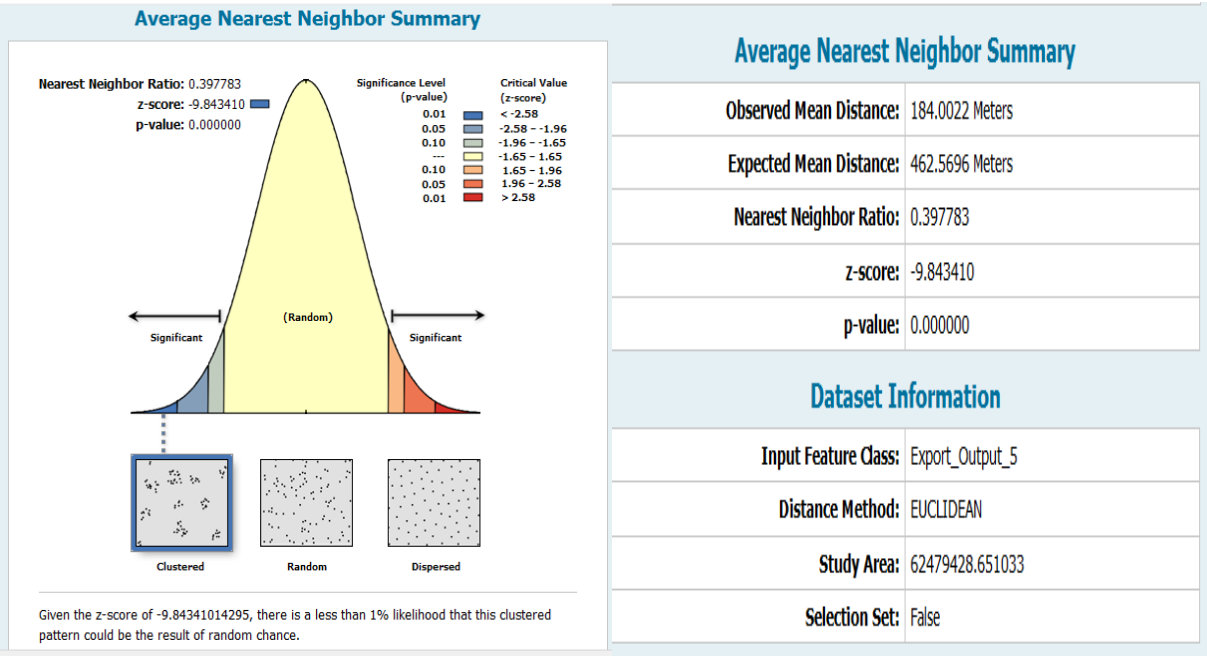

Figure 2: Nearest Neighbour summary

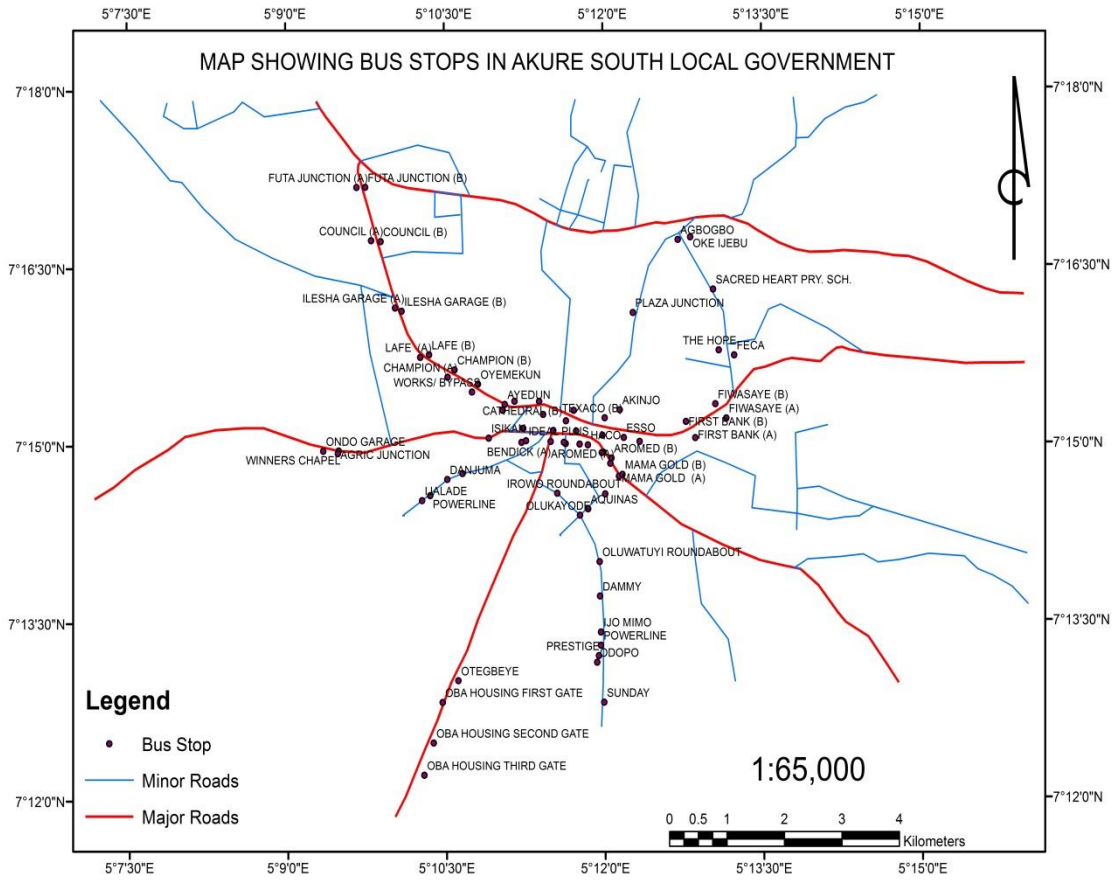

Figure 3: Map showing bus stops in Akure South Local Government

4.1 Proximity Analysis

The spatial join and the Near tool were used to allocate the closest bus stop to each chosen location (such as hospitals, churches, schools, hotels, etc.). Based on spatial proximity, the nearest bus stop attributes to each location in the dataset were linked together using the spatial join. The Near tool was used to conduct a nearby neighbourhood analysis, which involved calculating the distance between each location and its closest bus stop. Equation 1 was used to calculate the travel and walking time (in minutes) between the two nearest bus stops as well as the proximity analysis between the bus stops (Table 1). In this study, 300m was regarded as the maximum permitted walking or travelling distance. Additionally, the permitted walking speed is 4.5 km/h.

$$Walking\ Time\ (T) = \frac{Walking\ Distance\ (km)}{Walking\ Spead\ (km/hr)} * 60\ mins \quad (3)$$

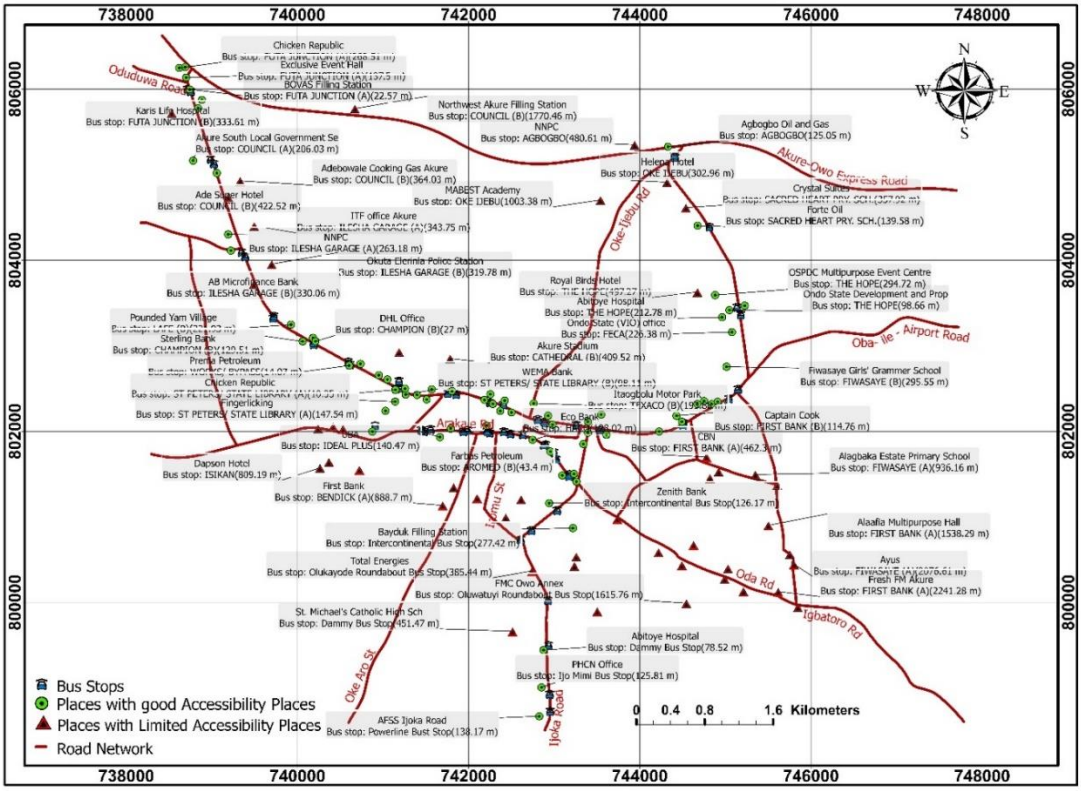

Figure 4: Proximity Analysis Result

The outcome of the proximity analysis is shown in Figure 4. 72 locations were discovered to be just a few minutes' walk from bus stations, indicating adequate accessibility to public transportation. Additionally, 48 locations are far from bus stations, which limits their access to public transportation. In light of this, a location for new bus stops was suggested.

Table 2: Walking time between bus stops

FROM	TO	Walking Distance (km)	Walking Time(mins)
Sammy Store (B)	Sammy Store (A)	0.023086793	0.307823903
Champion (B)	Champion (A)	0.024020824	0.320277657
Mama Gold (B)	Mama Gold (A)	0.025019992	0.333599893
Lafe (B)	Lafe (A)	0.025079872	0.334398299
First Bank (B)	First Bank (A)	0.027294688	0.363929175
Agbogbo	Oke Ijebu	0.027513633	0.36684844
Bendick (B)	Bendick (A)	0.034669872	0.462264955
Health Centre (B)	Health Centre (A)	0.035805028	0.477400368
Works/ Bypass	Oyemekun	0.037735925	0.50314566
Oyemekun	Futa Junction (A)	0.037735925	0.50314566
St Peters/ State Library (B)	Futa Junction (B)	0.045276926	0.603692343
St Peters/ State Library (A)	Council (A)	0.045276926	0.603692343
Futa Junction (B)	Futa Junction (A)	0.047010637	0.626808495
Council (B)	Council (A)	0.06463745	0.861832673
Ilesha Garage (B)	Ilesha Garage (A)	0.06670832	0.889444271

Ideal Plus	Bendick (A)	0.081908486	1.09211314
Texaco (B)	Lafe (B)	0.083216585	1.109554465
Texaco (A)	Champion (A)	0.083216585	1.109554465
Glober Plaza (A)	Glober Plaza (B)	0.083486526	1.113153678
Aromed (B)	Aromed (A)	0.088232647	1.176435294
Ayedun	Council (A)	0.08845903	1.179453734
Cathedral (B)	Council (B)	0.09773945	1.303192661
Cathedral (A)	Ilesha Garage (A)	0.09773945	1.303192661
The Hope	Feca	0.097989795	1.306530605
Haco	Glober Plaza (A)	0.144346805	1.924624061
Post Office (B)	Ilesha Garage (B)	0.153583853	2.047784711
Post Office (A)	Lafe (A)	0.153583853	2.047784711
Fiwasaye (B)	Fiwasaye (A)	0.155621335	2.074951137
Aquinas Bus Stop	Olukayode Round Bus Stop	0.167255639	2.230075192
Powerline Bust Stop	Ijo Mimi Bus Stop	0.202043772	2.693916956
Adegbemile	Champion (B)	0.283853836	3.784717808
Esso	Oyemekun	0.283853836	3.784717808
Intercontinental Bus Stop	Aquinas Bus Stop	0.379671762	5.062290161
Isikan	Futa Junction (B)	0.495654113	6.60872151
Oluwatuyi Bus Stop	Dammy Bus Stop	0.526967953	7.026239371
Sacred Heart Pry. Sch.	Oke Ijebu	0.906073397	12.08097862

4.2 Density Analysis

To visualize the spatial distribution and locate the concentrations of bus stops, Density Analysis was performed. To perform the Density Analysis on the bus stops dataset, which includes the X- and Y- coordinates of each bus stop the “Kernel Density” tool on ArcGIS Pro software was used.

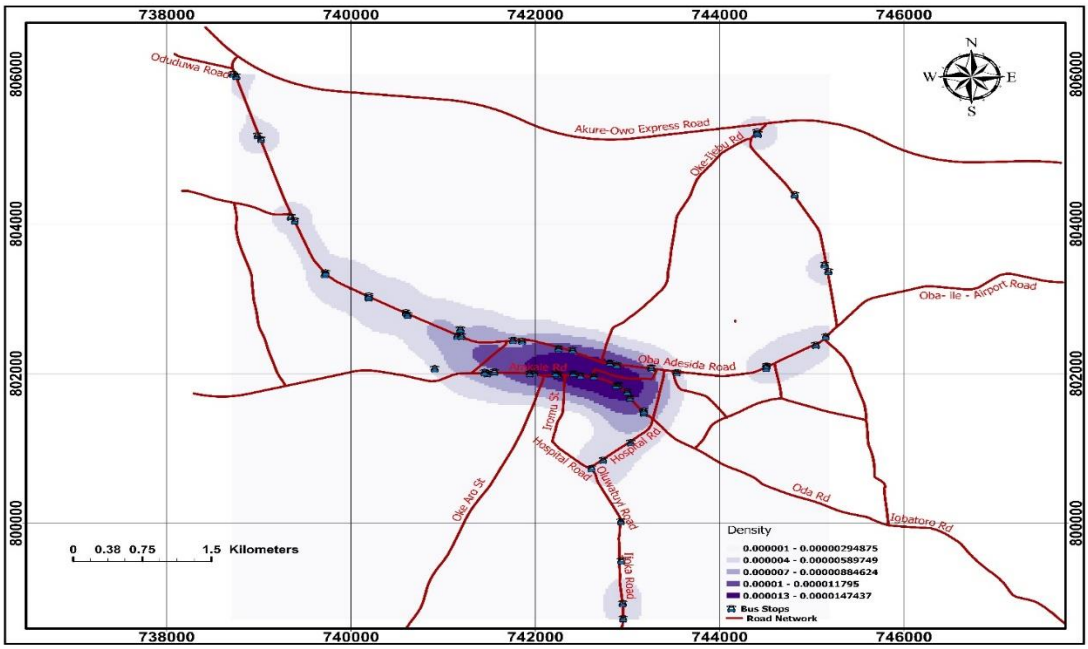

Figure 5: Density Analysis Result

In Figure 5, the density analysis revealed the concentration of bus stops. The result shows that bus stops are unevenly distributed across the study area. Notably, Mixed-use areas (banks, offices, restaurants, hotels, hospitals, petrol stations, etc.) emerged as prominent hotspots. These high-density cluster areas indicate that this area is well supported by public transportation and serves as an attractive destination for transit riders. However, the density analysis also reveals disparities in bus stop distribution. Some routes exhibit lower densities of bus stops, while others exhibit no bus stops. The outcomes of the density analysis provide valuable insights for infrastructure decision-making and urban planning. High-density areas around bus stops demand targeted investment in transportation infrastructure and enhanced transit services. Moreover, the identification of low-density areas underscores the need for expanding public transportation access and improving connectivity for residents. Addressing these planning considerations can lead to well-integrated urban development and more efficient transit systems.

4.3 Buffer Analysis

Buffer analysis involves creating a buffer zone around a point, line, or polygon feature. A buffer zone is a defined area around each feature within a specified distance. In this study, a buffer (which represents a walking distance) of 300 m was created around each bus stop (Figure 5). This is approximately 5 minutes at a walking speed of 4.5 km/hr. This analysis was carried out to give a clearer overview of the places that fall within a 300-meter walkable distance of each bus stop and to determine the area that is mostly in need of bus stops.

The buffer analysis successfully delineated service areas around each bus stop, representing the areas within a reasonable walking distance from the stops, and the result is shown in Figure 6. The result reveals that most places along Oba-Adesida and Arakale, the hospital, Oluwatuyi, and Ijoka Road fall within the coverage of each bus stop. Conversely, the buffer analysis has also revealed areas with limited-service coverage around certain bus stops. It can be seen clearly from Figure 5 that places along Oke-Aro, Oba-Ile-Airport, Oda, Oke-Ijebu, Igbatoro, and Akure-Owo express roads have limited coverage because there are inadequate or no bus stops along these roads. This reveals that more bus stops are needed in these areas with limited coverage (Underserved areas). Figure 7 presents the locations of new Bus stops.

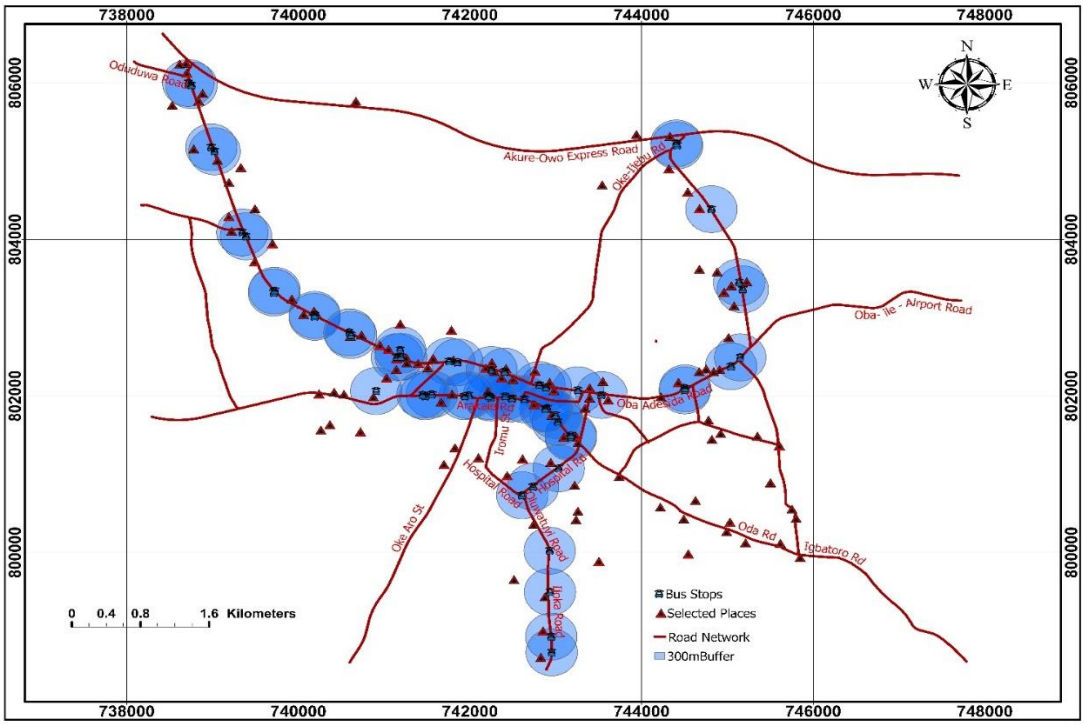

Figure 6: Buffer Analysis Result

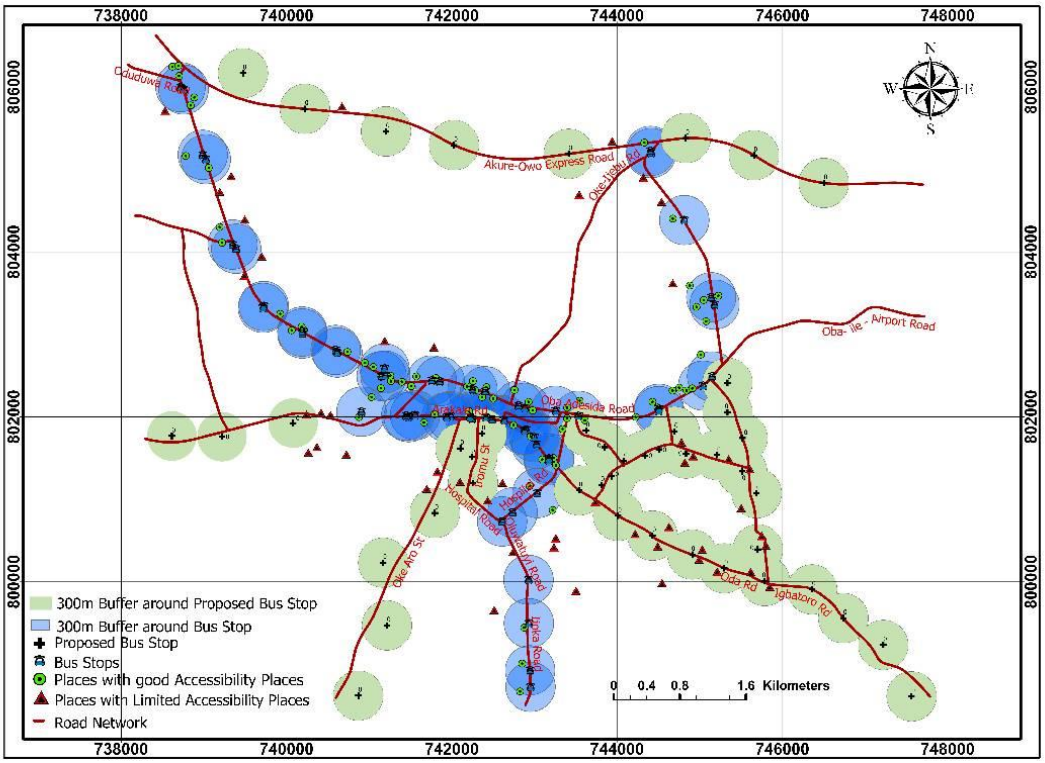

Figure 7 shows the locations of proposed Bus stops

5.0 CONCLUSION AND RECOMMENDATION

The study assesses the spatial distribution of Bus Stops in the Akure south local government area of Ondo state through the identification number of bus stops, mapping of the bus stops, generating the attribute data of bus stops creation of a GIS database for bus stops and , analysing the spatial distribution of bus stops in the study area. The Quadrat and the Nearest Neighbour analysis results shows that the bus stops are Clustered. Furthermore, proximity analysis between the bus stops at 300m was regarded as the maximum permitted walking or travelling distance. The outcome of the proximity analysis shows that 72 locations were discovered to be just a few minutes' walk from bus stations, indicating adequate accessibility to public transportation while 48 locations are far from bus stations, which limits their access to public transportation. The density analysis carried out revealed the concentration of bus stops. The result shows that bus stops are unevenly distributed across the study area. Notably, Mixed-use areas (banks, offices, restaurants, hotels, hospitals, petrol stations, etc.) emerged as prominent hotspots. The successful implementation of this study has the potential to positively impact the lives of residents by providing a more reliable, convenient, and sustainable public transportation system.

References

[1] Allison, N. (2002). Accessibility and the bus system: from concepts to practice. Thomas Telford, London. Pp.41-50.

[2] Bus Priority Team,(2006), Accessible bus stop design guidance, Bus Priority Team technical advice note BP1/06, Transport for London, pp2-10.

[3] Daudu, P. I.-U., Jibril, M.S. and Yashi, J. (2022) Spatial Analysis for Determining Accessibility to Bus Stops in Kaduna Metropolis. *Journal of Geographic Information System*, 14, 78-93. https://doi.org/10.4236/jgis.2022.141005

[4] Fatunmibi O (2018). Assessment of Bus Stops and its Effects on Major Roads in Ibadan Metropolis, Oyo State, Southwest Nigeria. *International Journal of Engineering Sciences & Research Technology*. **7(8) DOI**: 10.5281/zenodo.1336654

[5] Matisziw, T. A. (2006). Discrete Optimization Strategic route extension in transit networks. *European Journal of Operational Research*, 661-673.

[6] Murray, A., Davis, R., Stimson, R. and Ferreira, L, (1998) Public Transportation Access. *Transportation Research Part D*: *Transport and Environment*, **3**, 319-328. https://doi.org/10.1016/S1361-9209(98)00010-8

[7] O'Sullivan, D. M. (2000). Using desktop GIS for the investigation of accessibility by public transport: an isochrones approach. *International Journal of Geographical Information Systems 14 (1)*, 85–104.

[8] Olaogbebikan, J. E., I kpechukwu N., Akinsulire E. S. and Okoko, E., (2013). Traffic Management Problems in Lagos: A Focus on Alaba International Market Road, Ojo, Lagos State Nigeria. *Journal of Economics and Sustainable Development*. (4)4. 2013. Pp. 144-154

[9] Oyedepo, J. O. (2014). Assessment of socio-demographic characteristics of commercial motorcyclists in Akure, Nigeria. *African Journal of Engineering Research.* , 68-72.

[10] Olowosegun, A., & Okoko, E. E. (2012). The utility of geographic information system (GIS) in transport data integration for economic development: Evidence from Ibadan, Nigeria. *Global journal of human social science. Sociology, economics, and political science, 12*(14).

[11] Rodrigo, B.M., & Nick, W.L. (2004). Simulation modelling and analysis. An analytic investigation of optimal bus size. *Transportation Research*, 22B, 319- 337

[12] Tata Herbert and Matthew Nnonyelu Ono (2018). A Gravimetric Approach for the Determination of Orthometric Heights in Akure Environs, Ondo State, Nigeria. *International Journal of Scientific and Research Publications*, Volume 8, Issue 8, August 2018.

SUB THEME 07

Geospatial Sciences for Effective Delivery of Public and Social Services

GEOSPATIAL LANDUSE MAPPING IN CROP FARMING PURVIEW

Ogunlade, S.O.

Department of Surveying and Geoinformatics, Federal University of Technology, Akure

soogunlade@futa.edu.ng

Abstract

The applications of geospatial technology to land use have evolved salient positive interlocking innovations of land use mapping. The stretch of the interlock towards crop farming has evoked an intraoperative synergy between geospatial technology and agriculture. This study aimed at demonstrating the synergy between geospatial technology and agriculture through land use mapping in crop farming in the study area, Idi Ogun Village, Akinyele Local Government Area, Oyo State in Nigeria. A combined method of Global Positioning System and Total Station positioning and mapping was carried out on a farmland in the study area. The crop farming land use identified in the study is comprised of varied crops as follows: tomatoes, maize and cocoa. The locational data were acquired and processed for the general boundary of the farm and for the individual crop land use portion, thus resulting in the generation of the perimeter maps and the numerical data of the various crops land uses. The result showed that out of the total of 114392.051m^2 of land covering a perimeter of 1,438.369m, Cocoa plantation land use covered an area of 90,375.223 (79%); Maize land use -16,104.348m^2 (14.08%) and Tomato land use 7,912.480 m^2 (6.9%). Findings showed an inevitable intraoperative synergy of geospatial technology and agriculture and that geospatial land use mapping is a salient tool of high productivity in crop farming. The research concluded the availability of proper decision making in the management of farms through geospatial land use mapping; and an ease of further planning and decision making. The research was thus recommended as a tool for sustainable productivity and management of crop farms.

Keywords: Crop Farming, Data, Geospatial Technology, Land Use, Synergy

1.0 INTRODUCTION

Geospatial Technology is a field of study through which earth-related data are acquired to analyze, model and visualize part or whole of the earth surface. These data are referenced to the earth. Through them decisions to monitor the earth surface for sustainable management are thus made available. [3]. Thus, [8] and [19] viewed geospatial technology as part of a conglomerate of tools that are used to map and analyses the Earth and the ecosystem in this modern day. The component of geospatial technology includes Geographic Information System (GIS), Remote Sensing, and Global Positioning System (GPS) [8], Photogrammetry, Surveying and Geoinformatics [17]. It is a technology for the Earth (*geo*-) space (*spatial*) [17]. The concept of Land use in the field of geospatial technology is the human working, alteration, modification on the natural existence of the ecosystem [17] or the natural environment [6]. According to the [21],

it is the use to which a portion of land or the earth surface is put That is, the activities of man that is practiced at a given place. [20] viewed land use as a process. A process by which the use land in an area is identified by classifying the different types of land, distributing and using the space covered by land. The concept of mapping in geospatial technology is production of maps [9] from geographic data [2]. It is the transfer of features and their location (points) from the (curved or ellipsoidal) earth surface to a plane medium such as paper, cloth or screen. It is the creation of patterns of the features and their location in the environment of remote sensing techniques [7].

1.1 Scope

The concept of land use mapping is the production of map(s) that identifies the human activities (land use) taking place in an area. According to [7], from the perspective of using remote sensing techniques (such as LiDAR and RADAR), it is the method by which land use pattern are analyzed. The concept of Crop farming is the subset of the field of agriculture that deals with the production of crops. Other parts of agriculture are the production of livestock [11]. The purview of the crop farming indicates its environment, limit, and the operation within its scope. The applications of geospatial technology to land use have evolved salient positive interlocking innovations of land use mapping. The stretch of the interlock towards crop farming has evoked an intraoperative synergy between geospatial technology and agriculture. This study aimed at demonstrating the synergy between geospatial technology and agriculture through land use mapping in crop farming in the chosen study area.

2.0 MATERIAL AND METHODS

An area at Idi Ogun Village, Akinyele Local Government Area, Oyo State in Nigeria where several crop farming land uses is practiced was carefully sought for and chosen for a case study. It was a farmland where three crops (Cocoa, Tomatoes and Maize) were found to be grown. The GPS instrument was used to transfer ground control point from a first order control point located some distance away from the farmland. There were no reliable ground control points in the area to which the survey observation can be connected hence the need to establish some. The Total station instrument was used to obtain the locational data of the perimeter of the farmland and the perimeter of each of the existing crop farming land use by connecting to the established ground control points. The locational data were acquired and processed to generate the data for the general boundary of the farm and for the individual crop land use portion. The data were transformed in ArcGIS 10.5 software to generate land use planimetric maps for the whole farmland and for each of the crop farms. The resultant maps, geospatial data were stored in a database.

4.0 RESULTS AND DISCUSSION

The outcome of the fieldwork and data transformation were the planimetric locational data (Table 1) and maps of the perimeter of the whole farmland (Figure 1) and for each crop farming land use. The combination of these were used to generate a composite map (Figure 1)

Table 1: Locational of the farm land in its land use

Entire Farmland			**Cocoa Farm Land use**		
613863.964	831872.857	PL1	613927.005	831880.993	PL2
613927.005	831880.993	PL2	613970.961	831879.906	PL3
613970.961	831879.906	PL3	614021.81	831888.647	PL4
614021.81	831888.647	PL4	614026.252	831862.301	PL5
614026.252	831862.301	PL5	613948.354	831834.185	PL16
614030.383	831835.024	PL6	613905.518	831773	PL17
614076.934	831810.839	PL7	614031.494	831785.093	PL18
614030.167	831688.011	PL19			
614117.975	831660.736	PL20	Maize Farm Landuse		
Tomato Farm Landuse			614026.252	831862.301	PL5
614076.934	831810.839	PL7	614030.383	831835.024	PL6
614212.883	831697.88	PL8	614076.934	831810.839	PL7
614117.975	831660.736	PL20	614031.494	831785.093	PL18

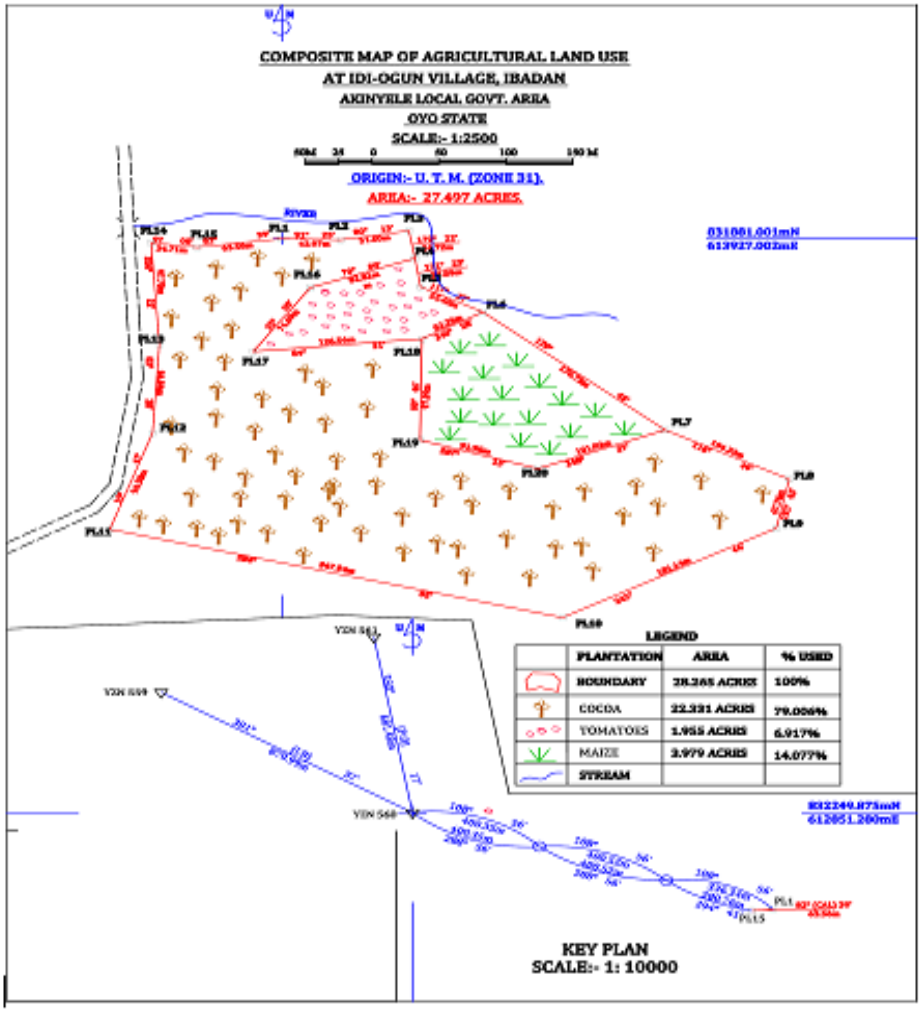

Figure 1: Composite Landuse planimetric map

(Source: Author's Work, 2023)

4.1 Findings

The results from the field work and data transformation are seen as veritable tools in the demonstration of the intraoperative synergy that exists between the field of geospatial technology and agriculture. From the results, the techniques of geospatial technology have made it easy to identify, describe and analyze the agricultural land use. The study area like many other farmlands require an identity of the ownership and the geographic location. So also is the description of its aerial extent and the geometric properties (such as the type of boundary lines, the color, length and bearing etc.). These were made available both graphically (Figure 1) and numerically (Table 1). More revealing from Figure 1 is the pattern and nature of the agricultural land use taking place within the study area. The map is loaded with the legends that guide in the interpretation of the contents. Many visual judgements were made available from the resultant

map. Table 2 is a summary of the dimensions of the agricultural (crop farming) land use identified in the study area.

Table 2: Summary of the dimensions of the agricultural (crop farming) landuse

LANDUSE	AREA (m^2)		Acres	Plots	PERIMETER (m)
ENTIRE	114392.051	%age	28.265	5	1438.369
COCOA	90375.223	79	22.331	4	1756.585
MAIZE	16104.348	14	3.979	0.7	519.937
TOMATOES	7912.480	7	1.955	0.3	416.336
TOTAL	114392.051	100	28.265	5	

Source: Author's Work, 2023

Out of the total of 114392.051m^2 of land covering a perimeter of 1,438.369m, Cocoa farm land use covered an area of 90,375.223 (79%); Maize land use 16,104.348m^2 (14.08%) and Tomato land use 7,912.480 m^2 (7%) (Table 2).

From table 2, the area of the farmland and its sub-divisions is made available at a glance, making it possible for decision and policy making such as shifting cultivation, suitability studies, modifications for other purposes and many fiscal and economic decision and policies. These data in digital form are replete with unlimited transformation and applications such as the multipurpose cadastre, Land Information System (LIS), and smart farming. Others are leasing, conveyancing or outright sale/purchase that require serious planning. In a nutshell, the geospatial information about the crop farming land use through the techniques of geospatial technology was made easy to access and assess, readily available, unambiguous for decision making, thus potentiate in boosting planning and productivity and sales. It is replete with other numerous potential benefits.

Geospatial technology applied to the agricultural field through the land use mapping of its sub-set of crop farming is a strong interoperative synergy. The crop farming purview has given geospatial technology a boost and vice versa. The geospatial technology family are having prospects in its application to agricultural fields while the agricultural family are having solace in the numerous benefits of geospatial technology. The inter-relationship is synergized to put smiles in the face of men.

5.0 CONCLUSION AND RECOMMENDATION

The study is mainly to demonstrate that there is an inevitable intraoperative synergy between the field and techniques of geospatial technology and the field of agriculture; and to appreciate it for maxima and optima benefit. Geospatial land use mapping has been discovered as a salient tool for high productivity in crop farming as it assists in proper and in-depth planning, hence, the availability of proper decision making in the management of farms; and an ease of further planning and decision making. The world and the environment are dynamic. Technology is

advancing. The correct appreciation of the positive influence of the field of geospatial technology in other disciplines and field is germane to the ubiquitous benefits it bestows on humanity.

The research is advocating the appreciation of the intraoperative synergy that exists between geospatial technology and agriculture as demonstrated in the crop farming purview as a case study. The use of geospatial technology in optimizing productivity in the field of agriculture should be intensified. More research in this corridor as in [17] is highly encouraged. More appreciation of geospatial technology and other fields is so invaluable in this modern era of deluge of geospatial information

References

[1] Bannister A., Raymond S. and Baker R. (1998). Surveying 7th Edition published by Person Education Limited, England.

[2] bls.gov (2022). Surveying and Mapping Technicians: Occupational Outlook Handbook. Retrieved from https://www.bls.gov › ooh › architecture-and-engineering on 8th August 2023

[3] Bronx Community College (2018). What is Geospatial Technology? 2155 University Avenue, Bronx, New York 10453. Retrieved from http://www.bcc.cuny.edu/academics/geospatial-center-of-the-cuny-crest-institute/what-is-geospatial-technology/ Accessed on 29th July 2023

[4] Deckshatulu, B.C. and George, J. (1993). Science of Remote Sensing: Current Science. Special Issue on Remote Sensing for National Development. Volume 61, No 3 and 4. Indian Academy of Science, August 1991.

[5] Di Gregorio, A. and Jansen, L.J.M. (1998). Land Cover Classification System (LCCS): Classification Concepts and User Manual for Software Version 1.0. Rome: Food and Agriculture Organization of the United Nations.

[6] Ellis, Erle; Goldewijk, Kees Klein; Gaillard, Marie-José; Kaplan, Jed O.; Thornton, Alexa; Powell, Jeremy; Garcia, Santiago Munevar; Beaudoin, Ella; Zerboni, Andrea (2019). "Archaeological assessment reveals Earth's early transformation through land use". *Science*. **365** (6456): 897–902.

[7] Fenstermaker (2023). what-is-land-use-mapping? Retrieved from https://blog.fenstermaker.com/what-is-land-use-mapping/

[8] GeoSLAM (2021) What is Geospatial Technology. Retrieved from https://geoslam.com › what-is-geospatial-technology. Accessed on 29th July 2023

[9] Geoinfotech (2023). Difference Between Mapping and Surveying. Retrieved from https://geoinfotech.ng › difference-between-mapping-. on 07/08/2023

[10] Nathan, W. (2000). Remote Sensing for Agricultural Applications. Agriculture and Natural Resources Extension Technology. Ohio State University Extension, 2000.

[11] National Geographic (2022). The Science and Art of Agriculture. Retrieved from https://education.nationalgeographic.org/resource/agriculture/ Accessed on 30th July 2023

[12] Norman, D. (1993). The Farming Systems Perspective: The Key to Building Sustainable Agriculture in Southern Africa. Invited Keynote Address at the Southern African Farming Systems Research-Extension Conference, Ezulweni, Swaziland, I et-3rd June1993.

[13] NPC (2006). National Population Commission, Nigeria Census Report, 2006.

[14] Obamiro, E. (2008). Farming Systems and Policy Options for Food Security in Southwestern Nigeria. International Institute of Tropical Agriculture, Ibadan, Nigeria Land Use/Land Cover Mapping. Paper presented at the National Workshop on Satellite Remote Sensing (NigeriaSat-1) and GIS: A Solution to Sustainable National

[15] Ogunlade, S.O (2018): Geomatics Techniques for Landuse Pattern Identification In Apatapiti Suburb of Akure Metropolis, Ondo State Nigeria. '*JOGER' Journal of Geomatics and Environmental Research.* Vol.1 No.1, 2018. http://ejournals.unilorin.edu.ng/journals/index.php/joger

[16] Ogunlade, S.O (2019): Spatiotemporal Land use Pattern Mapping For Sustainable Development of Akure City. *Journal Of Environmental Technology, School Of Environmental Technology, Federal University Of Technology Akure, Nigeria.* Vol. 1, No.1, 2019 21-28.

[17] Ogunlade, S.O. (2020): Site Suitability Mapping For Fish Farming: a Geospatial Approach. 3rd World Environmental Conservation Conference (WECC)- 'Strategies for Improved Quality of Life: Inclusive, Innovative, Integrated and Multi-stakeholder's Participation' Wesley University Ondo, Ondo State, Nigeria. 6th July, 2020 30-43 [Nigeria]Pretty, J.N. (1995). Regenerating Agriculture: Policies and Practice for Sustainability and Self-Reliance. London: Earthscan, Extensive practical strategy.

[18] Raji, B.A. (2004). Agricultural Land Use Planning and Management in Kadawa Irrigation Scheme, Kano State. Paper presented at the National Workshop on Satellite Remote

[19] ScienceDirect (2021). Geospatial Technology - an overview. Retrieved from https://www.sciencedirect.com › topics › geospatial-technology. Accessed on 29th July 2023.

[20] TeamCFL (2020). Types Of Crops | Classification and Basics of Agriculture. Retrieved from https://cropforlife.com/classification-types-of-crops-basics-of-agriculture, Accessed on 29th July 2023

[21] United States Environmental Protection Agency (2023) . What is the meaning of land use? Retrieved from https://www.epa.gov › report-environment › land-use on 7th August 2023

SPATIAL PATTERN ANALYSIS OF COVID_19 IN NIGERIA

Akpee, D., Eludoyin, O, S. and Ogoro, M.

Centre for Disaster Risk and Development Studies, University of Port-Harcourt, Rivers State

Corresponding author's email: -akpee2001@gmail.com

Abstract

The COVID-19 pandemic has significantly affected many countries, including Nigeria. Spatial pattern analysis of the pandemic in Nigeria provides insight into the spread and the extent of the outbreak across the country. This study aims to analyze the spatial pattern of COVID-19 cases in Nigeria using data visualization techniques and spatial statistics. The study uses publicly available data from the Nigeria Centre for Disease Control (NCDC) on the number of confirmed COVID-19 cases/deaths in Nigeria between March 2020 and November 2022. The data is analyzed using spatial statistical techniques, including Moran's I and high and low clustering. The result shows that the observed evidence of autocorrelation is due to randomness and not a meaningful relationship. For deaths, the results also show no clear pattern or relationship in the spatial distribution of covid-19 deaths across the country. The analysis identifies several clusters of high COVID-19 cases in specific states, including Lagos, FCT, Rivers State, Kaduna, and Oyo State. The study also examines the spatial autocorrelation between COVID-19 cases and population density. The results show a positive correlation between the number of confirmed cases/death and population density or urbanization. Additionally, the study created an interactive dashboard to visually represent the findings and provide a tool for monitoring the spread of COVID-19 in Nigeria. In conclusion, the spatial pattern analysis of COVID-19 in Nigeria provides insights into the distribution and factors associated with the pandemic. The study highlights the importance of utilizing spatial statistical techniques in understanding the complex spatial patterns of COVID-19 and developing effective strategies for controlling the disease.

Keywords: COVID-19, Spatial Analysis, Spatial Autocorrelation

1.0 INTRODUCTION

The coronavirus disease (COVID-19) first broke out in the city of Wuhan, Hubei Province in China in late December 2019 [6]. With the rapid spread in countries especially in Europe, COVID-19 was declared a pandemic by the World Health Organization (WHO) on March 12, 2020 [6]. The virus has spread to nearly all countries and continents wreaking havoc in catastrophic dimensions in different countries at an alarming pace. The first case of the virus emerged in Nigeria on February 28, 2020, and increased rapidly within two years to 264,000 cases with 3,148 deaths as of November 30, [6]. Compared with the number of cases and causalities in Asia, America, and Europe, Africa currently has a lower burden of COVID-19. These may be ascribed to differences in environmental conditions and the fact that the breakout started later in Africa than in most places

thereby providing a window of opportunity for preparedness and mitigation efforts such as lock-down.

However, Africa has the largest proportion of less developed countries than other continents. The continent nonetheless suffers a dearth of medical supplies, a very low baseline of and access to hospitalization capacity, particularly intensive and sub-intensive care. Other parameters such as larger household sizes, higher intergenerational mixing within households, poorer environmental conditions including overcrowded urban settlements, inadequate water, and sanitation, and pre-existing disease burden with higher prevalence of both undiagnosed, poorly managed, and unmanaged non-communicable diseases. These health outcomes may be risk factors for COVID-19 severity. Bearing in mind that Africa had the highest burden of infectious diseases, such as HIV, TB, malaria, Ebola, etc., which might have a negative impact on the long-time severity of COVID-19. There is a need for multi-sectoral efforts to stimulate understanding of the spread and severity of the virus in Africa and Nigeria in particular. This has necessitated undertaking this research on Mapping and Spatial Analysis of the COVID-19 Pandemic in Nigeria. Besides sharing the peculiarities of other African countries, Nigeria has a fragile healthcare system that could be overwhelmed easily. There are concerns that the current situation may worsen. Nigeria, as the most populous African country, occupies a delicate and strategic position in the continent. Inefficient management of the pandemic may affect other African countries negatively.

Spatial Pattern Analysis and modeling the spread of the virus worldwide has remained a big task because most virus parameters are unknown. Since the virus was declared a pandemic, professionals consisting of Geographic information system experts, engineers, Mathematicians, Statisticians, and data scientists have been presented with the daunting task of understanding and modeling the nature, the spread as well as other characteristics of the virus [3].

The current state of research on COVID-19 in Nigeria lacks sufficient focus on the spatial and temporal distribution of the disease. Existing studies have primarily centered around national-level data during the initial six months of the outbreak. Therefore, this research aims to bridge the gap by analyzing extended timeframe data to gain deeper insights into the disease outbreak. By doing so, it seeks to identify states with higher infection risks and facilitate targeted interventions to curb transmission effectively. The analysis revealed the existence of low clustering of COVID-19 cases/deaths in different parts of Nigeria, though not statistically significant. This information can be useful in targeting interventions and resources to the areas that need them the most. Visualizations of Covid-19 data will help to create a shared understanding of the changing nature of the pandemic and to enable a more unified response. Spatiotemporal analysis can inform forecasting of the potential future burden of the disease, help identify drivers of local transmission and populations at higher risk and guide the designing of targeted interventions in resource-limited settings [1]. Recognizing the temporal and spatial dynamics of the infection can provide insights into the epidemiological characteristics of the disease and the identification of disease hotspots.

Since the start of the pandemic in Nigeria, government agencies and other private and non-profit agencies in Nigeria often work at cross purposes. This research will create maps and tools that can bring together disparate government agencies and other private and non-profit partners to work together using common data and in turn, serve as a platform for information sharing. These visualizations will help to create a shared understanding of the changing nature of the pandemic and to enable a more unified response.

1.1 Aim and Objectives

The aim of this study is to carry out a spatial pattern analysis of the Covid-19 pandemic in Nigeria. The Objectives are: -

i. To create visual representations/Graphs/maps that showcase Nigeria's spatial and temporal distribution of pandemic data.

ii. Determine the spatial relationship between covid-19 cases/deaths and location in Nigeria.

iii. To develop a thorough representation of the COVID-19 cases and fatalities in Nigeria and examine the pattern of their geographical distribution.

iv. Develop the COVID-19 Dashboard for Nigeria

The study shows the importance of spatial pattern analysis in understanding the patterns and trends of pandemic. The analysis of spatial autocorrelation, of high and low clustering highlights the areas that are most affected by the pandemic and can be used to prioritize resource allocation and intervention efforts. Furthermore, the use of GIS and Spatial Analysis proved to be effective in identifying areas with a high incidence of COVID-19 cases and in detecting spatial patterns in the distribution of cases.

3.0 METHODOLOGY

The research design is shown in Fig. (1)

3.1 Data Collection

The research design is shown in Fig. (1) The data collection process involves gathering comprehensive datasets from multiple sources to analyze the spatial aspects of the COVID-19 pandemic in Nigeria. The primary data sources include:

a) COVID-19 Case Data: Daily or weekly COVID-19 case data at the subnational level (states or local government areas) are collected from official sources such as the Nigeria Centre for Disease Control (NCDC) and relevant government agencies. The data includes information such as the number of confirmed cases, deaths, recoveries, and demographic details. Data on confirmed cases, discharged cases, total active cases, total active cases, and deaths of COVID-19 was obtained from the Nigerian Centre for Disease Control (https://covid19.ncdc.gov.ng/). Using ArcMap and ArcGIS Pro, the collected data on covid 19 was downloaded and cataloged using an

Excel spreadsheet. These were then inputted into the ArcGIS software for visualization and spatial analysis. The spatial patterns and distribution trends in these data sets were analyzed using Geographical Information Systems (GIS).

b) Population Data: Accurate and up-to-date population data, including population datasets for the various states in Nigeria, were obtained from the National Population Commission websites and other online sources. This data is crucial for normalizing and analyzing COVID-19 cases in relation to the population.

c) Geospatial Data: Various geospatial datasets are collected and integrated into the analysis. These may include administrative boundaries (states, local government areas), road networks, and other relevant spatial data. These datasets enable the exploration of spatial relationships and potential factors influencing the spread of COVID-19.

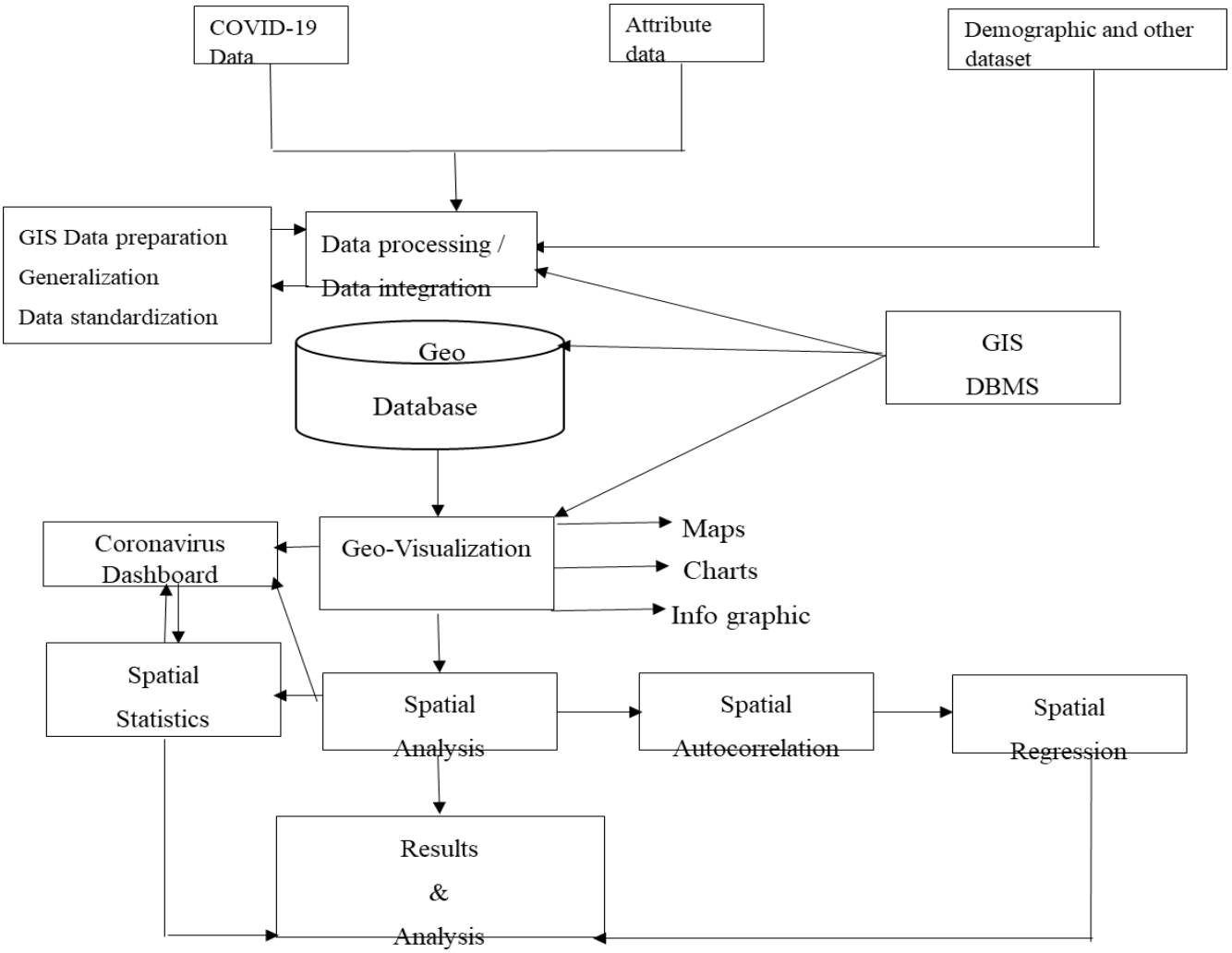

Figure1. Flowchart of research methodology

3.2 Data Preprocessing and Integration

The collected data undergoes preprocessing to ensure data quality and compatibility. Steps such as data cleaning, standardization, and georeferencing are performed. The datasets are then integrated based on spatial and temporal attributes, enabling comprehensive spatial analysis across different layers of information. Visualization using ArcGIS software and Power Bi to create maps showing the distribution of confirmed cases/deaths across Nigeria. ArcGIS Online and Power BI were deployed to create an interactive dashboard. Statistical Analysis techniques were used to identify patterns and determine spatial relationships that are associated with the spread of Covid-19 in Nigeria. For example, High and low clustering tests were carried out to see whether Covid 19 cases and deaths are clustered, Spatial autocorrelation or Global Moran 1 was used to examine the relationship between Covid-19 cases and factors such as population density, and location. Spatial autocorrelation analysis was carried out using Global and Local Moran's I while Getis-Ord will be used for cluster analysis. Spatial clustering analysis was carried out for low and high clustering of pandemic data.

Spatial autocorrelation was applied to assess the spatial correlation between variables through matching location similarity and attribute similarity. All data are presented in tables, graphs, charts, and maps.

4.0 RESULTS AND DISCUSSION

nga_aamonaa_aam1_osgof_201612

FID *	Shape *	admin1Name	Shape_Leng	CASES	ADMISSION	DISCHARGE	DEATHS	POP_2019	LAT	LONG	STATES	ORIG_FID	POINT_X	POINT_Y	START_X	START_Y
1	Point	Abia	4.695135	2253	14	2205	34	3841943	5.44045	7519150	ABIA STATE	0	7.52319	5.453302	3.40644	6.46542
2	Point	Adamawa	11.525443	1203	68	1103	32	4536948	9.29472	12.387	ADAMAWA STATE	1	12.400241	9.323227	3.40644	6.46542
3	Point	Akwa Ibom	5.26383	4989	38	4907	44	4780581	5036380	7.9122	AKWA IBOM	2	7.846395	4.907245	3.40644	6.46542
4	Point	Anambra	3.59596	2825	46	2760	19	5599910	6.2072	6.93601	ANAMBRA STATE	3	6.932186	6.222776	3.40644	6.46542
5	Point	Bauchi	13.952005	1990	18	1948	24	7540663	10.7482	9.97651	BAUCHI STATE	4	9.876172	10.301636	3.40644	6.46542
6	Point	Bayelsa	5.046708	1363	10	1325	28	2394725	4.76982	6.06958	BAYELSA STATE	5	6.080418	4.766315	3.40644	6.46542
7	Point	Benue	9.40808	2129	340	1764	25	5787706	7.32684	8.73557	BENUE STATE	6	8.751908	7.341086	3.40644	6.46542
8	Point	Borno	13.714364	1629	5	1580	44	5751590	11.8743	13.1463	BORNO STATE	7	13.153347	11.88898	3.40644	6.46542
9	Point	Cross River	8.779796	882	5	852	25	4175020	5.8344	8.57609	CROSS RIVERS	8	8.599106	5.874565	3.40644	6.46542
10	Point	Delta	7.372526	5664	382	5170	112	5307543	5.68798	5.93012	DELTA STATE	9	5.876631	5.499709	3.40644	6.46542
11	Point	Ebonyi	4.489355	2064	28	2004	32	3007155	6.24323	8.00804	EBONYI	10	8.016266	6.262027	3.40644	6.46542
12	Point	Edo	7.889425	7821	102	7398	321	4461137	6.33144	5.60327	EDO STATE	11	5.930215	6.633537	3.40644	6.46542
13	Point	Ekiti	3.395633	2457	12	2417	28	3350401	7.71004	5.3081	EKITI STATE	12	5.309516	7.72008	3.40644	6.46542
14	Point	Enugu	4.319893	2952	13	2910	29	3350401	7.71004	5.5081	ENUGU STATE	13	7.440611	6.536245	3.40644	6.46542
15	Point	Federal Capital Territory	3.498412	29257	164	28845	249	2702443	9.07448	7.39786	FCT	14	7.254198	8.825591	3.40644	6.46542
16	Point	Gombe	5.955286	3310	6	3238	66	3623462	10.3274	11.1776	GOMBE STATE	15	11.191995	10.383588	3.40644	6.46542
17	Point	Imo	2.878088	2655	7	2590	58	5467722	5.56113	7.05692	IMO STATE	16	7.062308	5.57302	3.40644	6.46542
18	Point	Jigawa	11.771497	669	2	649	18	6779080	12.2039	9.56159	JIGAWA STATE	17	9.563558	12.23842	3.40644	6.46542
19	Point	Kaduna	12.613678	11541	37	11415	89	8324285	10.3448	7.69431	KADUNA STATE	18	7.705979	10.392367	3.40644	6.46542
20	Point	Kano	8.244195	5263	112	5024	127	14253549	11.9997	8.59172	KANO STATE	19	8.529557	11.745202	3.40644	6.46542
21	Point	Katsina	9.105637	2418	0	2381	37	9600382	12.98	7.26179	KATSINA STATE	20	7.628834	12.378301	3.40644	6.46542
22	Point	Kebbi	14.968981	480	10	454	16	5001610	11.459	4.22955	KEBBI STATE	21	4.161723	12.138429	3.40644	6.46542
23	Point	Kogi	10.476383	5	0	3	2	4153734	7.7274	6690580	KOGI STATE	22	6.57867	7.803185	3.40644	6.46542
24	Point	Kwara	12.046963	4691	452	4175	64	3259613	8.95008	4.39119	KWARA STATE	23	3.599367	9.455692	3.40644	6.46542
25	Point	Lagos	4.28777	103463	320	102372	771	12772884	6.5232	3.37968	LAGOS STATE	24	3.586975	6.522424	3.40644	6.46542
26	Point	Nasarawa	9.537188	2777	393	2345	39	2632239	8.47821	8.1978	NASARAWA STAT	25	8.197963	8.510447	3.40644	6.46542
27	Point	Niger	18.921559	1183	165	998	20	6220617	8.47821	8.1978	NIGER	26	5.590435	9.933226	3.40644	6.46542
28	Point	Ogun	9.649774	5810	11	5717	82	5945275	6.98197	3.47374	OGUN STATE	27	3.473262	6.995135	3.40644	6.46542
29	Point	Ondo	7.751109	5173	315	4749	109	4969707	7.25607	5.20532	ONDO STATE	28	5.192575	7.104774	3.40644	6.46542
30	Point	Osun	4.66014	3311	29	3190	92	4237396	7.7809	4.54086	OSUN STATE	29	4.517762	7.562919	3.40644	6.46542
31	Point	Oyo	8.624586	10329	2	10125	202	7512885	8.11804	3.61465	OYO STATE	30	3.612912	8.158827	3.40644	6.46542
32	Point	Plateau	8.575527	10317	10	10232	75	4400974	9.5652	9.08255	PLATEAU STATE	31	9.596843	8.96153	3.40644	6.46542
33	Point	Rivers	5.814545	17831	173	17503	155	7034973	4.80467	6.89986	RIVERS STATE	32	6.918181	4.845392	3.40644	6.46542
34	Point	Sokoto	10.503159	822	0	794	28	5863187	13.0146	5.30333	SOKOTO STATE	33	5.31881	13.037993	3.40644	6.46542
35	Point	Taraba	13.696255	1474	63	1377	34	3831885	7.97501	10.774	TARABA STATE	34	10.509575	7.943946	3.40644	6.46542
36	Point	Yobe	11.096937	638	4	625	9	3398177	12.2624	11.4315	YOBE STATE	35	11.437066	12.29868	3.40644	6.46542
37	Point	Zamfara	9.466144	375	0	366	9	5317793	12.0944	6.2198	ZAMFARA STATE	36	6.246535	12.101505	3.40644	6.46542

Figure 2. Covid-19 X Y to point table.

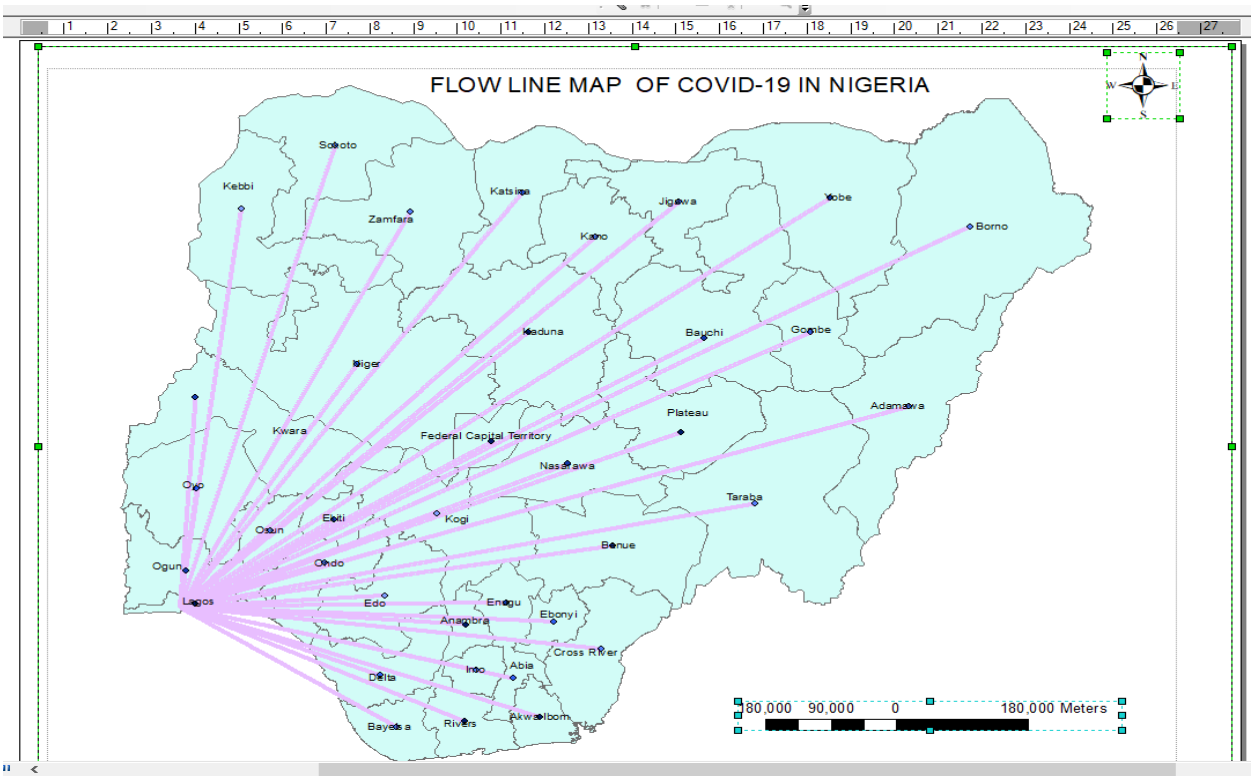

Figure 3. Flow map of COVID-19 in Nigeria

Title
nga_admbnda_adm1_osg

Metadata Geography Table

	admin1Name	Shape_Leng	CASES	ADMISSION	DISCHARGE	DEATHS	POP_2019	LAT	LONG	STATES	OBJECTID *	Shape__Area *	Shape__Length *	Shape *
10	Delta	7.372526	5664	382	5170	112	5307543	5.68798	5.93012	DELTA STATE	10	1.394082	7.372526	Polygon
11	Ebonyi	4.489355	2064	28	2004	32	3007155	6.24323	8.00804	EBONYI	11	0.51805	4.489355	Polygon
12	Edo	7.889425	7821	102	7398	321	4461137	6.33144	5.60327	EDO STATE	12	1.595809	7.889425	Polygon
13	Ekiti	3.395633	2457	12	2417	28	3350401	7.71004	5.3081	EKITI STATE	13	0.471634	3.395633	Polygon
14	Enugu	4.319893	2952	13	2910	29	3350401	7.71004	5.5081	ENUGU STATE	14	0.624323	4.319893	Polygon
15	Federal Capital Territory	3.498412	29257	164	28845	249	2702443	9.07448	7.39786	FCT	15	0.607222	3.498412	Polygon
16	Gombe	5.955286	3310	6	3238	66	3623462	10.3274	11.1776	GOMBE STATE	16	1.438747	5.955286	Polygon
17	Imo	2.878088	2655	7	2590	58	5467722	5.56113	7.05692	IMO STATE	17	0.414097	2.878088	Polygon
18	Jigawa	11.771497	669	2	649	18	6779080	12.2039	9.56159	JIGAWA STATE	18	1.928873	11.771497	Polygon
19	Kaduna	12.613678	11541	37	11415	89	8324285	10.3448	7.69431	KADUNA STATE	19	3.645639	12.613678	Polygon
20	Kano	8.244195	5263	112	5024	127	14253549	11.9997	8.59172	KANO STATE	20	1.685607	8.244195	Polygon
21	Katsina	9.105637	2418	0	2381	37	9600382	12.98	7.26179	KATSINA STATE	21	1.991947	9.105637	Polygon
22	Kebbi	14.968981	480	10	454	16	5001610	11.459	4.22955	KEBBI STATE	22	3.035227	14.968981	Polygon
23	Kogi	10.476383	5	0	3	2	4153734	7.7274	6690580	KOGI STATE	23	2.368882	10.476383	Polygon
24	Kwara	12.046963	4691	452	4175	64	3259613	8.95008	4.39119	KWARA STATE	24	2.766244	12.046963	Polygon
25	Lagos	4.28777	103463	320	102372	771	12772884	6.5232	3.37968	LAGOS STATE	25	0.300166	4.28777	Polygon
26	Nasarawa	9.537188	2777	393	2345	39	2632239	8.47821	8.1978	NASARAWA STATE	26	2.197927	9.537188	Polygon
27	Niger	18.921559	1183	165	998	20	6220617	8.47821	8.1978	NIGER	27	5.930956	18.921559	Polygon
28	Ogun	9.649774	5810	11	5717	82	5945275	6.98197	3.47374	OGUN STATE	28	1.364021	9.649774	Polygon
29	Ondo	7.751109	5173	315	4749	109	4969707	7.25607	5.20532	ONDO STATE	29	1.233546	7.751109	Polygon
30	Osun	4.66014	3311	29	3190	92	4237396	7.7809	4.54086	OSUN STATE	30	0.704549	4.66014	Polygon
31	Oyo	8.624586	10329	2	10125	202	7512885	8.11804	3.61465	OYO STATE	31	2.264918	8.624586	Polygon
32	Plateau	8.575527	10317	10	10232	75	4400974	9.5652	9.08255	PLATEAU STATE	32	2.180996	8.575527	Polygon
33	Rivers	5.814545	17831	173	17503	155	7034973	4.80467	6.89986	RIVERS STATE	33	0.830196	5.814545	Polygon
34	Sokoto	10.503159	822	0	794	28	5863187	13.0146	5.30333	SOKOTO STATE	34	2.679547	10.503159	Polygon
35	Taraba	13.696255	1474	63	1377	34	3831885	7.97501	10.774	TARABA STATE	35	4.802474	13.696255	Polygon
36	Yobe	11.096937	638	4	625	9	3398177	12.2624	11.4315	YOBE STATE	36	3.726688	11.096937	Polygon
37	Zamfara	9.466144	375	0	366	9	5317793	12.0944	6.2198	ZAMFARA STATE	37	2.782855	9.466144	Polygon

Figure 4. States, cases, deaths, and population data.

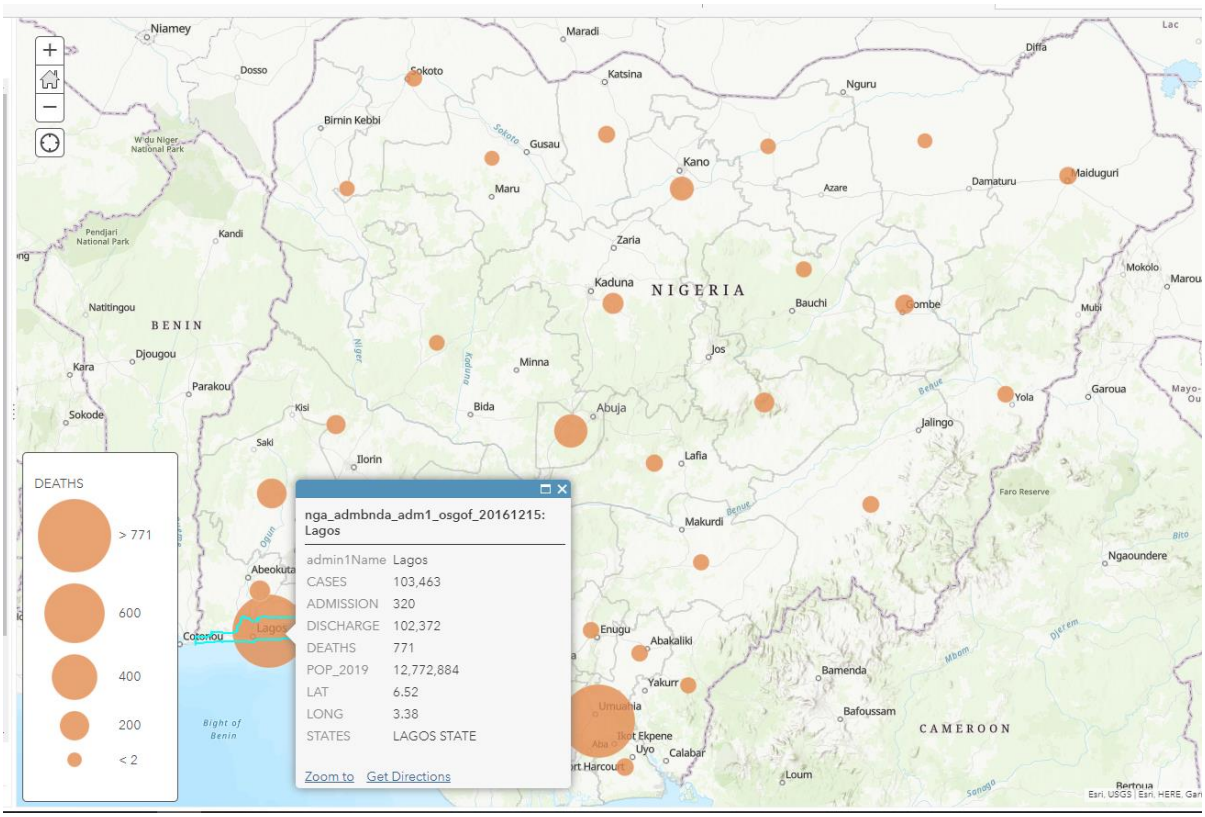

Figure 5. Cartograms of COVID-19 deaths in Nigeria

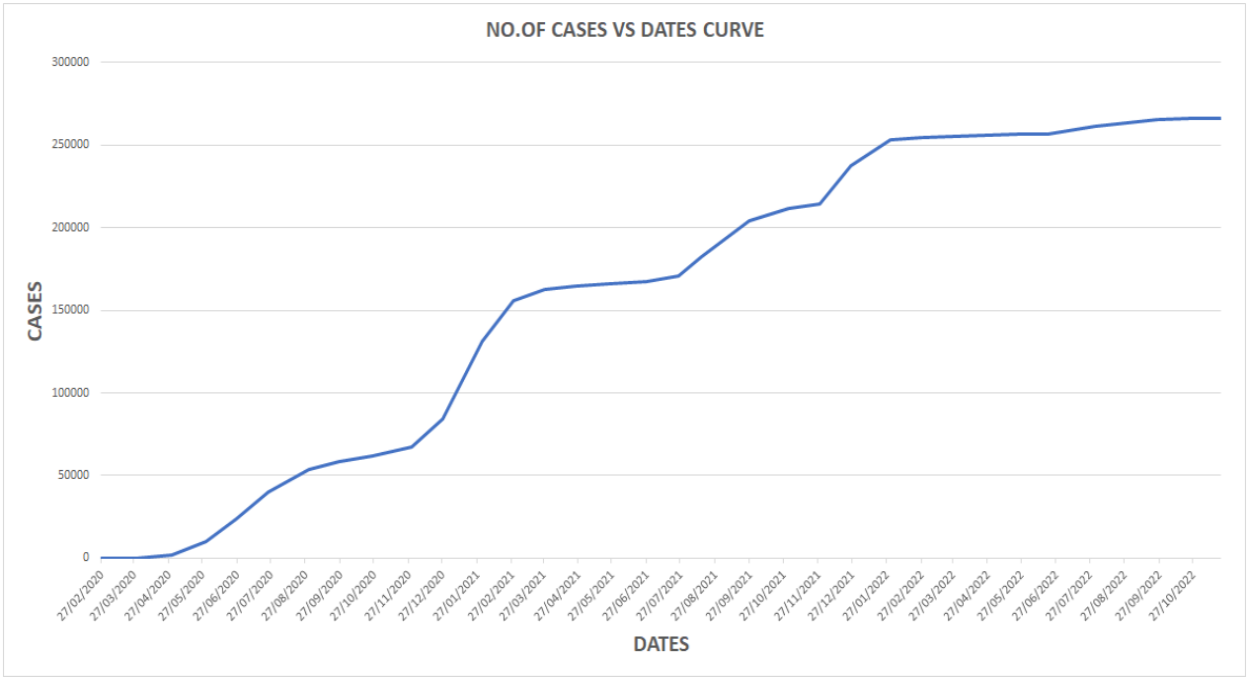

Figure 6. Linear logarithmic (time series) of total cases/dates

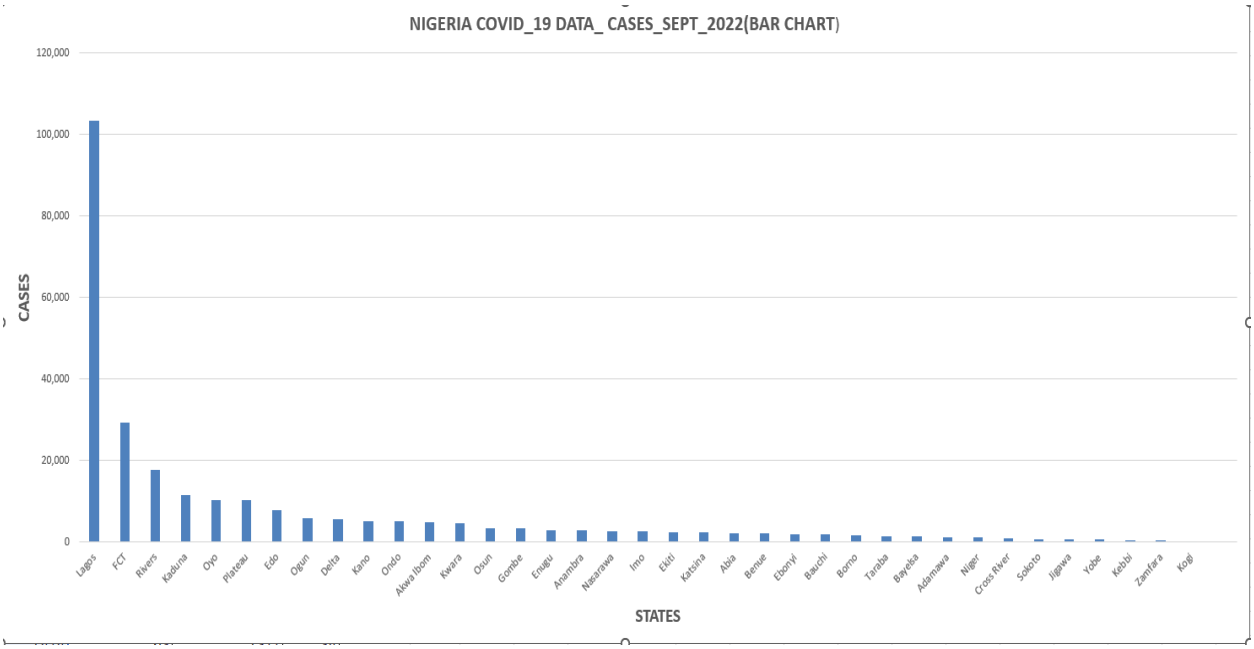

Figure 7. Bar chart of Covid-19 cases across states in Nigeria

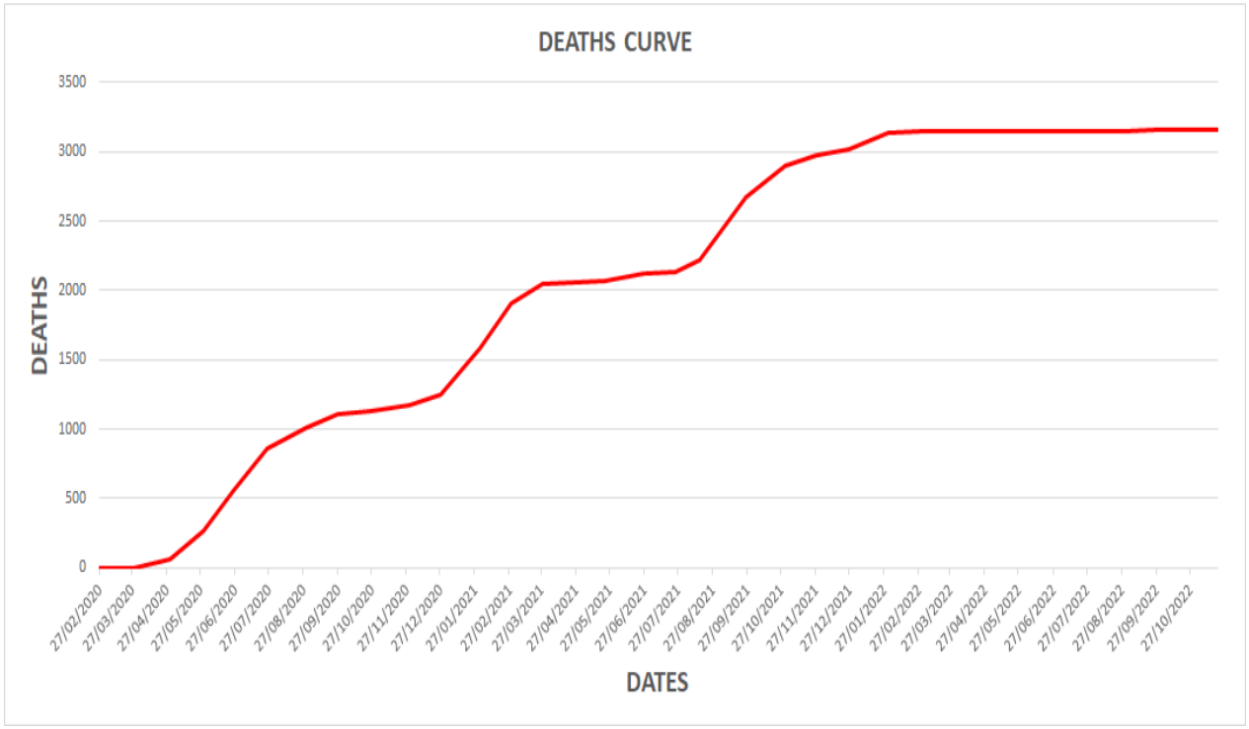

Figure 8. Time series graph of Covid-19 deaths across states in Nigeria

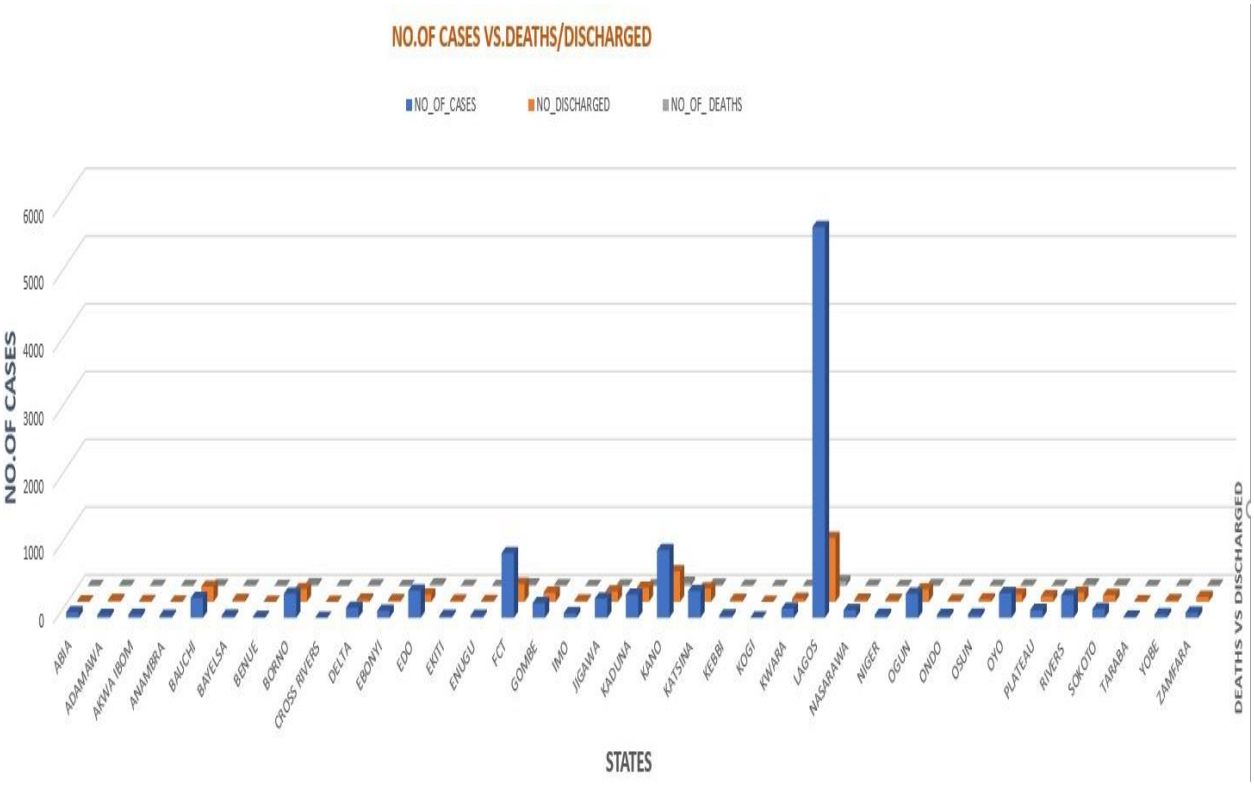

Figure 9. 3D chart showing no. of cases, discharged and deaths for the first 100 days.

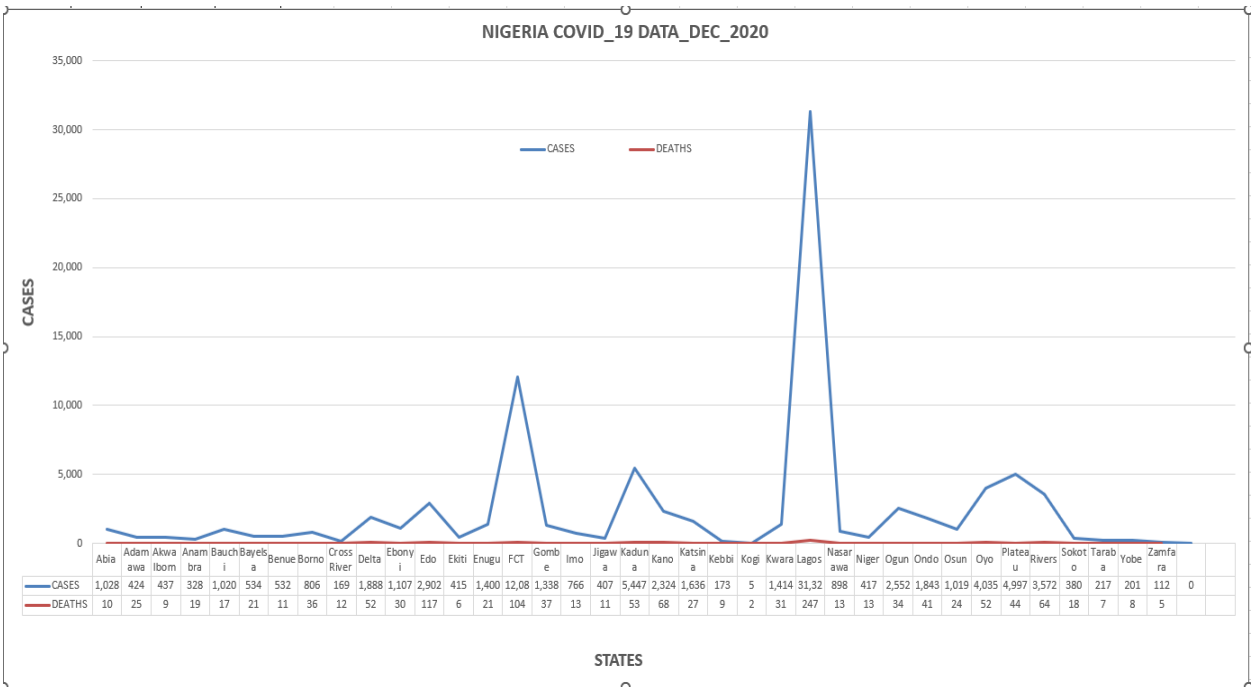

	Abia	Adamawa	Akwa Ibom	Anambra	Bauchi	Bayelsa	Benue	Borno	Cross River	Delta	Ebonyi	Edo	Ekiti	Enugu	FCT	Gombe	Imo	Jigawa	Kaduna	Kano	Katsina	Kebbi	Kogi	Kwara	Lagos	Nasarawa	Niger	Ogun	Ondo	Osun	Oyo	Plateau	Rivers	Sokoto	Taraba	Yobe	Zamfara	
CASES	1,028	424	437	328	1,020	534	532	806	169	1,888	1,107	2,902	415	1,400	12,08	1,338	766	407	5,447	2,324	1,636	173	5	1,414	31,32	898	417	2,552	1,843	1,019	4,035	4,997	3,572	380	217	201	112	0
DEATHS	10	25	9	19	17	21	11	36	12	52	30	117	6	21	104	37	13	11	53	68	27	9	2	31	247	13	13	34	41	24	52	44	64	18	7	8	5	

Figure 10. Time series (Dec 2020)

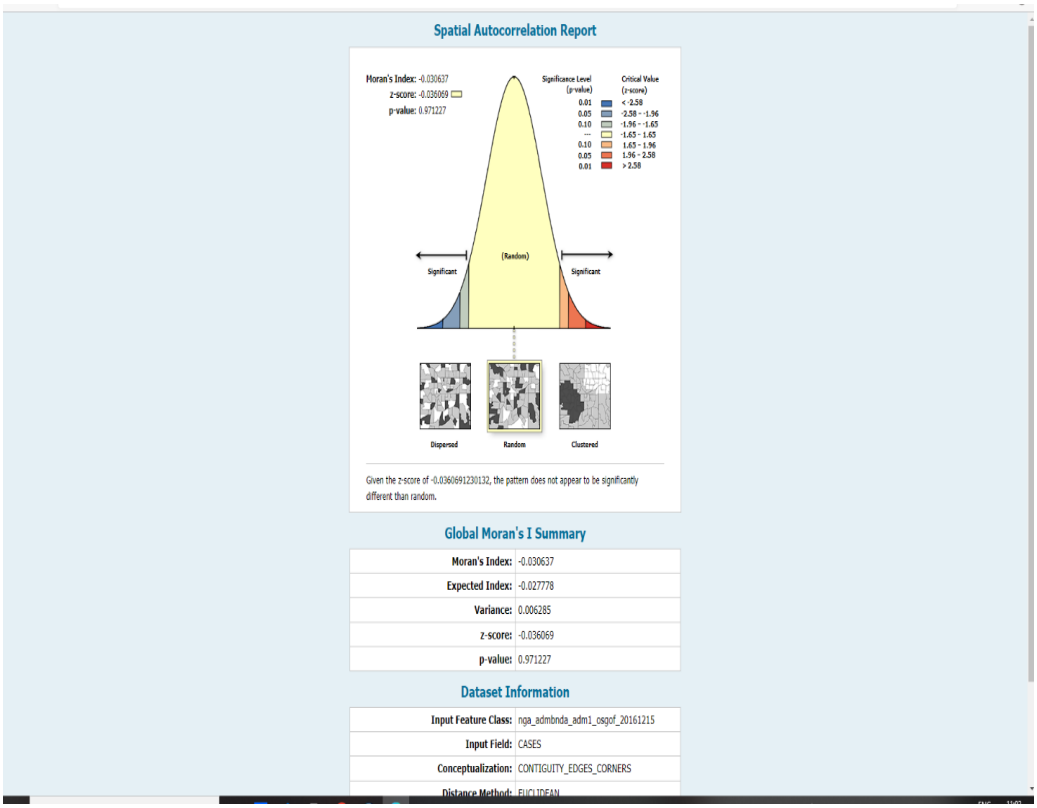

Figure 11. Spatial autocorrelation test result for Deaths

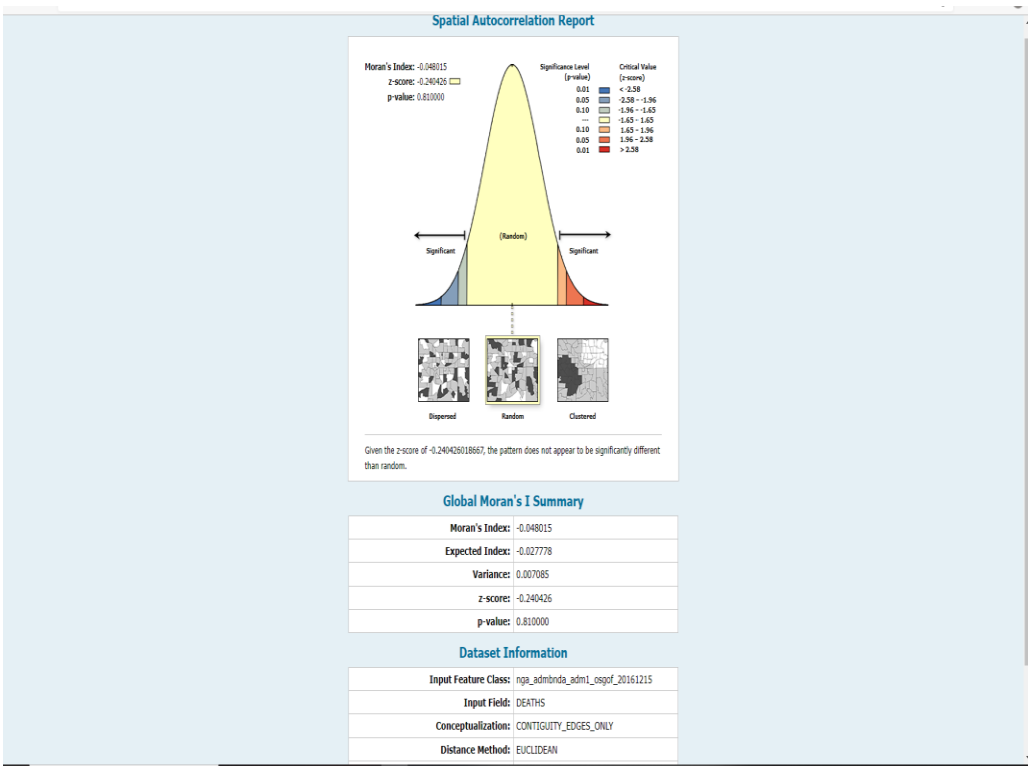

Figure 12. Spatial autocorrelation test result for cases

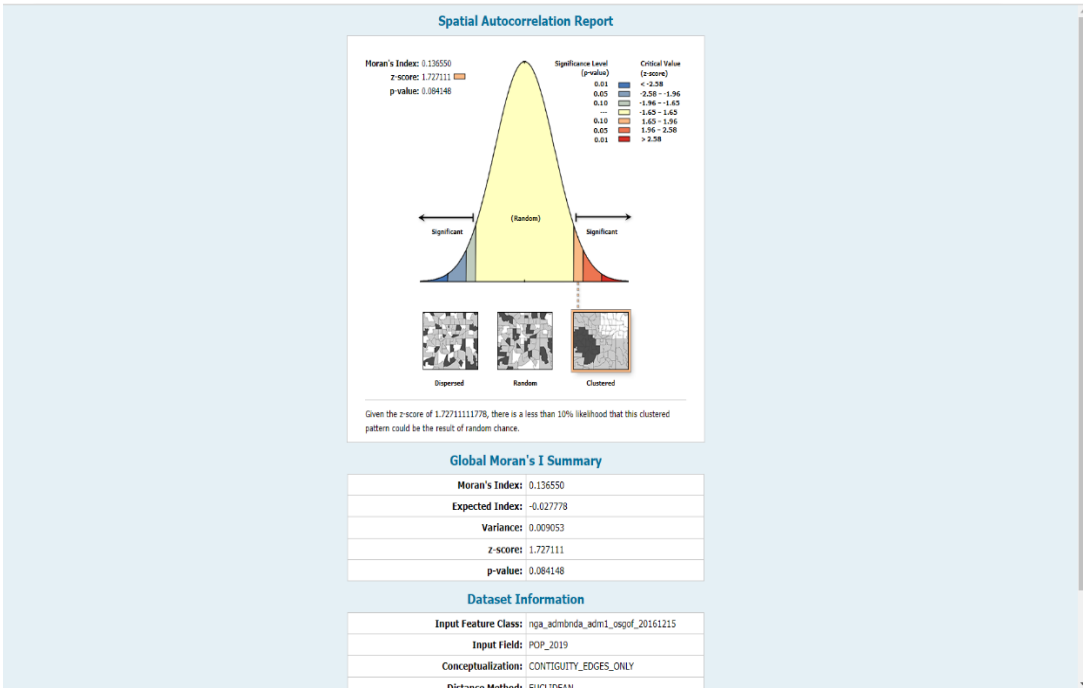

Figure 13. Spatial autocorrelation for population density

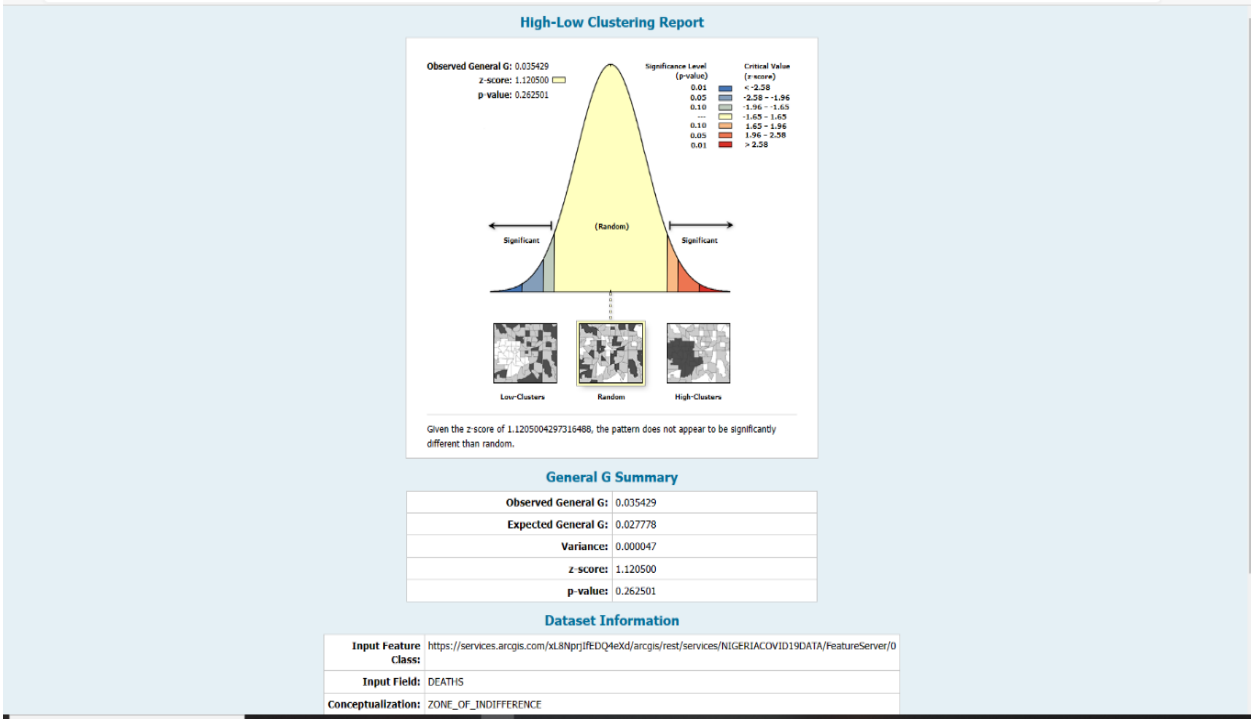

Figure 14. High/low clustering of COVID-19 deaths

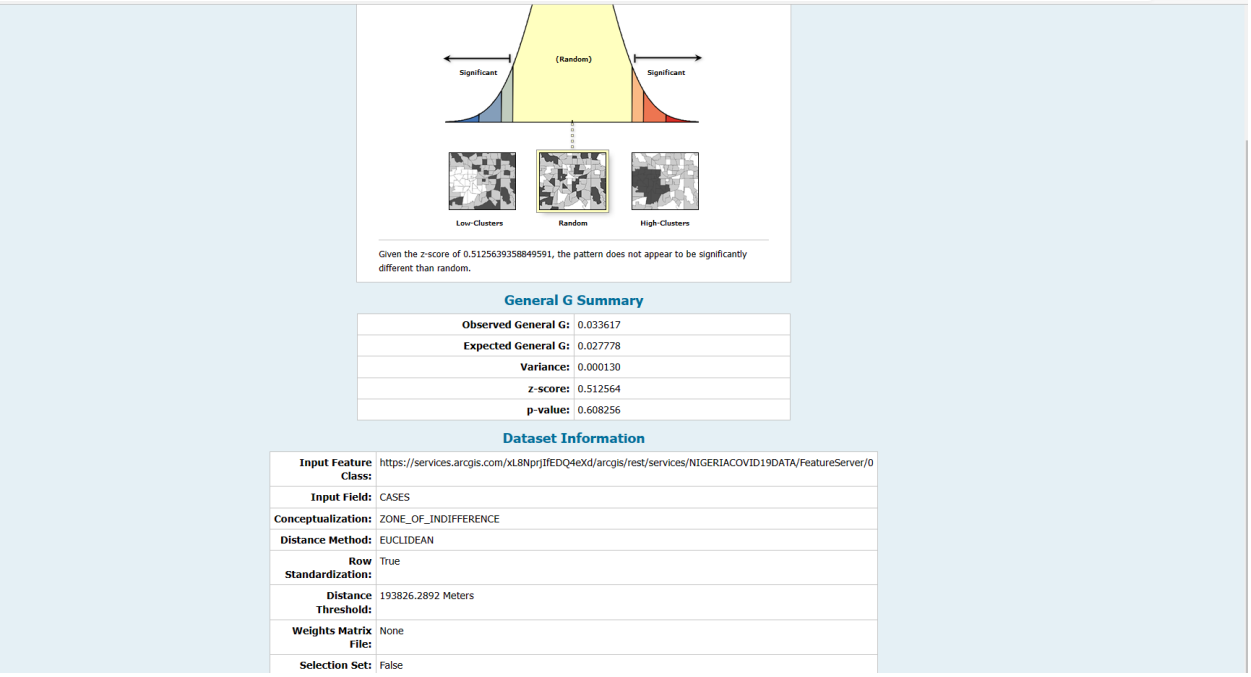

Figure 15. High/low clustering of COVID-19 cases

4.1 Discussion

(a) Time Series Graphs/Cartograms/ Bar Charts/Maps

The Time series graph, Cartograms, Bar charts, and maps generated from the research data obtained from the Nigerian Centre for Disease Control (NCDC). Nigeria recorded a total of 264,000 cases and 3144 deaths for the period under review. The states with the highest caseloads were Lagos (103,463 cases), FCT (29,258 cases), Rivers State (17,831 cases), Kaduna (11,541 cases), and Oyo State (10,329). States with the least COVID-19 cases were Kogi (5), Zamfara (375), Kebbi (480), Yobe (638), and Jigawa state (669). The virus started in Nigeria on February 28, 2020, and it spread slowly until April 2020. The curve shows that COVID_19 cases were on the rise from April 2020 to the early part of September 2020. There was a reduction in the number of cases from part of September 2020 to November 2020. From December 2020, Covid_19 cases were on the rise through March 2021. There was a substantial reduction in the number of cases from April through July 2021. It peaked again from August through October. The curve was flat in November 2021. There was a rise again from December 2021 through February 2022. The curve was flattened from February through May 2022. It started to peak again from June 2022 through September 2022. From October 2022 till now November 2022, the curve flattened. The highest recorded instances of caseload were from December 2021 through January 2022. Over 4000 daily cases were recorded on 28th December 2021. The second instance of the highest caseloads was from December 2020 through February 2021. This period recorded over 1000 daily confirmed cases, and it peaked at 2300 confirmed cases on the 30th of January 2021.

Figures 6 and 7, show the bar chart and time series graph of COVID-19 deaths across Nigeria. There was a slow start from the inception of COVID-19 in February 2020, and it remained so till April 2020. Death cases rose from May 2020 through August 2020. Things started slowing down in late September through November 2020. There was a sharp rise in death cases from December 2020 and it kept rising till March 2021. The curve was fattened from April 2021 through July 2021. Thereafter, there was a steady climb or rise in cases from August 2021 and it peaked in January 2022. The death curve was flattened from February 2022 through October 2022.

Lagos state has the highest recorded deaths of 771 cases. Edo state has the second highest death cases of 321. The Federal Capital Territory has the 3rd highest deaths count of 249 cases. The Oyo state came 4th with a total death count of 202, followed by Rivers State came with a total death count of 155 deaths. The last death counts were recorded in Kogi (2), Zamfara and Yobe (9), and Kebbi (16).

At the beginning of the COVID-19 outbreak, there was much fear about Africa and Nigeria due to the health crisis in Africa, however, the predictions did not play out and it's sparking global interest in understanding what may be responsible and the peculiarities in the Covid-19 outbreak dynamics that lead to the milder outbreak than initially projected for Nigeria and Africa at large. Nigeria has done substantially well in managing or responding to the COVID-19 outbreak if we look at data from other African countries. South Africa had 4,054522 cases and 102595 deaths, Morocco recorded 1,272186 cases and 16296 deaths, Tunisia had 1,152033 cases and 29219 deaths, Egypt had 515645 and 26613 deaths, Ethiopia had 499354 and 7572, Kenya 342792 cases 5688 deaths, Botswana had 328581 and 2795 deaths and Algeria had 271354 and 6881 deaths while Nigeria had 266453 cases and 3155 deaths as of January 2023. Africa has been predicted to be the most vulnerable continent in terms of COVID-19 infection and mortality and was predicted as the region where COVID-19 will have a major impact. The prediction was based on the continent's weak healthcare system and large immune-compromised population (Lone and Ahmed, 2020). However, the present reality proved the prediction otherwise. Some researchers have attributed the low impact of COVID-19 in Nigeria to the low volume of air travel, large youthful population, favorable climate and immunity from prior immunizations, and poor reports of events (David et al., 2020). Other factors could be low testing and serious underreporting.

4.1.1 Low/High clustering

Figures 14 and 15 are the results obtained from low/High clustering analysis. The clustering is a statistical measure used to assess the degree of spatial clustering, in this instant- COVID-19 cases in Nigeria. Specifically, these values relate to the calculation of the General G statistic, which is a common index used to measure the degree to which similar values (in this case, COVID-19 cases) are clustered together in geographic space.

The General G statistic considers both the observed and expected number of cases within a particular geographic unit (e.g., states). The expected number of cases is calculated based on the overall prevalence of COVID-19 in Nigeria and serves as a baseline against which to compare the

observed number of cases. If the observed number of cases is higher than the expected number, this suggests that there may be spatial clustering of cases in that area. the observed General G value is 0.033617, indicating some degree of spatial clustering of COVID-19 cases in Nigeria. The expected General G value is 0.027778, which suggests that there may be some deviation from what would be expected by chance alone, although this difference is not statistically significant.

The Z-score is another important statistic that is used to assess the significance of the clustering pattern. In this case, the Z-score is 0.512564, which is relatively low and indicates that there is no strong evidence for spatial clustering of COVID-19 cases in Nigeria. Overall, the clustering values obtained suggest that there may be some degree of spatial clustering of COVID-19 cases in Nigeria, but that this clustering pattern is not statistically significant. This could be due to various factors, such as differences in testing rates and reporting, differences in population density and mobility, and differences in adherence to public health measures.

For COVID-19 deaths, The Z-score of 1.120500 and P-value of 0.262501 suggest that the observed general G statistic 0.035429 is not significant and the clustering of COVID-19 Deaths in Nigeria is not different from random. It also indicates that the observed clustering is not statistically significant and likely occurred by chance. This means that there is a relatively high probability that the death cases occurred by chance and is therefore not statistically significant.

4.1.2 Spatial autocorrelation

Spatial autocorrelation refers to the degree to which the values of a variable in geographic space are like one another. The Moran Index is a statistical measure used to determine whether there is spatial autocorrelation in a set of data. It ranges from -1 to 1, where -1 indicates perfect negative spatial autocorrelation, 0 indicates no spatial autocorrelation, and 1 indicates perfect positive spatial autocorrelation.

From Figure 11 in the context of COVID-19 cases across Nigeria, a Moran index of -0.030637 suggests that there is a weak negative spatial autocorrelation in the data. This means that areas with high COVID-19 cases are slightly more likely to be surrounded by areas with lower COVID-19 cases. This is true for Lagos with the highest covid cases but surrounded by Ogun, Osun, and Ondo states respectively with relatively low COVID cases. The same is true for FCT with high covid cases but surrounded by states with low COVID cases like Kogi, Nasarawa, and Niger state. Rivers State with the third highest COVID-19 cases is also surrounded by low COVID-burden states like Bayelsa, Akwa-Ibom, Imo, and Abia State. However, the negative correlation is weak, indicating that there is no clear pattern of clustering or dispersion of COVID-19 cases across Nigeria. Again, In the case of COVID-19 negative spatial autocorrelation, means that there is no clear pattern of clustering or dispersion of COVID-19 cases across the country. In other words, the distribution of COVID-19 cases in Nigeria is somewhat random and not dependent on geographic proximity. The Z-score of -0.036069 and P-value of -0.971227 provide additional information about the statistical significance of Moran's I value. The Z-score measures the number of standard deviations from the mean, and a Z-score of -0.036069 suggests that Moran's I value is not statistically significant. The

P-value represents the probability of obtaining a Moran's I value as extreme as the one observed if there were no spatial autocorrelation in the data. A P-value of -0.971227 suggests that there is a very high probability that the observed Moran's I value is due to chance rather than a true spatial pattern. Overall, these values suggest that COVID-19 cases in Nigeria are not significantly clustered or dispersed in any way, and there is no clear geographic pattern to the spread of the virus, the spread of COVID-19 cases in Nigeria is random. For COVID-19 deaths (see Figure 4.34 and Figure 4.42), the Moran's I index for COVID-19 deaths across Nigeria is -0.48015. This value suggests a negative spatial autocorrelation or dispersion of COVID-19 deaths across Nigeria. This means that areas with higher COVID-19 death rates are not necessarily close to each other and may be scattered throughout the country. States with the highest COVID-19 deaths are Lagos (771), Edo State (321), FCT (249), Oyo State (202), Rivers State (155), and Kano (127). In other words, the spatial distribution of Covid-19 deaths across Nigeria is random. This means that COVID-19 deaths are not clustered in any area of the country and are distributed randomly across Nigeria. This suggests that there is no strong spatial clustering of COVID-19 deaths in Nigeria, and the pandemic has affected different regions of the country equally.

Overall, these results suggest that there is no strong evidence of spatial clustering or dispersion of COVID-19 deaths across Nigeria, and the observed pattern could be due to random chance. It is important to note that these results only provide a snapshot of the spatial pattern of COVID-19 deaths at a point in time of this data, and further analysis is needed to understand the spatial dynamics of the pandemic and its spatial patterns over time.

With regards to population density and how it affects COVID-19 spread, results obtained suggest there is a borderline significant clustering of COVID-19 cases/deaths because of population density in the Nigeria space (See Figure 4.45). The Moran index (I) of 0.136550 indicates that there is positive spatial autocorrelation in the COVID-19 cases/deaths because of high or low population data. This means that areas with high population density tend to have high COVID-19 cases/deaths, and areas with low population density tend to have low COVID-19 cases/deaths across the Nigerian space. In other words, there is the clustering of COVID-19 cases in space with respect to population density. The positive value of the Moran index indicates that the clustering is stronger than would be expected by random chance. The Z-score of 1.727111 tells us how the standard deviations are away from the mean of the observed Moran index. A Z-score of 1.727111 suggests that the observed Moran index is statistically significant and unlikely to have occurred by chance.

5.0 CONCLUSION AND RECOMMENDATION

The study's first significant finding underscores the crucial role of spatial analysis in comprehending pandemic patterns. By examining spatial autocorrelation and identifying high and low clusters, the most impacted regions emerge, guiding the prioritization of resources and intervention strategies. The effectiveness of GIS and Spatial Analysis is evident in pinpointing areas with elevated COVID-19 cases and revealing spatial distribution patterns.

The second key insight from the analysis reveals the presence of both high and low clusters of COVID-19 cases and deaths across different Nigerian regions, although not reaching statistical significance. Despite this, the information remains valuable for directing interventions and resources to areas in greatest need.

The third important observation involves the identification of spatial autocorrelation in the distribution of COVID-19 cases in Nigeria. This suggests that the occurrence of cases in one location might influence the likelihood of cases appearing in nearby locations.

Finally, the study's implementation of a pandemic dashboard enabled real-time monitoring and visualization of disease spread, empowering policymakers to make informed decisions and optimize resource allocation. Altogether, the utilization of GIS and Spatial Analysis tools has proven highly valuable in gaining insights into the spatial patterns and distribution of COVID-19 in Nigeria, thereby informing targeted interventions and resource allocation strategies.

References

[1] David Wilson, Daniel T Halperin (2008) “Know your epidemic, know your response”: a useful approach if we get it right. *The Lancet* Volume 372, Issue 9637, 9–15 August 2008, Pages 423-426.

[2] Ivan Franch-Pardo, Brian M. Napoletano, Fernando Rosete-Verges, and Lawal Billa (2020). *Journal Science of the Total Environment*. Volume 739, 15 October 2020, 140033

[3] Fong, S.J., Li, G., Dey, N., Crespo, R.G., & Herrera-Viedma, E. (2020). Finding an accurate early forecasting model from small dataset: A case of 2019-ncov novel coronavirus outbreak. arXiv preprint arXiv:2003.10776.

[4] Kayode P. Ayodele, Hafeez Jimoh, Adeniyi F. Fagbamigbe, Oluwatoyin H. Onakpoya, The dynamics of COVID-19 outbreak in Nigeria: A sub-national analysis, *Scientific African*, Volume 13,2021. https://doi.org/10.1016/j.sciaf.2021.e00914.

[5] Lawal, O., & Nwegbu, C. (2022). Movement and risk perception: Evidence from spatial analysis of mobile phone-based mobility during the COVID-19 lockdown, Nigeria. *Geojournal*, 87(3), 1543-1558. https://doi.org/10.1007/s10708-020-10331-z

[6] World Health Organization (2020). Who Announces Covid-19 Outbreak a Pandemic, World Health Organization [Internet].

NATIONAL SPACE RESEARCH
AND DEVELOPMENT AGENCY

@AS-SEHIIND CREATIVITIES: 07062389161